

Rochester Institute of Technology

RIT Digital Institutional Repository

Theses

12-15-2016

Harvesting a Sustainable Energy Future: Examining the effect of chemical composition on the electromechanical properties of polymer gel beads

Kaushik Kudtarkar
kak6093@rit.edu

Follow this and additional works at: <https://repository.rit.edu/theses>

Recommended Citation

Kudtarkar, Kaushik, "Harvesting a Sustainable Energy Future: Examining the effect of chemical composition on the electromechanical properties of polymer gel beads" (2016). Thesis. Rochester Institute of Technology. Accessed from

This Thesis is brought to you for free and open access by the RIT Libraries. For more information, please contact repository@rit.edu.

Harvesting a Sustainable Energy Future: Examining the effect of chemical composition on the electromechanical properties of polymer gel beads

By:

KAUSHIK AJIT KUDTARKAR

A thesis submitted in partial fulfillment of the
requirements for the degree of Master of
Science in Mechanical Engineering

Department of Mechanical Engineering
Kate Gleason College of Engineering

Rochester Institute of Technology
Rochester, New York
Submitted Dec 15, 2016

Harvesting a Sustainable Energy Future: Examining the effect of chemical composition on the electromechanical properties of polymer gel beads

By:

KAUSHIK AJIT KDUTARKAR

A thesis submitted in partial fulfillment of the
requirements for the degree of Master of
Science in Mechanical Engineering

Department of Mechanical Engineering
Kate Gleason College of Engineering

Approved by:

Dr. Michael Schertzer, Assistant Professor Date
Thesis Advisor, Department of Mechanical Engineering

Dr. Thomas Smith, Professor Date
Committee Member, Department of Chemistry & Material Science

Dr. Patricia Iglesias Victoria, Assistant Professor Date
Committee Member, Department of Mechanical Engineering

Dr. Agamemnon Crassidis, Graduate Director/Professor Date
Department Representative, Department of Mechanical Engineering

ABSTRACT

Clean energy is required to ensure global prosperity and economic growth. Increased industrialization is expected to increase energy demand by 50% by 2035. This will result in increased air pollution. Carbon dioxide emissions have been linked to global warming and other pollution related problems. These emissions can be reduced by recapturing the waste energy in the form of heat, vibration, and friction.

Common applications like transportation can lose as much as 78% of the energy they generate. Energy harvesters can be used to recapture energy lost through vibration, heat, etc. This recaptured energy will be reused and hence, we don't need to produce as much energy using traditional methods. Equipment with low power needs such as sensors can use this recaptured energy and hence, the need for external battery or energy source will be minimized.

This investigation will focus on the effects of chemical composition on the electromechanical properties of the gel beads.

Electrostatic energy harvesters consist of a proof mass that translates or deforms relative to an electrode array. When an electrical field is applied, this causes a change in capacitance which drives a current through a load resistance to generate power.

Ionic liquid polymers have been used in dye-sensitized solar cell energy harvesters. This work will examine whether the flexibility offered by Polymeric Ionic liquid (PIL) gel beads could be leveraged in other energy harvesting devices. To that end, this investigation works to examine the effect of the chemical composition of PIL beads on electromechanical properties. This will be accomplished using:

1. Microfluidic fabrication of conductive gel beads
2. Experimental testing of electromechanical properties of the beads
3. Metallization of IL resins and IL gel beads fabricated from the microreactor.
4. Optimization of those properties through a chemical understanding of the components required for use in electrostatic energy harvesters.

The IL beads are fabricated and tested for electromechanical properties to study the effects of the percentage of IL present in the chemical composition of the monomer solution. As the IL proportion was decreased, the gel beads had stronger physical properties such as stiffness but poor conductivity. To improve their conductivity, these IL gel beads were metallized with a gold salt solution. In metallization process, Cl⁻ ions of the IL were replaced by gold AuCl₄⁻ ions which were subsequently reduced to Au⁰ with the agency of Hydrazine. The metallization process resulted in significant increase in conductivity of the IL gel beads.

ACKNOWLEDGEMENTS

I would like to thank Dr. Michael Schertzer, Dr. Thomas Smith, Dr. Patricia Iglesias, Dr. Ron Aman and Dr. Agamemnon Crassidis for guiding me at every stage of my thesis proposal and inspiring me to work harder every day.

I would also like to thank Dr. Agamemnon Crassidis for providing me an academic scholarship for my thesis which inspired me to work even harder on my thesis work.

I would also like to thank the mechanical engineering department for providing me with all necessary components to build three experimental facilities and conduct experiments on those facilities.

TABLE OF CONTENTS

ABSTRACT.....	iii
ACKNOWLEDGEMENTS.....	v
TABLE OF CONTENTS.....	vi
LIST OF FIGURES	viii
LIST OF TABLES.....	x
NOMENCLATURE	xi
1.0 INTRODUCTION	1
1.1 The need for polymerized ionic liquid gel beads.....	1
2.0 RESEARCH QUESTION.....	22
3.0 EXPERIMENTAL METHODOLOGY	24
3.1 PIL Gel Bead Synthesis	24
3.2 Mechanical Characterization	31
3.3 Electrical Characterization	34
3.4 Metallization of ionic liquid beads	39
4.0 RESULTS AND DISCUSSION	47
4.1 Fabrication and testing of gel beads.....	47
4.1.1 Fabrication and testing of gel beads without ionic liquid	47
4.1.2 Polymer Gel Bead Synthesis and effects of chemical composition on the electromechanical properties of the beads	53
4.1.3 Fabrication and testing of gel beads with ionic liquid	63
4.2 Metallization process	70
4.2.1 Metallization and testing of IONAC A554 Cl- resin	70
4.2.2 Metallization and testing of IL gel beads	79

4.3 Metallization and testing of IL gel beads	89
5.0 CONCLUSIONS.....	94
5.1 Fabrication of non-IL gel beads using the microreactor	94
5.2 Fabrication of IL gel beads using the microreactor	94
5.3 Metallization of IL gel beads and resin.....	94
5.4 Contribution of my thesis.....	95
6.0 FUTURE WORK.....	96
REFERENCES	97

LIST OF FIGURES

Figure 1 Climate responses after peak concentration are reached due to thermal expansion [6]...	1
Figure 2 Types of energy and Transformation among them [55].....	4
Figure 3 Seebeck effect [13].....	5
Figure 4 Operation of Photovoltaic cell [15].....	5
Figure 5 Sensor replacement in future automobiles [21].....	6
Figure 6 Electromagnetic energy harvester [16].....	7
Figure 7 Schematic overview of a dye-sensitized solar cell [26].	9
Figure 8 Top (a) and side (b) views of an electrostatic energy harvester	12
Figure 9 Capacitance by position in the energy harvester	12
Figure 10 Accumulated output energy vs. time for mercury droplet, D = 1.2 mm, inclination angle $\theta = 20^\circ$ [41]	13
Figure 11 Mercury droplet with a diameter of 1.2 mm on 400 μm -wide electrodes under an optic [39].....	14
Figure 12 Photo of IL marble with a diameter of 1.2 mm on 500 μm -wide electrodes [25].....	15
Figure 13 Accumulated output energy vs. time for IL marble, D = 1.2 mm, inclination angle $\theta = 20^\circ$ [25]	16
Figure 14 Microfluidics-based vibrational energy harvester (VEH) [42]	16
Figure 15 Charge flow in micro fluidically based VEH (a) to (e) [28]	17
Figure 16 Comparison of power generation of the [EMIm][BF ₄] bridge	18
Figure 17 (a) The effective power versus vibrational amplitude for five typical IL with $f \frac{1}{4} 10 \text{ Hz}$ and $RL \frac{1}{4} 30 \text{ MU}$. (b) The effective power versus vibrational frequency f for five typical IL with $L = 0.35 \text{ mm}$ and $RL = 30 \text{ MU}$ [41].	19
Figure 18 Micro-reactor.....	25
Figure 19 Polymerized beads.....	27
Figure 20 Droplet formation	28
Figure 21 Sketch and image of the microreactor facility.....	28
Figure 22 Microreactor droplet generation [56]	29
Figure 23 Facility used for side and top view imaging of synthesized beads.....	30
Figure 24 Side View Bead Measurement	30
Figure 25 Stiffness measurement of a gel bead [54].....	31
Figure 26 Stiffness measurement facility	32
Figure 27 Conductivity experiment facility.....	34
Figure 28 Digital Indicator on sample holder	35
Figure 29 Contact area measurement experimental setup	38
Figure 30 1cm ² area plate.....	39
Figure 31 Front view of 1cm ² area plate	39
Figure 32 Gold salt 1/10th molar solution	41
Figure 33 IONAC A554 Cl ⁻ form resins beads	42
Figure 34 Resin beads in gold solution.....	42
Figure 35 Excess hydrazine being weighed.....	43

Figure 36 before adding Hydrazine (left) and after adding Hydrazine (Right)	43
Figure 37 Chemical reactions for gold metallization process of IONAC A554 Cl- form resins..	44
Figure 38 Chemical reactions for platinum metallization process of IONAC A554 Cl- form resins	45
Figure 39(a) Front view of bead & (b) Top view of bead	47
Figure 40 Images of the side and top view images from gel beads. Ratio of monomer to oil flow rate increases from (a) through (d).....	51
Figure 41 Graph for Bead aspect ratio (l/w) as a function of ratio of carrier and dispersed fluid flow rates (Q_c/Q_d). Circles represent aspect ratios of beads fabricated from Table 5	52
Figure 42 Graph of force vs deformation of bead A.....	55
Figure 43 Spring Constant of Beads A, B, C, D and E. di-vinyl monomer percentage of beads A, B, C, D and E is shown.	56
Figure 44 Graph of stiffness vs compression for bead A, C, and D	57
Figure 45 Graph of stiffness vs compression of beads B and E	57
Figure 46 Graph showing increase in contact area of a single bead A with increase in compression from 5% to 20%.....	58
Figure 47 Graph showing increase in Capacitance as beads A are compressed from 5% to 20%	59
Figure 48 Graph showing increase in dielectric constant as beads A are compressed from 5% to 20%	59
Figure 49 Graph of dielectric constant vs compression of beads A, B, C, D and E	60
Figure 50 Graph showing decrease in impedance as beads A are compressed from 5% to 20%.	61
Figure 51 Graph of resistivity vs compression of bead A	62
Figure 52 Graph of resistivity vs compression of beads A, B, C, D and E	62
Figure 53 Swollen gel beads with 45% IL.....	63
Figure 54 Comparison of force acting on the IL at 45% and on non-IL gel bead at compression ranging from 5% to 20% of the original size of the gel beads.....	64
Figure 55 Graph of stiffness of non-IL gel beads vs. IL gel beads w.r.t. compression ranging from 5% to 20%.....	65
Figure 56 Graph of dielectric constant of Non-IL gel beads vs IL gel beads.....	65
Figure 57 Graph of resistivity of non-IL gel beads vs IL gel beads	66
Figure 58 Graph of dielectric constant vs compression of IL gel beads.....	68
Figure 59 Graph of resistivity vs compression of IL beads	68
Figure 60 Graph of Force acting on IL gel beads when compressed from 5% to 20% of original size.	69
Figure 61 Graph of stiffness vs compression of IL beads	70
Figure 62 Graph of dielectric constant vs compression of resin, Platinum and gold metallized beads	72
Figure 63 Graph of resistivity vs compression of resin, platinum resins and gold metallized resin beads	73
Figure 64 Graph of stiffness vs compression of resin, platinum resins and gold metallized resin beads	73
Figure 65 Graph of force vs compression to calculate spring constant of resin, platinum coated resins and gold coated resins.....	74

Figure 66 Graph of Resistivity of platinum and metallization stages of gold beads vs compression	76
Figure 67 Graph of dielectric constant of platinum and metallization stages of gold beads vs compression	77
Figure 68 Graph of force vs compression to calculate spring constant of metallization stages of gold coated resins.....	77
Figure 69 Graph of Stiffness of platinum and gold beads vs compression	78
Figure 70 Ruptured beads with 45% IL composition	80
Figure 71 Ruptured beads with 10% IL composition	81
Figure 72 Heat treatment for metallization process	84
Figure 73 Metallized stage III IL beads	85
Figure 74 Graph of dielectric constant vs compression of metallized IL beads	86
Figure 75 Graph of resistivity vs compression of metallized IL beads	87
Figure 76 Graph of stiffness vs compression of metallized IL beads	87
Figure 77 Spring constant of IL gel beads and metallized IL gel beads	88
Figure 78 Dielectric constant at 20% compression.....	90
Figure 79 Resistivity of polymerized gel beads at 20% compression	91
Figure 80 Spring constant of IL beads at 20% compression	91

LIST OF TABLES

Table 1 Energy Harvesting Techniques	4
Table 2 Desired properties of PIL beads for different energy harvesters	21
Table 3 Monomer ingredients	27
Table 4 Updated monomer solution.....	49
Table 5 Effect of flow rates on formation of beads	50
Table 6 Composition of non-IL gel beads	54
Table 7 Monomer solution for gel bead with 45% IL	63
Table 8 Chemical Composition with varying proportions of IL monomers.....	67
Table 9 Metallization composition of IONAC A554 Cl ⁻ resin beads with platinum.....	71
Table 10 Metallization composition of IONAC A554 Cl ⁻ with Gold salt NaAuCl ₄ *2H ₂ O	71
Table 11 Metallization composition of IONAC A554 Cl ⁻ with 3 stages of Gold salt NaAuCl ₄ *2H ₂ O	75
Table 12 Metallization composition of IL beads with 45% IL monomer.....	79
Table 13 Metallization composition of IL beads with 10% IL monomer.....	80
Table 14 Metallization composition of IL beads with 5% IL monomer.....	82
Table 15 Metallization composition of IL beads with 2.5% IL monomer.....	83
Table 16 Suggested IL gel beads for energy harvesting applications.....	92

NOMENCLATURE

ϵ_0 = Dielectric Constant

C = capacitance

A = contact area,

d = distance between the plates

ρ = Resistivity

R = electrical resistance

l = dispersed phase plug length

w = width of the microchannel

k = emulsion co-efficient

Q_c = Continuous phase flow rate

Q_d = dispersed phase flow rate

Ca =capillary number

μ = viscosity of the carrier fluid

u = velocity of the carrier fluid

γ = interfacial tension

n = number of moles

x = Dry Weight

M = Molecular weight

y = Number of grams of beads

Z = impedance and

θ = phase angle

1.0 INTRODUCTION

1.1 The need for polymerized ionic liquid gel beads:

Energy consumption is expected to increase by 50% by 2035 due to increasing industrialization and commercialization [1]. Increased energy consumption increases industrialization which eventually leads to pollution in air, land or water pollution [2]. Measures must be taken to create clean energy to secure a healthy environment without hampering global development [3]. Worsening air pollution has also been directly linked to increased mortality [4] as according to a research there are approximately 1500 premature respiratory deaths [5].

Current research suggests that there will be an increase in carbon dioxide emissions content in the near future [1], [6]. These studies suggest that an increase in carbon dioxide concentration from 385 parts per million (current) to 600 parts per million, would lead to a series of changes in climate including rainfall reductions, higher atmospheric temperature and unstoppable sea rise as

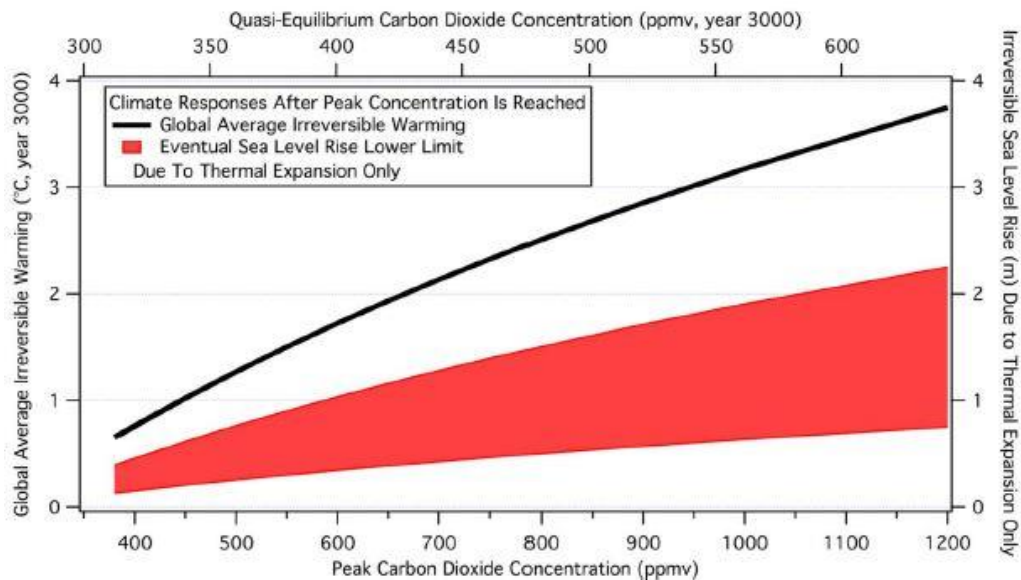


Figure 1 Climate responses after peak concentration are reached due to thermal expansion [6]

shown in Figure 1 [6]. These predictions highlight the need for a global shift toward the production of clean, affordable energy.

By recapturing lost energy in various industrial or commercial processes green energy can be generated. Reducing the energy wasted in various industrial and commercial processes will lead to a reduction in carbon emissions [7]. Energy harvesting devices seek to reduce emission by reclaiming energy that would normally be wasted in the form of heat, vibration or friction. While the energy reclaimed in these devices is often small, it can be used to improve process efficiency or power wireless sensors and wearable devices [3].

Various types of sensors are used in electronic components as they provide real-time information with minimal energy requirements [8]. These small low-powered sensors are used for many applications including pressure sensors, temperature sensors, etc. where they are either located on a moving component or situated on a fixed structure or sometimes within a human body for medical purposes. In these applications, wireless sensors are often preferred because they require reduced set-up time and long term maintenance. For example, the Guemdang Bridge in South Korea was equipped with 14 wireless sensor units for which a total cost of \$1,400. An equivalent wired sensors array could have cost \$10,000-15,000 [9]. The total setup required only an hour. Use of wireless electronics reduces the number of wires which will save complexity and materials. For example, if we reduce wires in various applications a considerable amount of copper can be saved in countries like United States, Germany, Japan, etc. every year [10]. It has also been observed that the use of GPS circuits is increasing due to increased flexibility in the mobile applications. Due to which there is an increased need for a power source which would supply continuous energy to these wireless devices [11].

While wireless sensors provide many benefits, they need to be powered by a battery, which

needs to be replaced at periodic intervals. These batteries may pose harmful effects on the environment and hence must be treated carefully. Batteries have various harmful materials including mercury, cadmium, etc. When these batteries are disposed of, these harmful materials are mixed in soil and water, which eventually will be consumed by humans or animals. Various health problems such as nausea, excessive salivation, abdominal pain, liver and kidney damage, skin irritation, headaches, asthma, nervousness, decreased IQ in children and sometimes even cancer can result from exposure to such metals for a sufficient period of time [9]. Energy harvesters provide a means to satisfy the increased need for a power source to continuously supply energy to these wireless devices as it stores energy, which would increase the lifespan of the battery. It thus creates a need for the harvesting energy which would be able to generate energy to increase the efficiency of any equipment and improve the ability to set up any process with fewer wires or less with tedious complexity.

According to Newton's first law, "Energy can neither be created nor destroyed, it can be only converted from one form into another." Energy harvesters make use of this principle to scavenge energy that would normally be wasted and convert it into usable electrical energy. Various types of energy harvesting processes have been developed to reclaim different types of waste energy are categorized and shown in Table 1 below [9].

Table 1 Energy Harvesting Techniques

Source of energy	Effects employed
1. Light	Photoelectric
2. Temperature Difference	Thermoelectric (Peltier and Seebeck) effects
3. Electromagnetic Radiation	Electromagnetic Induction
4. Vibration	Piezoelectric, Electrodynamic & Electrostatic

A wide range of energy harvesting technologies has been developed to convert various types of energy into electric energy (Table 1). These devices can be employed in a variety of industrial processes to improve efficiency. Methodologies for these transformations are shown in Figure 2.

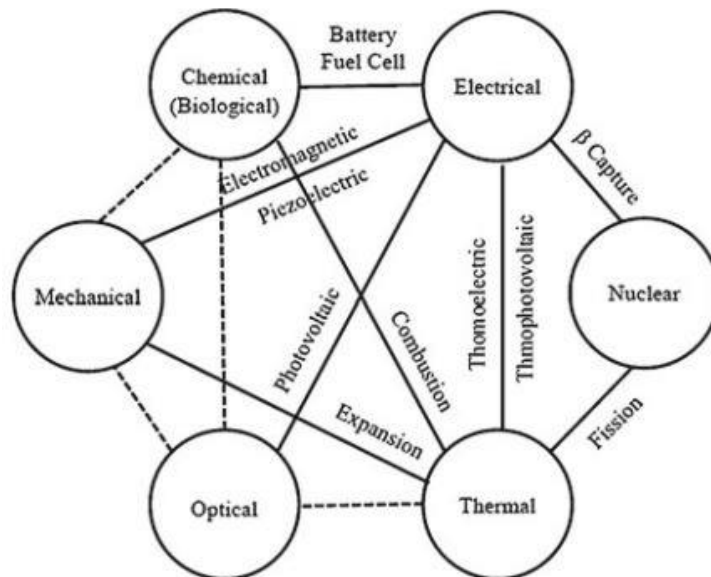


Figure 2 Types of energy and Transformation among them [55]

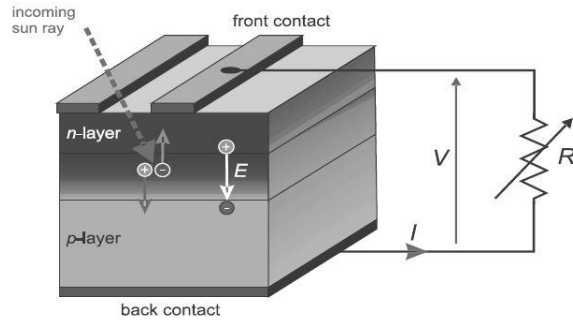


Figure 4 Operation of Photovoltaic cell [15]

Optical energy can be converted into electrical energy using photovoltaic cells. Photovoltaic cells have the capability to convert radiation into electrical energy using semiconductor diode. These devices consist of two layers or regions separated by an electric field barrier as shown in Figure 4. The p-layer consists of holes while n-layer consists electrons. When light falls on the cell, electrons diffuse into p-layer and holes diffuse into n-layer are generated, this causes an increase in minority charges which then pass through the electric field barrier. If a resistor is applied across the circuit then current flows through it and electricity is generated [12].

Thermoelectric energy can be converted into electric energy using the Seebeck effect. The

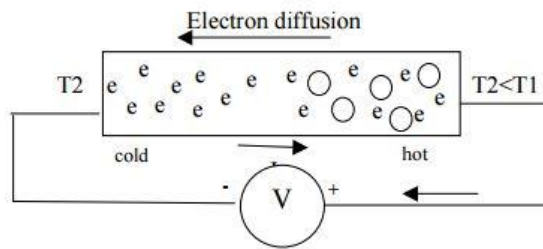


Figure 3 Seebeck effect [13]

Seebeck effect is produced when an electromotive force in a closed loop connected by two dissimilar materials at two different temperatures and due to which electric current is generated as shown in Figure 3 [13], [14].

Many energy harvesting technologies seek to convert vibrational energy into electrical energy. Vibrational energy can be converted into electrical energy using piezoelectric, electromagnetic and capacitive transducers [15]–[20]. Piezoelectric transducers are attractive as the electromechanical coupling is high and also no input energy is required for operation [21]. For



Figure 5 Sensor replacement in future automobiles [21]

example, for automobiles, piezoelectric material technology can be used to scavenge vibrational energy from various sources [21].

As shown in Figure 5 piezoelectric material technology can be used to absorb vibrations from various sources and provide energy to power the sensors which provide feedback to the operating [21]. Since these sensors are self-powered, they do not require wiring or the need for replacement batteries.

Electromagnetic transducers can be used for harvesting vibrational energy. These devices consist of a mass spring damper system, a magnet, and a coil. The basic model of an electromagnetic transducer system is shown in Figure 6. Here, frame vibrations are transferred to the magnet (with mass m) which is displaced from its original position. Due to change in magnetic flux in the coil, an electrical potential is generated in the coil. If an electrical load is connected across the coil, current will flow and electrical power is generated [16].

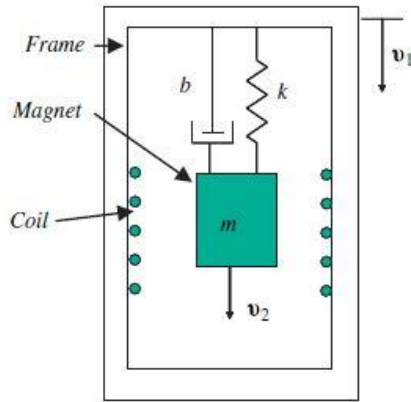


Figure 6 Electromagnetic energy harvester [16]

While piezoelectric and electrodynamic energy harvesters can be used to power electronic devices, they have drawbacks which may limit these energy harvesters to a certain application. The cost of fabrication of piezoelectric crystals is high [22]. While for electromagnetic transducers, due to non-contact nature of transducer, the complexity and preparation time is increased to perform inspections [23]. These two types of energy harvesters work well at resonance, but they do not give same results over a wider range of frequencies [24].

Ionic liquids (IL) are another option for the fluidic proof mass. IL's are non-volatile, highly conductive, non-flammable, etc. solvents composed of cations and anions having low melting points [25]. Ionic Liquids can be used under various operating conditions due to their favorable properties. Ionic liquids show different properties depending upon their composition as their properties can be altered by changing the anions or cations of the IL. For example, Ethyl methyl Imidazolium chloride is solid at room temperature while ethyl methyl Imidal trifloral sulphanal emide is liquid at room temperature. Also, trifluoromethane sulfonamide TFSI and Triflate are thermally stable, while IL with chloride are not thermally stable. Various properties of ionic liquids are: Ionic liquids are more viscous than molecular solvents, and vary over a range of 10 to 1000 cP at room temperature. The viscosity of IL's is difficult to find as they do not follow the ordinary Arrhenius behavior [26]. The surface tension of IL's is less well explored and understood. It is an

important factor for mass and heat transfer at an interface [27]. Surface tension of ionic liquids at room temperature are lower than that of water (72.7 N m^{-1} at $20 \text{ }^\circ\text{C}$) but higher than n-alkane (16.0 N m^{-1} for pentane to 25.6 N m^{-1} for dodecane, all at $20 \text{ }^\circ\text{C}$) Also, as the length of the alkyl chain in ionic liquid increases it is observed that the surface tension decreases at room temperature [28]. Surface tension is an important factor if there is translating motion required for electrostatic energy harvesters. Also, surface tension is an important characteristic to calculate the emulsion stability criteria, which helps us to know the flow rate of liquids in the microreactor. In terms of toxicity, IL's are less toxic than various organic solvents [26]. Also as compared to mercury ionic liquids are non-volatile [29]. But ionic liquids are corrosive on certain surfaces with certain chemical compositions [30]. So, corrosion might be reduced if polymerized ionic liquid gel beads are used instead of it in liquid form on the electrostatic energy harvester.

A dye-sensitized solar cell (DSSC) is a relatively new kind of low-cost solar cell that shows great promise because of its low-cost materials and its simplicity [31]. A schematic overview of a dye-sensitized solar cell is shown in Figure 7. The anode is transparent, like glass, so that sunlight can be absorbed by the inner parts of the solar cell. Between the anode and the cathode is a mesh of titanium dioxide nanoparticles that act like a roadway for the electrons coursing through the cell. The TiO_2 nanoparticles are coated with a light absorbing dye that converts photons into electrons. An electrolyte (usually iodide) fills the spaces between the TiO_2 nanoparticles and helps transfer electrons from the cathode to the dye molecules. After the dye releases an electron, it needs another electron to replace the one it lost. On the other end of the cell is the cathode, typically a film of graphite or platinum. The anode sends electrons from the solar cell through a wire to whatever the cell is powering; then the electrons loop back to the cathode [31]–[33].

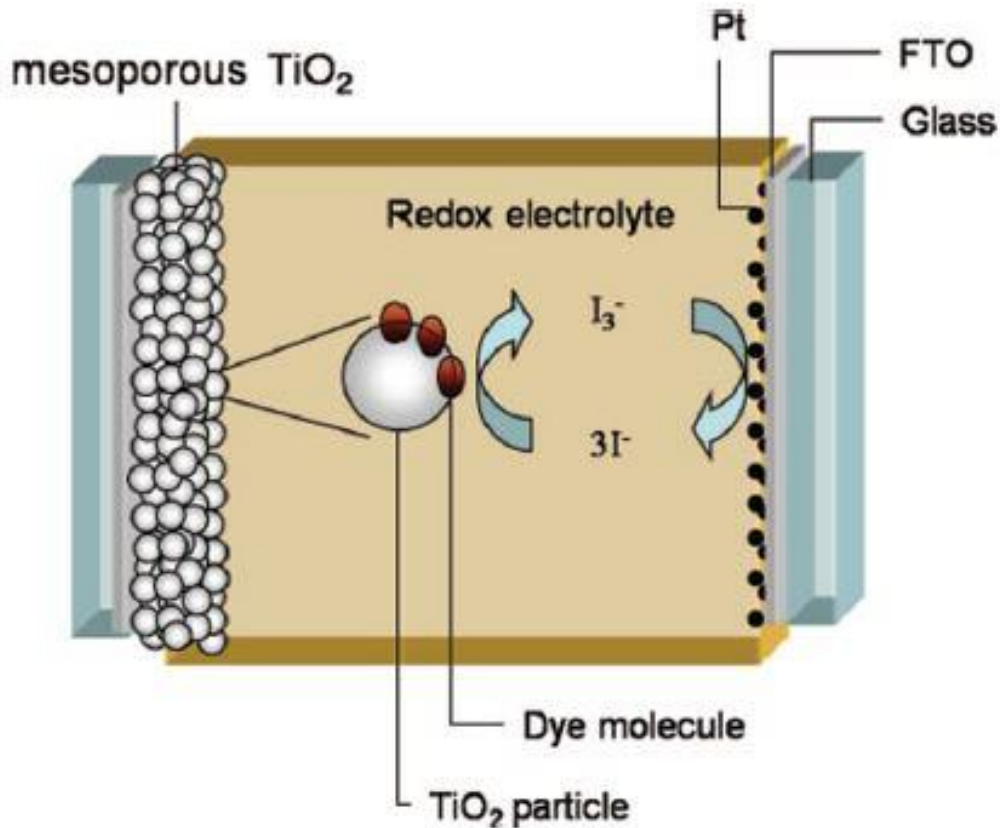


Figure 7 Schematic overview of a dye-sensitized solar cell [26].

For anything to generate electricity, it needs to generate an electric current. In a DSSC, this means that electrons need to be flowing from one end of the cell to the other: in this case, from the cathode to the anode. The electrons travel through the electrolyte (iodide) and the TiO₂ nanoparticles to create an electric current [31]. In a DSSC, TiO₂ nanoparticles are normally used as conductors because of their unique ability to be welded together and form one huge network for the electrons to travel through [34]. Also, TiO₂ nanoparticles are transparent. The electrons originate from the dye molecules coating the TiO₂ nanoparticles when they are hit by photons.

Different color dyes can absorb different wavelengths of light, which in turn carry different amounts of energy [35]. The dye nanoparticles are covered all over except where the nanoparticles are connected to other nanoparticles. The spaces in between the TiO₂ nanoparticles are filled with an electrolyte (iodide), which transfers electrons from the cathode to the dye. It may appear that

the electrons would have no trouble traveling from one end of DSSC to the other, but, it can take quite a lot of work for an electron to get from the cathode of the DSSC to the anode [31]. The electrons travel randomly from one TiO₂ nanoparticle to another until they reach the anode. The size and density of the TiO₂ nanoparticles can affect the journey of an electron. The smaller the nanoparticle size, the more defects in the nanoparticle, which results in electron loss to the iodide solution [36]. However, the smaller the nanoparticles for a fixed volume, the more surface area you can coat with dye. A lower density of nanoparticles will have the same result, but that also means electrons have fewer paths to take to the anode [37]. Finding the optimal size and density of TiO₂ nanoparticles one of the challenges in building a DSSC, creating the maximum amount of surface area while also creating the maximum number of safe pathways for the electrons. When a photon strikes a dye molecule, the energy of the photon is absorbed by the dye molecule. The dye molecule enters an excited state and emits an electron. The emitted electron travels through the TiO₂ nanoparticles until it reaches the anode or it is lost to the iodide solution because of defects in the TiO₂ nanoparticles [31]. Because the dye molecule just emitted one of its own electrons, it will start to decompose, unless it receives another electron to replace the one it lost. In this state, the dye molecule cannot emit any more electrons. The dye-coated TiO₂ molecules are hence, immersed in a solution of iodide; the iodide is able to replace the electrons lost by the dye molecules. The iodide molecules in the iodide solution can give up an electron to a dye molecule that needs it. When this occurs the iodide molecules are oxidized into triiodide, which will float around until it comes in contact with the cathode [31], [33]. The triiodide recovers its missing electrons from the cathode, which reduces triiodide back to three iodide molecules. When all these processes work together, an electric current is generated. The electrons emitted from the dye flow from the anode to whatever is powered by DSSC, and then flow back into the cell through the

cathode. Then, the electrons from the cathode restore the electrons needed by the iodide, which restores the electrons needed by the dye molecules, and the whole process starts over again.

The liquid electrolyte in DSSC has some disadvantages such as leaking, sealing, flammability issues, shape flexibility and electrochemical stability. Liquid electrolytes also stood challenges for integration of large area modules, photo-degradation of attached dyes and corrosion of counter electrode, which eventually led to lower performance and lifetime of the photovoltaic cell. So to avoid this, instead of liquid electrolyte, a polymer gel based electrolyte can be used in DSSC [33]. In DSSC polymerized IL BEMA: PEGMA (70:30)–NaI/I₂ gave output efficiency of 5.35% while liquid electrolyte used Poly Imidazolium ion based IL, PEO-co-BImI/I₂–SiO₂ gave output efficiency of 5.25%. IL's have been used in DSSC and results have shown an increase in efficiency and higher stability, non-volatile, non-flammable and high ionic conductivity [38]. The IL polymer was fabricated using the swelling technique. Good chemical stability was observed as the ionic conductivity did not vary over storage time. Raised cell durability, photocurrent, electron lifetimes and reducing the photo-corrosion effects of counter electrode by iodine radical was observed [33]. Due to advantages of using polymeric based IL electrolyte in DSSC, we can observe that polymerized ionic liquid can also be used various other energy harvesting applications. Polymerized IL can be used in various energy harvesting applications such as electrostatic energy harvester and vibrational based energy harvester. These energy harvesting applications are discussed below.

Fluidic energy harvesters have also been used to scavenge energy from vibrations. These

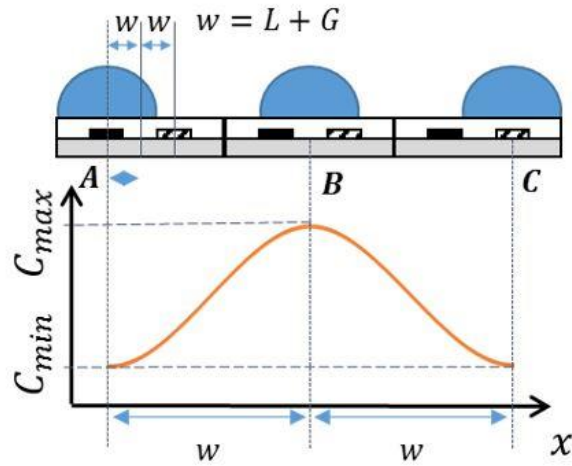


Figure 9 Capacitance by position in the energy harvester

devices operate on electrostatic effects which occur when a conductive droplet translates through

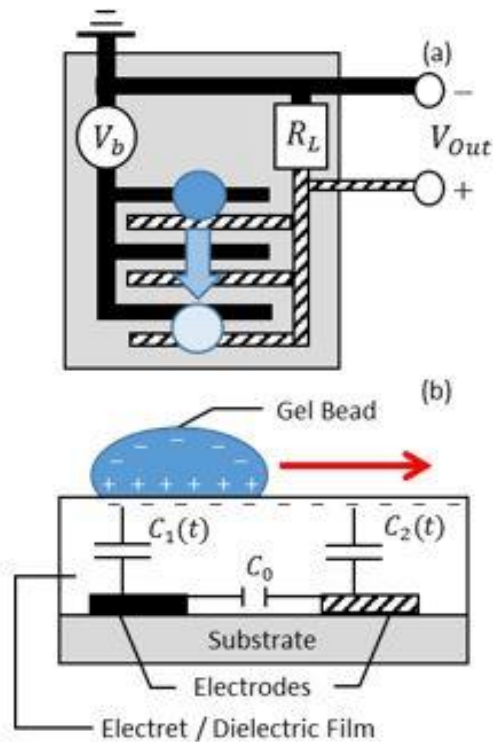


Figure 8 Top (a) and side (b) views of an electrostatic energy harvester

an electric field [39]. In fluidic energy harvesters, a droplet translates through an electric field as shown in Figure 8. Fluidic energy harvesters recapture mechanical energy by making droplets translate [39], [40] or deform[41], [42] relative to an electrode array. The capacitance between the

electrodes changes with droplet position. When capacitance varies in the electrode array a transient voltage is developed. The bias between electrodes can be achieved by applying an external voltage, or by embedding charge in a dielectric layer to create an electret material. Adopting the use of an electret material eliminates the need to power the energy harvester.

Due to the potential for miniaturization and application in industrial and commercial operations electrostatic energy harvesters have been considered as a potential alternative for harvesting energy [39]. As shown in Figure 9, electrostatic energy harvesters consist of a conductive droplet on a dielectric coated electrode array. In this case, the electrode array consists of an interdigital electrode (IDE). An interdigital electrode is a geometric structure consisting a wide variety of sensor and transducer designs depending upon the type of applications [43]. Various fluids have been used as proof masses including mercury and ionic liquids [39], [40]. As shown in Figure 9, the capacitance between opposite halves of the IDE as the mass passes over the array the capacitance changes. As the capacitance changes between the electrodes, a current pass through a load between opposite sides of the IDE. This results in a transient output voltage across the load [44].

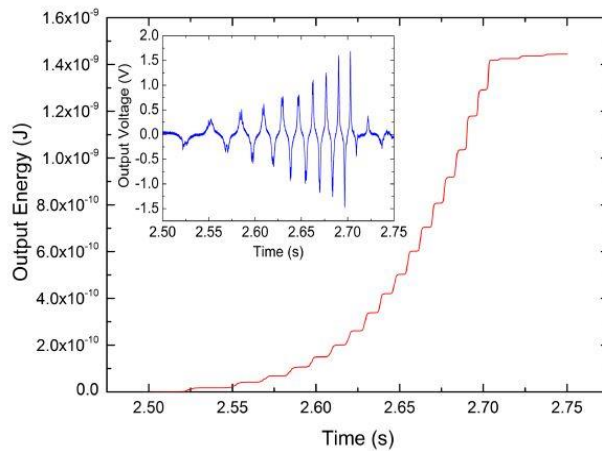


Figure 10 Accumulated output energy vs. time for mercury droplet, $D = 1.2 \text{ mm}$, inclination angle $\vartheta = 20^\circ$ [41]

Selection of liquid media in electrostatic energy harvesters is important. Various aspects are taken into consideration for the liquid droplet like the ability to evaporate, toxicity and corrosiveness to the dielectric layer. Mercury is attractive due to its high conductivity, low evaporation rate and low vapor pressure and hence can be suited for future hermetic encapsulation with vacuum in the enclosure [39], [44]. Mercury has been tested for an electrostatic energy harvester, is shown in Figure 11.

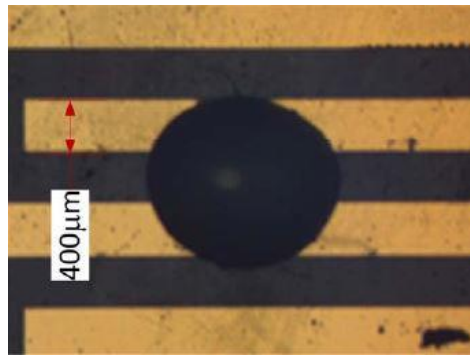


Figure 11 Mercury droplet with a diameter of 1.2 mm on 400 µm-wide electrodes under an optic [39]

The instantaneous output obtained using mercury droplet of 1.2 mm diameter is $0.18\mu\text{W}$ and mean output for one cycle is $7.78\mu\text{W}$, shown in Figure 10. Since mercury is neurotoxic in nature, it makes it an impractical solution [39]. While water is nontoxic, but its relatively low conductivity and high evaporation rates result in low power output that degraded with time [45]. Ionic liquids (IL) are another option for the fluidic proof mass. IL's are green and environment-friendly solvents composed of cations and anions having low melting points [25]. Ionic Liquids can be used under various operating conditions due to their favorable properties. Ionic liquids show different properties depending upon their composition.

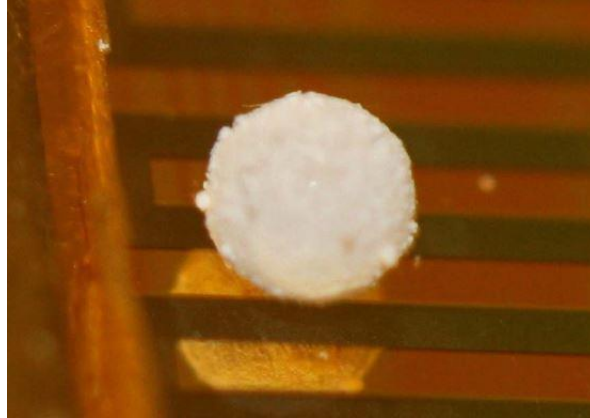


Figure 12 Photo of IL marble with a diameter of 1.2 mm on 500 μm -wide electrodes [25]

Ionic liquid marbles have been tested on an electrostatic energy harvester by Yang 2014. Ionic liquids are salts of an organic cation (e.g. ammonium, imidazolium or phosphonium), which have good electrical conductivity, thermal stability and solvation capability [39], [41]. Hence, these features they can be used for a broad range of organic, inorganic and biological molecules. Due to high ionic conductivity, ionic liquids gel beads can be used for harvesting energy [46], [47]. The IL marble consisted of an ionic liquid coated with PTFE powder, 1 micron in particle diameter [39]. The IL marble is shown in Figure 12. But PTFE powder on the marble's surface tends to aggregate in small clusters which resulted in increasing the gap between the IDE's and the IL present in the marble and hence resulted in a reduction in conductivity of the IL marble. The output performance of the IL marble was 2 orders by magnitude less than mercury, is shown in Figure 13 [39].

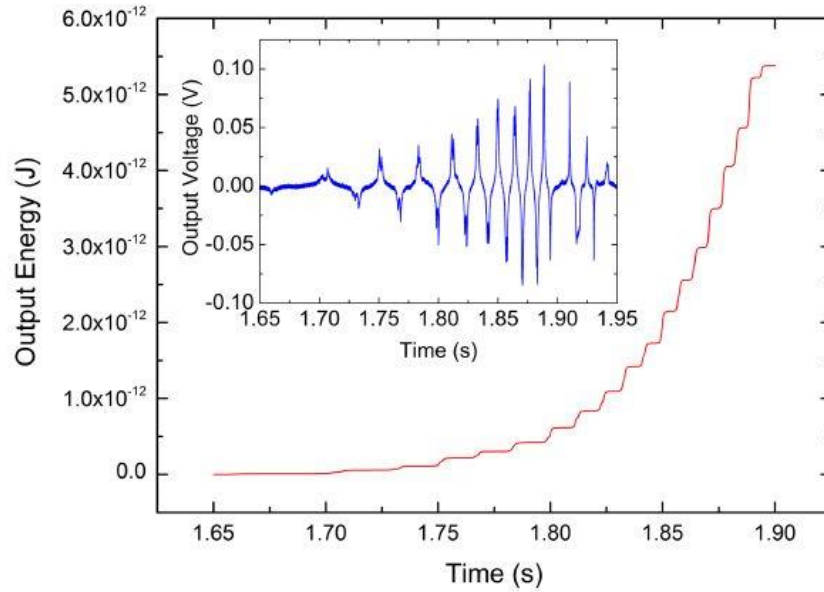


Figure 13 Accumulated output energy vs. time for IL marble, $D = 1.2 \text{ mm}$, inclination angle $\vartheta = 20^\circ$ [25]

Since, IL marble have low conductivity due to PTFE coating, polymerized IL's can replace the PTFE coating, probably increasing the conductivity of the electrostatic energy harvester. Also, ionic liquids are corrosive on certain surfaces with certain chemical compositions [30]. So, corrosion might be reduced if polymerized ionic liquid gel beads are used instead of it in liquid form. Hence, we might be able to use IL gel beads in an electrostatic energy harvester resulting in increasing its output than IL marble and making the energy harvester safer to use as compared to mercury.

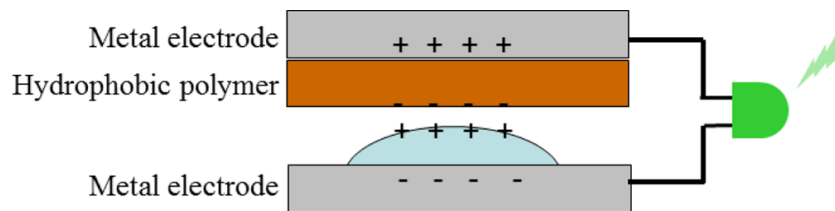


Figure 14 Microfluidics-based vibrational energy harvester (VEH) [42]

Apart from electrostatic energy harvester, polymerized IL gel beads could be used in microfluidics-based vibrational energy harvester (VEH). VEH works on a principle as shown in Figure 14, which consists of a liquid droplet resting on a metal electrode, causes electrification if

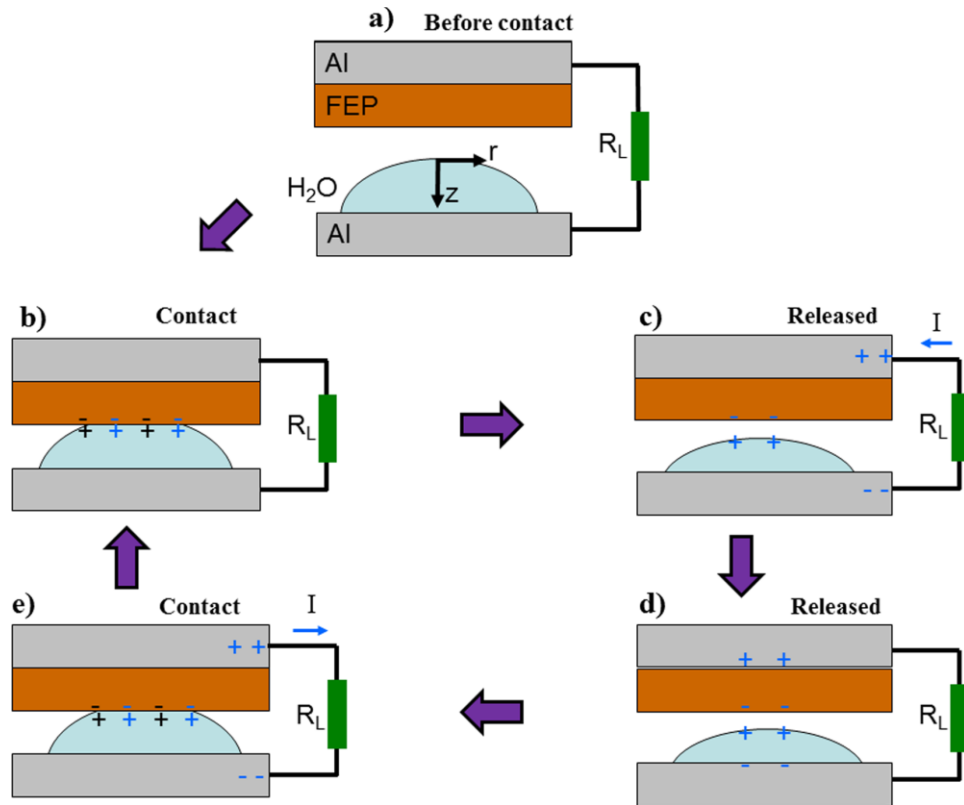


Figure 15 Charge flow in micro fluidically based VEH (a) to (e) [28]

brought periodically in contact with hydrophobic polymer film [42]. In this type of energy harvester (Helseth 2015), fluorinated ethylene propylene FEP was used as the hydrophobic polymer and it was observed that as the volume of the water droplet increased, the maximum current increased, which is in accordance with the power law. The power law is a functional relationship between two quantities, where a relative change in one quantity results in a proportional relative change in the other quantity. Charge flow in such type of VEH is shown in Figure 15. As shown in Figure 15b, when the water droplet is in contact with FEP, a negative charge is developed on the polymer surface and positive charge on water surface [42].

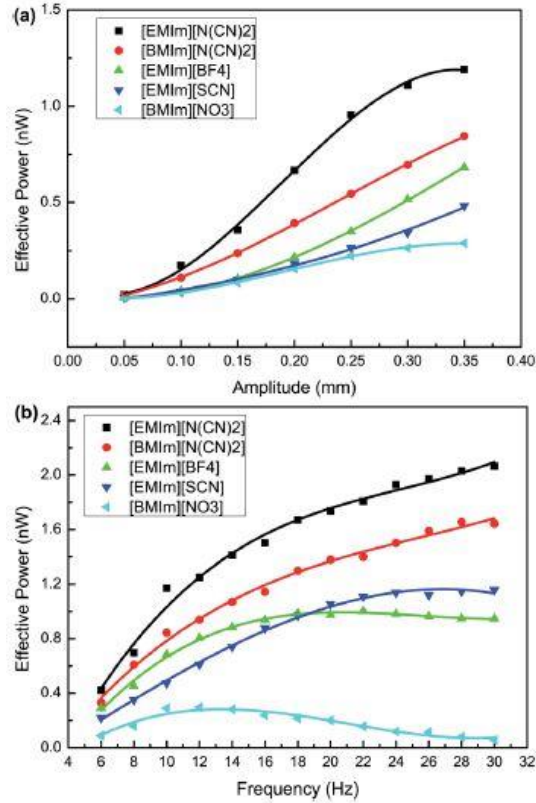


Figure 16 Comparison of power generation of the [EMIm][BF4] bridge

When the contact between the water droplet and FEP occurs, electrons started to flow from the FEP into the metal surface because of the charges of the electric double layer at the FEP-water contact surface. Electron flow out from the metal surface in contact with the water droplet, thereby neutralizing the net charge [42]. This energy harvester gave an average power of $0.7 \mu\text{W}$ and peak power of $5 \mu\text{W}$ at 5 Hz frequency [42]. Since water evaporates under normal conditions in the air, the output of this energy harvester will decrease with time. Also, this water-based system will not work at higher or lower temperature [41]. Room temperature ionic liquids can be used instead of water as they can be operated at high or low temperatures, they are electrochemically stable, non-toxic and most importantly, properties of IL's can be greatly regulated as per applications by changing the ions [41]. Five imidazolium IL, [EMIm][N(CN)2], [BMIm][N(CN)2], [EMIm][BF4], [EMIm][SCN] and [BMIm][NO3] were tested in Kong 2014 on a microfluidically

based VEH. The effective power of each IL versus vibrational amplitude and against frequency is shown in Figure 16 [41]. According to Figure 16, the output power follows the order [EMIm][N(CN)2] > [BMIm][N(CN)2] > [EMIm][BF4] > [EMIm][SCN] > [BMIm][NO3]. It is mainly because of two reasons namely differences in the charge densities near the interface

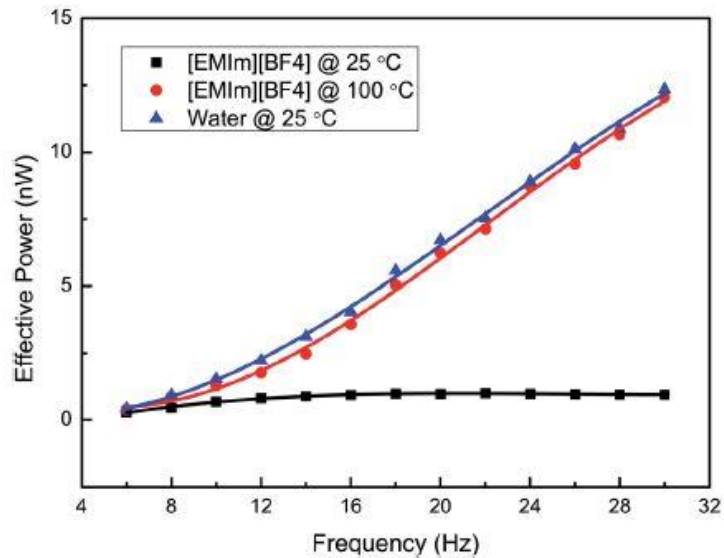


Figure 17 (a) The effective power versus vibrational amplitude for five typical IL with $f \approx 10$ Hz and $RL \approx 30$ MU. (b) The effective power versus vibrational frequency f for five typical IL with $L = 0.35$ mm and $RL = 30$ MU [41].

between top plates and IL, and due to different viscosities of IL [41]. In Kong 2014, it has been observed that for IL's with lower viscosity provided higher output power at higher frequencies. It can be observed that output power of IL is lower than water at 25°C and it is shown in Figure 17, mostly because of low viscosity of water (1cP). As shown in Figure 17, water based VEH generated more power than [EMIm][BF4] bridge at 25°C, especially at higher frequencies. But when the temperature is increased to 100°C, the output of [EMIm][BF4] increased significantly, when compared to that at 25°C [41]. Hence, IL's can be used in VEH for higher temperatures and they also don't require any air tight containers as water based VEH requires.

Although IL's can be used in VEH, but they have few drawbacks. IL's once compressed, cannot be brought back to their initial shape due to wettability and because of high viscosity, IL

cannot keep up the motion of the shaker [48]. To avoid this drawback, polymerized IL gel beads can be used, as they have the ability to regain their initial shape after decompression. Also, IL gel beads can be easily regulated so that they would keep up with the motion of the shaker. Properties of IL gel beads can be modified as per requirement of the application, resulting in a better controlled and efficient microfluidics-based VEH.

Polymerized ionic liquid gel beads can be used for various solid state electronic applications such as lithium batteries, actuators, field-effect transistors, light emitting electrochemical cells, and electrochromic devices [49].

Literature survey shows that for PIL gel beads can be used for various applications. But, for every application, the properties of the PIL gel beads had to be varied as per required application. The desired properties for each application are shown in Table 2. As shown in Table 2, every application requires PIL gel beads with different electromechanical properties. For any energy harvesters, PIL beads should have a high dielectric constant in order to increase the capacitance of the system, and low resistivity for higher conductivity. But, properties such as stiffness and rolling resistance should be altered as per type of energy harvesters. For electrostatic energy harvester, PIL should roll smoothly on the dielectric plate which can be attained is PIL beads have low rolling resistance and low stiffness. While for VEH and DSSC, the PIL bead's position will be fixed and hence PIL beads should have low stiffness and high resistance.

Table 2 Desired properties of PIL beads for different energy harvesters

	Electrostatic Energy Harvester	Vibrational based Energy Harvester
Dielectric Constant	High [1.007(Hg)][50]	High [1.007(Hg)][50]
Resistivity	Low [9.8×10^{-7} ohm m (Hg)] [51]	Low [9.8×10^{-7} ohm m (Hg)] [51]
Rolling Resistance (Data N/A)	Low	High
Stiffness	High	Low

Hence, altering properties of these PIL beads can be achieved by, (i) micro reactor synthesis and (ii) metallization of IL beads, in latter sections. The goal of this work is to determine the effect of (i) chemical composition and (ii) metallization on the electro-mechanical properties. To do so this investigation has created a systematic method to fabricate polymer gel beads and characterize their electro-mechanical properties.

2.0 RESEARCH QUESTION

How does the chemical composition of an ionic liquid gel bead affect its electro-mechanical properties?

This proposed investigation will answer the research question by examining the effect of chemical composition on the electromechanical properties of polymerized ionic liquid (PIL) gel beads. PIL beads will be synthesized using the methodology presented in Rahman 2013 [46]. Characteristics of interest include conductivity, dielectric coefficient, and elasticity (stiffness).

The maximum performance of the electrostatic energy harvester presented in Yang et al. 2014 [39] occurred with a Mercury droplet. While mercury is attractive due to its high conductivity and low evaporation rates, its high level of toxicity makes it a poor choice for practical applications. Ionic liquids may provide an alternative option that can be fairly conductive with little or no toxicity. This is in part due to dielectric layer thickness and due to PTFE coating on the IL which erodes and results in changes in shape. This drawback can be avoided using polymerized ionic liquid gel beads as they won't require PTFE coating hence reducing dielectric layer thickness and increasing conductivity. Also, for the vibrational based energy harvesters, with small molecular ionic liquids and aqueous solutions thereof the size of the IL droplet decreased due often fragmented to instability and decreased in size due to evaporation [8]. This drawback can be avoided by using elastomeric PIL gel beads, as due to elasticity property of PIL gel beads they that will retain their original shape due to vibrations when vibrated. Dye-sensitized solar cells also used IL in the electrolyte solution, which increased the output efficiencies of the solar cells [52]. Drawbacks of DSSC such as leakages of electrolytes can be eliminated using PIL gel beads.

Understanding how chemical composition affects EM properties would give engineers the ability to enhance performance for a particular application by engineering a bead with particular properties. In particular, works in the literature discuss two methods of changing the properties of PIL (i) chemical composition (ii) metallization. As such, there is a need to gain a deeper understanding of the effects

This investigation will develop and implement a systematic experimental method to rapidly synthesize and characterize the electro-mechanical properties of PILs. Beads will be synthesizing in a microreactor as described by Rahman 2013 [46]. Electrical characterization will be performed by commissioning conductivity measurement facility which would enable us to characterize properties of PIL beads such as dielectric constant, resistivity, capacitance, etc. Mechanical characterization will be performed by commissioning conductivity measurement facility which would enable us to characterize stiffness of PIL beads. The understanding provided here will provide insight into strategies that can be employed to optimize the electromechanical properties of PIL proof masses for a variety of applications including Electrostatic energy harvester, VEH, DSSC, etc. Methodologies for testing these properties will be similar to those presented in [53], [54].

This work makes the following contributions:

- Commissioning of a facility for microfluidic bead synthesis and examination of the effect of chemical composition on the stability and shape of beads generated in the facility.
- Development of a methodology for testing electrical properties.
- Commissioning of a facility for testing mechanical properties.
- Examination of the effect of the chemical composition of PIL beads on electromechanical properties.

3.0 EXPERIMENTAL METHODOLOGY

This investigation seeks to determine how the chemical composition of an ionic liquid gel bead affects its electro-mechanical properties. This question will be answered by performing a series of well-controlled experiments to:

1. Synthesize PILs with various chemical compositions in a microfluidic reactor similar to Rahman 2013 [46] and characterize the effects of chemical composition on the shape of the gel beads;
2. Characterize the mechanical properties of PIL gel beads;
3. Characterize the electrical properties of PIL gel beads;
4. Metalize microfluidically synthesized PIL gel beads and characterize their electro-mechanical properties.

A detailed description of the experimental methodology used to perform these tasks is provided in this chapter.

3.1 PIL Gel Bead Synthesis

The microfluidic gel bead synthesis used in this investigation is based on the method published by Rahman 2013 [46]. This process requires the generation of monodispersed droplets in a continuous carrier fluid. The droplets are polymerized through exposure to UV light. This process was performed in the facility shown in Figure 18.

The microfluidic reactor is responsible for creating monodispersed droplets of the monomer solution in the silicon oil. The reactor consists of a monomer solution, silicone oil, a microfluidic reactor syringes and syringe pumps, PEEK cross section, PFA tubing, and a UV lamp.

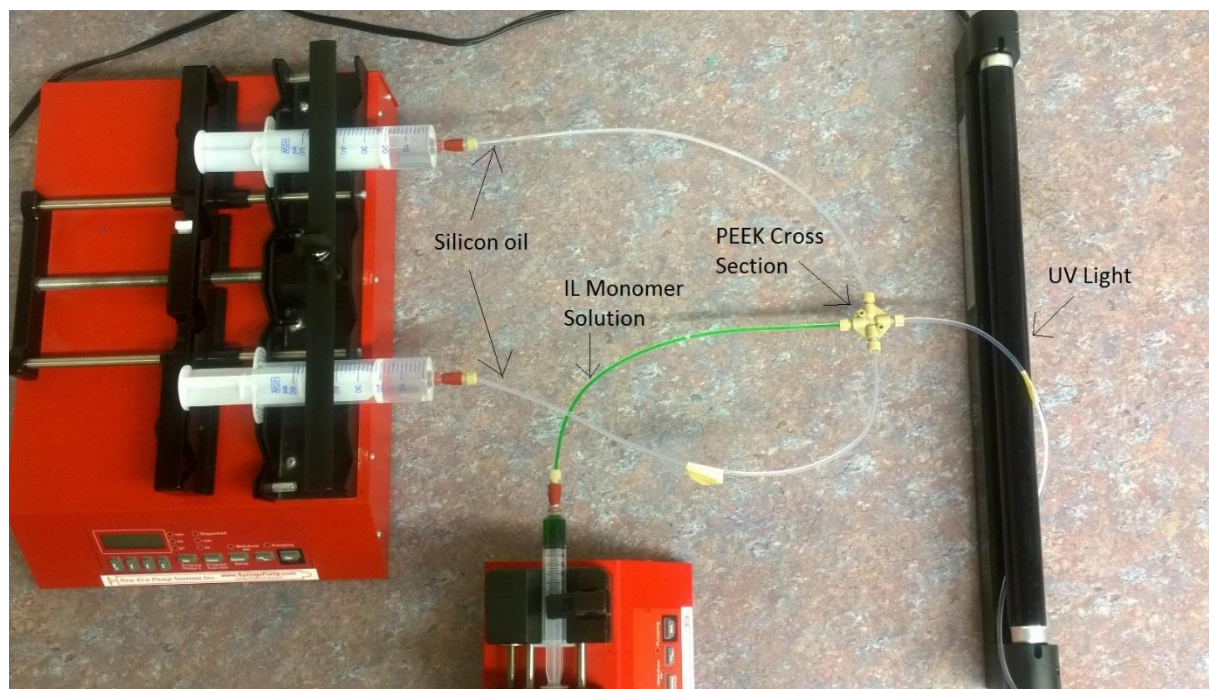


Figure 18 Micro-reactor

Detail specification of the components required for fabricating the micro-reactor are as following:

1. The ultimate monomer mixture was composed of a polymerizable ionic liquid ([2-(Methacryloyloxy) ethyl] trimethylammonium chloride), a difunctional acrylic monomer PEGDA (Polyethylene glycol diacrylate, average M_n 700, Sigma-Aldrich) that serves as the crosslinker, a photoinitiator (Darocur 1173), and water. PEGDA is a water miscible cross-linker which is extensively used in polymeric microgel synthesis [46]. PEGDA also helps in rapid polymerization and to suppress the phase separation of water-immiscible photoinitiator [46]. Deionized water was used as the base of the dispersed phase in the reactor. It is selected because it is immiscible in the oil carrier fluid.
2. Silicone Oil: Silicone oil with a viscosity of 10cst is used for this process. It is used as it is an immiscible carrier fluid, which can be used to carry the monomer fluid throughout the process which would eventually lead polymerized ionic liquid gel beads.

3. Syringes and Syringe pump: Syringe pumps are used to deliver the monomer solution and silicone oil from the syringes at different pumping velocities. For the monomer solution, NE300 syringe pump, and 10mL Luer lock inert syringe is used, while for silicone oil NE1600 syringe pump and two 50mL Luer lock inert syringes are used. A two-channel syringe pump (NE1600) are used to pump silicon oil. Flow rates from this device range from 0.454 $\mu\text{L/hr}$ to 1163mL/hr. A single channel syringe pump (NE300) is used to pump the monomeric fluid. This flow rate can be adjusted between 0.73 $\mu\text{L/hr}$ to 1257 mL/hr. Luer lock syringes are used because PFA (Perfluoroalkoxy) tubing will be easily connected to the syringe. This gives an easy interchangeability between tubes of different sizes.
4. Tubing: PFA (Perfluoroalkoxy) tubing is used for this process. PFA belongs to a class of melt-processible fluoroplastics. PFA tubing is selected as it has excellent UV transmission ratings which are required for polymerizing ionic liquid [55]. PFA tubing is also known for its gas and vapor permeability properties. PFA tubing has better heat resistance and a smoother surface. PFA is also clearer and more flexible than PTFE. Tubes used had an inner diameter ranging from 0.8 mm – 1.2 mm.
5. PEEK cross section: PEEK (Polyether ether ketone) cross section is used as a medium where silicone oil and monomer solution mixes and due to which the monomer solution separates into small spherical division and are carried forward with the carrier silicone oil.

6. UV light: UV light is used to polymerize the ionic liquid into gel beads. UV light of 365 nm wavelength is used. The tube is wrapped around the UV light so that the length of the tube can vary as per the time required for the monomer solution to be polymerized. In the process described by Rahman et al. [46], the micro-reactor generates droplets of a monomer solution in a silicon oil carrier fluid. Upon exposure to UV light (365 nm), these monomers droplets are polymerized (Figure 19).



Figure 19 Polymerized beads

The silicon oil was pumped through the microreactor at flow rates between 25 $\mu\text{L}/\text{min}$ – 200 $\mu\text{L}/\text{min}$ per channel from NE1600 syringe pump and the monomer solution at flow rates between 0.5 $\mu\text{L}/\text{min}$ - 20 $\mu\text{L}/\text{min}$ from NE300 syringe pump. The monomer solution with chemical composition was initially used referring to [46] and it is shown in Table 3.

Table 3 Monomer ingredients

Monomer Ingredients	Qty.
Ionic Liquid monomer	65% w/w
PEGDA cross-linker	18% w/w
Darocur 1173	7% w/w
Milli-Q Water	10% w/w

A systematic approach was used to commission the microreactor. Initial testing examined the effects of flow rates of silicone oil and monomer solution, on the formation of monodispersed

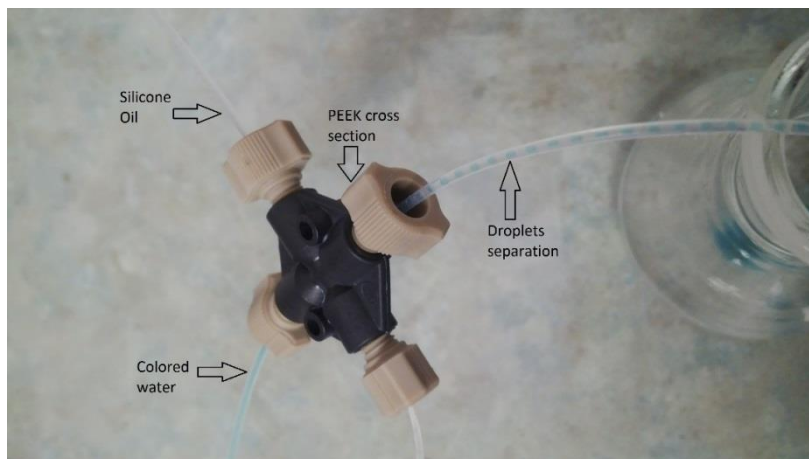


Figure 20 Droplet formation

droplets in the microreactor. In these experiments, colored water was used instead of the monomer solution described above. This resulted in the formation of uniform evenly spaced droplets shown in Figure 20. Similar results were reported in Rahman 2013 [46]. The components are assembled together and are termed as micro-reactor as shown in Figure 18.

After successfully creating monodispersed water droplets in the microreactor, experiments were performed to demonstrate bead polymerization. In these tests, a monomeric solution without ionic liquid was used as the dispersed phase in the microreactor. The monomer solution with

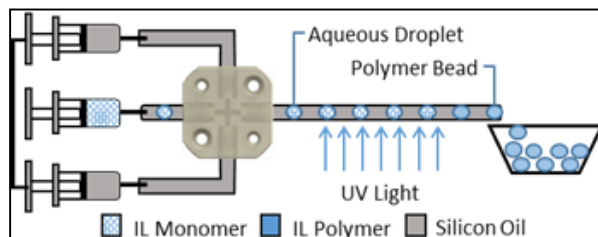


Figure 21 Sketch and image of the microreactor facility

chemical composition was based on that presented in Rahman 2013 [46]. Here, the monomer solution included a crosslinker (Polyethylene glycol diacrylate with average Mn 700 PEGDA), a

photoinitiator (Darocur 1173), and Mili-Q water. The effect of the relative contribution of these components is discussed in section 4.1.1. In energy harvesting applications, ionic liquids will also be included in this solution to increase conductivity. Silicone oil (10cst viscosity) was chosen as the carrier phase as it is immiscible with the dispersed phase.



Figure 22 Microreactor droplet generation [56]

These fluids meet at a PEEK cross section (0.050" bore diameter) where there is the formation of emulsions of monomeric solution due to cross flow mechanism as shown by Tan 2008 et. al (Figure 22[56]). As shown in Figure 22, in a cross flow mechanism the continuous phase liquid is disrupted by another immiscible liquid at a cross junction where dispersed phase liquid meets the continuous phase liquid at right angles as shown in Figure 22. Due to this cross flow, the continuous phase liquid is divided into emulsions.

After synthesis, an optical inspection was performed to provide determine the circularity of the bead. Cross-sectional images of the beads in the horizontal and vertical planes were taken using AmScope WF10x/20 microscope and Ramé Hart respectively as shown in Figure 23. Measurements in the vertical plane were made using DROP image V2.8.02 software. Measurements of the beads were made by selecting two points to measure the distance on the major and minor axis of the image of the bead, as shown in Figure 24. Measurements in the horizontal plane were taken using an AmScope WF10x/20 microscope with a CMOS USB camera. The circularity of the beads by measuring the ratio of length and width of the beads, as the ratio tends towards one, the bead shape is circular.



Figure 23 Facility used for side and top view imaging of synthesized beads

Ramé Hart 250 standard goniometer was also used to measure the contact surface area of the beads. PIL beads which will be created must be tested for various factors such as stiffness, elasticity, conductivity, rolling resistance, and toxicity.

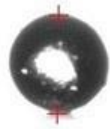


Figure 24 Side View Bead Measurement

Evaluation of these factors will allow for assessment of their viability for electrostatic energy harvesters. Furthermore, understanding the effect of chemical composition on these factors will allow PIL beads to be optimized for particular applications.

Ionic liquids were added to the monomer solution after synthesis of monodispersed gel beads. [2-(Methacryloyloxy) ethyl] trimethylammonium chloride solution was used as an IL in the monomer solution for the microfluidic gel bead fabrication. Results observed from the IL gel beads fabrication are discussed in section 4.1.2. To characterize the effect of various properties of IL gel beads, electromechanical properties need to be calculated. Mechanical properties such as stiffness and electrical properties such as dielectric constant and resistivity should be calculated. Hence, to calculate these properties, experimental facilities of stiffness measurement was developed and experimental facilities for electrical properties such as resistivity and dielectric constant were developed. The experimental facilities are discussed in detail in next sections.

3.2 Mechanical Characterization

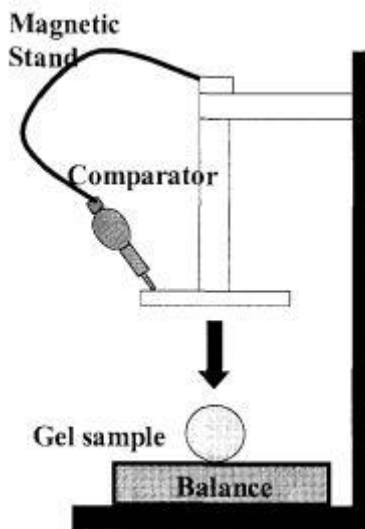


Figure 25 Stiffness measurement of a gel bead [54]

The goal of the proposed research project is to develop a reliable method to synthesize and systematically characterize the electromechanical properties of PIL beads. The elasticity of the beads has been tested in the past using various experimental facilities. As per Tiihonen 2001 et. al [53] the elasticity of a bead was measured using mechanical measurement techniques which

consisted of beads placed between two parallel plates connected by a micrometer screw and micro load cell. Deformation of the beads was observed visually and shear modulus was calculated. In another method, the compression measurement was calculated using a different mechanical apparatus as shown in Figure 25 [54]. As shown in Figure 25, the gel bead was placed on a digital balance scale and the load was applied on the gel bead vertically. The force acting on the bead is measured by the digital balance and the deformation is measured using the comparator. So, elasticity or stiffness of the beads can be calculated using any of the above measurement techniques. Stiffness can be calculated using the formula: $\text{Stiffness} = \text{Load} / \text{Deformation}$ [57]. An experimental facility has been designed and fabricated as Melekaslan 2003 and is shown in Figure 26.

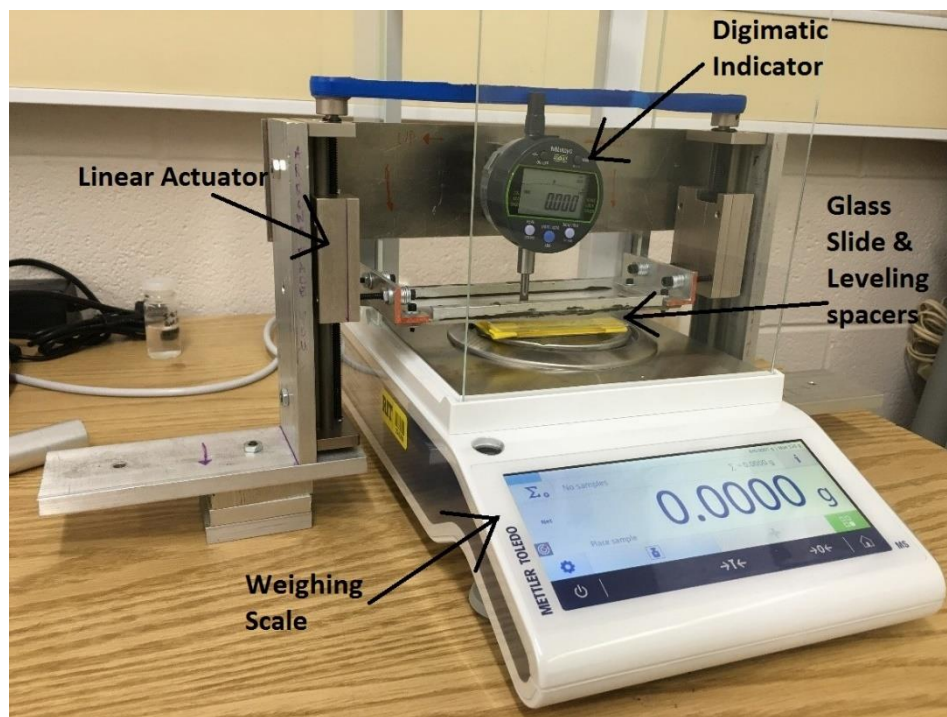


Figure 26 Stiffness measurement facility

The major components of the stiffness measurement facility shown in the Figure 26 are:

1. Linear actuator

2. Digimatic indicator (Mitoyo 543-262)
3. Glass Slide
4. Weighing scale (Mettler Toledo MS104TS)

As shown in Figure 26, the linear actuator was supported by aluminum plates. These aluminum plates are connected to the linear actuator so that it can position vertically. Two linear actuators have a rotating knob at the top which when rotated will displace the actuator vertically. To ensure the same displacement of the linear actuators, these knobs are connected by a belt as shown in Figure 26. A glass plate is connected to the linear actuator which applies force on the beads as it descends. A digital micrometer is used to measure the displacement of the glass plate. Compressive force on the beads is measured using a high precision analytical balance (Mittler Toledo model MS104TS). The readability of this device is reported by the manufacturer as 0.0001g, respectively. Before conducting the experiment, the digital indicator dial, and the balance scale must be reset to zero.

Measured values of compressive force and displacement can be used to calculate the stiffness of a bead using the formula: $\text{Stiffness} = \text{Load} / \text{Deformation}$ [57]. In each case, a bead was placed on a glass plate and compressed using the glass connected to the linear actuator. The bead was compressed from 0-20% of original diameter with increments of 5. The beads were compressed till 20% as they maintained elastic behavior at 20% compression. Hence, the beads were compressed to 5% initially and force acting on the bead was observed using the weighing scale and deformation of the bead was observed using the Digimatic Indicator. Stiffness was calculated using the data obtained from the experimental facility. This procedure was repeated for bead compressed at 10%, 15%, and 20%. Stiffness was calculated and was plotted vs compression to characterize the stiffness (elasticity) for each gel beads fabricated.

3.3 Electrical Characterization

Conductivity and dielectric constant are important properties of proof masses in translational and vibrational energy harvesters. An impedance analyzer was used to measure both of these properties. Impedance is like resistance, except resistance has the only magnitude, while impedance has magnitude as well as phase angle. Resistance can be measured from impedance using the following formula:

$$R = Z \cos \theta$$

Where, R is resistance, Z is impedance and θ is the phase angle. So, at $\theta = 0$, $R = Z$. Hence, the units of impedance are ohms at 0 phase angle.

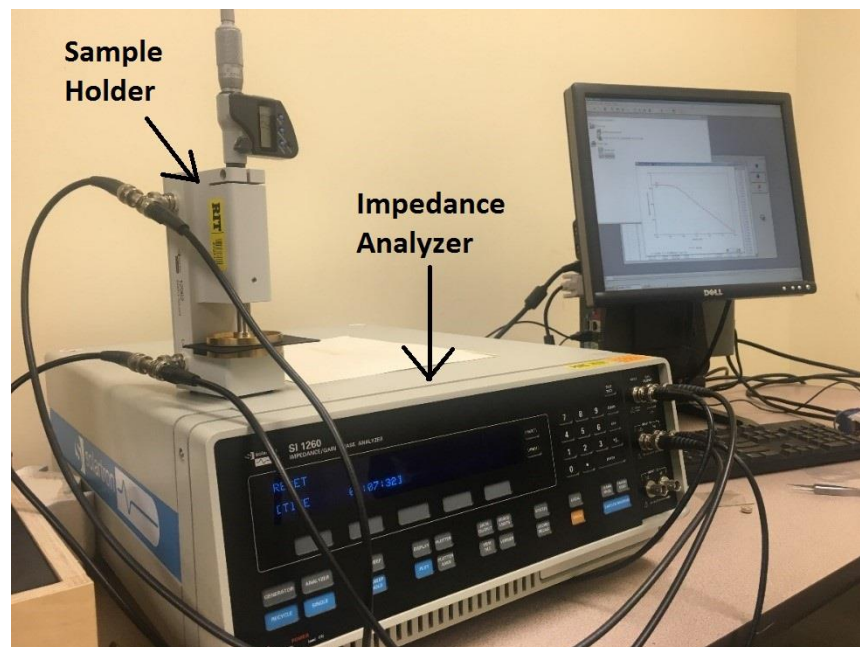


Figure 27 Conductivity experiment facility

Solartron 12962 sample holder was used to hold the gel beads in place for the impedance analyzer Solartron SI 1260. The impedance analyzer and sample holder are shown in Figure 27. As shown in Figure 27, the sample holder is connected to the impedance analyzer using the input and output wires which send/receive the signals from the sample holder to the impedance analyzer. A digital dial is located on the sample holder which displays the distance between the two plates of the sample holder. A rotating dial on top of the sample holder helps to move the plate in the vertical direction. As shown in Figure 27, a conductive polymer sheet is tested for conductivity. SMaRT impedance measurement software was used to operate the impedance analyzer.

As shown in Figure 27, the polymer sheet INCOBLEND elastomer was initially placed in



Figure 28 Digital Indicator on sample holder

the sample holder. The top plate of the sample holder was moved vertically downwards using the rotating dial on top of sample holder as shown in Figure 28. When the polymer sheet is fixed, the distance between the plates was recorded as the initial distance. The input-output terminals were connected from the impedance analyzer to the sample holder. Now, the impedance analyzer is switched on and using the SMaRT impedance measurement software, impedance reading of the

polymer sheet can be measured. In the SMaRT software, we can generate various types of graphs such as Impedance vs Frequency, Real Impedance vs Imaginary Impedance, etc. Also, using SMaRT software, the frequency can be either be fixed to a value or can be decremented from a given value to zero. This enables us to know the impedance of the material at different frequencies. SMaRT software provides a self-generated report after an experiment has ended, which includes, impedance (in ohms), phase angle (in radians/degrees) admittance and capacitance (pF) per each frequency reading. Any material is measured after being compressed in the sample holder at 5%, 10%, 15% and 20% to analyze the change in impedance of the sample placed. Using the data from the SMaRT impedance measurement software, we can calculate various electrical properties of any specimen. The most important properties, we require are the dielectric constant and the resistivity.

Dielectric constant can be calculated using the formula:

$$\epsilon_0 = \frac{C \cdot d}{A}$$

Where, ϵ_0 = Dielectric Constant, C is capacitance, A is contact area, and d is the distance between the plates.

Resistivity (ρ) can be calculated using the formula:

$$\rho = \frac{R \cdot A}{l}$$

Where, ρ = Resistivity, R is electrical resistance, A is area and l is the distance between the plates of the sample holder.

According to the data sheet provided by the manufacturer, the elastomer had conductivity more 1 S/m. For this elastomer, the resistance and distance between the plates were observed from the impedance analyzer. Using the formula of resistivity shown above, resistivity was calculated as 0.6988 ohm m. As conductivity is a reciprocal of resistivity, we calculate that the conductivity of elastomer sheet was 1.43 S/m. Hence, comparing the data from manufacturer's data we can say that the experimental facility is working correctly.

Hence, from the data obtained from the impedance analyzer and the formulas mentioned above, we can calculate the dielectric constant and resistivity of any given specimen.

The conductivity of beads can also be measured using the experimental setup mentioned above. But, provisions need to be made to keep all the beads in a fixed position. Initially, a single bead was placed inside the sample holder and tested. The cross-sectional area of a bead at each compression rate (from 5% till 20%) was observed and noted using Rame-Hart and sample holder/stiffness measurement setup and is shown in Figure 29. As shown in Figure 29, a sample holder is used to hold a bead between two plates. Rame hart provide the capability to capture an image of the bead deformed when under compression. The contact area can be measured from Rame Hart measuring tool as shown in Figure 29. It has been observed that whenever a gel bead was compressed, the contact area increased. The contact area found from above setup was used initially as only a single bead was tested for conductivity. Since, for any energy harvesting application, there will be more than one bead in a confined space.



Figure 29 Contact area measurement experimental setup

To confine beads in a fixed amount of space a special arrangement was done. An aluminum plate was cut into two square pieces and an electric insulating tape was used to confine an area of 1cm^2 . The plate with beads confined to the area of 1cm^2 as shown in Figure 31. The plate shown

in Figure 31 is filled with beads and is covered with another aluminum plate as shown in Figure 30.



Figure 30 1cm² area plate



Figure 31 Front view of 1cm² area plate

This configuration is then inserted into the sample holder to calculate the resistivity and dielectric coefficient of the beads. Aluminum plates allow all the beads to compress uniformly when compressed in the sample holder.

3.4 Metallization of ionic liquid beads:

The addition of ionic liquids to the beads improves their electrical properties. The conductivity of these ionic liquid gel beads can be increased by depositing metal inside these beads making them more ionically charged [58]. The process of metallization can be done using two methods, cation exchange, and anion exchange methodology. Selection of the method depends on upon

which metal is used to metallize the beads. Metal ions from the metal salt sample can replace the free radical ions from the ionic liquid solution. Since silver has positive ions, it can be replaced by a cation exchange process. Gold ions are negative, so they would be replaced by anion exchange process. Experiments performed here used gold and platinum. Anion exchange was used for both metals since they both have negative ions.

A metal salt is selected to metallize the beads of resins or beads fabricated from the microreactor. The beads are placed in a test tube with a metal salt solution. The entire solution is mixed together until all metal salt solution has replaced the free radical ions in the IL gel bead. The beads are decanted and washed using distilled water. Now, Hydrazine is added in excess to the beads to reduce the metal salt solution to metal ions in the beads.

Materials required for this process are as following:

- 1) Resin beads or gel beads fabricated from microreactor
- 2) Metal salt solution
- 3) Distilled water
- 4) Hydrazine ($\text{N}_2\text{H}_4 \cdot 2\text{H}_2\text{O}$)

Pretreatment: To create metallized gel beads, initially the dry weight of the gel bead is calculated in order to find the amount of salt present in a gel bead which would be replaced by gold or any given metal IONAC A554 Cl⁻ form was reported by the manufacturer to have 4.2 millimoles quaternary ammonium groups per ml (3 grams) of wet resin are calculated, it gives us the number of moles of gold is required to replace Cl⁻ ions with gold from the resin. Distilled water and Hydrazine are added in excess.



Figure 32 Gold salt 1/10th molar solution

Metallization was initially performed on commercially available IONAC A554 Cl⁻ resins beads. Gold was added to these beads using gold salt NaAuCl₄. A 0.1 molar solution was created by diluting 4 grams of gold salt in 100 ml of distilled water as shown in Figure 32. This concentration was chosen to avoid any shortage of gold salt for future experiments.

Resin beads weighing 3 grams are measured on a weighing scale. They are later decanted and washed using distilled water. The resin beads are collected in a test tube and are shown in Figure 33.

Since 4.2 mil-moles of gold are required to replace 4.2 mil-moles of IONAC A554 Cl⁻ form resin beads, we would need 42 ml of (1/10th molar) gold solution, which will react with the resin



Figure 33 IONAC A554 Cl⁻ form resins beads



Figure 34 Resin beads in gold solution

beads replacing Cl⁻ with Au⁺ and leave Na⁺ and Cl⁻ ions in the solution. Hence, these resin beads are added with 42 ml of gold solution as shown in Figure 34.

The mixture is shaken vigorously until all the gold salt is deposited in the solution turning the solvent transparent in color. To check if all the gold solution is deposited in the resin beads, add more gold salt solution and check if the solvent is turning transparent in color or not. If the color of the solvent is still yellow, it suggests that all gold has been deposited in the resin beads and no extra gold can be further deposited.

After metallization, the resin beads are decanted and washed in distilled water to remove any residual chemicals in the resin beads. After washing, the resin beads contain AuCl⁻, which should be reduced to Au (i.e. gold only).



Figure 35 Excess hydrazine being weighed

To obtain that state we add an excess of hydrazine (Figure 35). Hydrazine reacts with gold deposited resin quickly reducing AuCl_4^- to Au^0 . This results in the metalized beads shown in Figure 36.

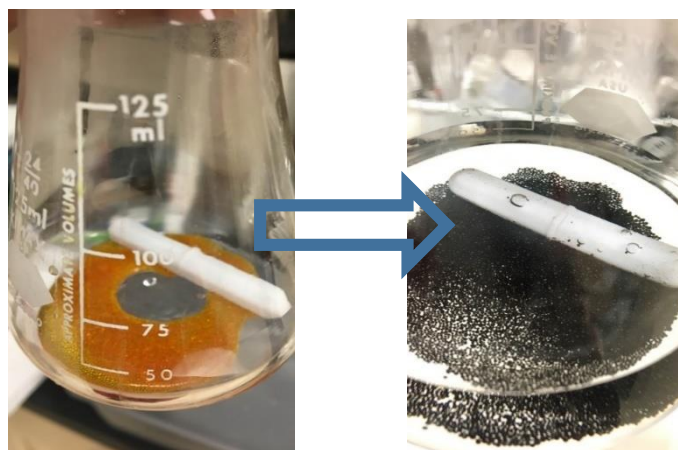


Figure 36 before adding Hydrazine (left) and after adding Hydrazine (Right)

Using the anion exchange method for metallization we have converted 3 grams of IONAC A554 Cl^- form resins to gold deposited resins. Assuming the above procedure as the first metallization of gold, we can now take 1 gram of gold beads for their stiffness and conductivity testing and proceed for 2nd gold metallization process. Since we have 2/3rd of beads, we can repeat

the above process with 2/3rd of a 1/10th molar gold solution of which used earlier i.e. 28 ml of gold and repeat the entire process again. When the 2nd metallization process is completed, we will remove 1 gram of gold beads for their stiffness and conductivity testing. Now, we are left with 1/3rd of original beads, with which we can proceed to 3rd gold metallization process Again since we have 1/3rd of beads, we can repeat the above process with 1/3rd of a 1/10th molar gold solution of which used earlier i.e. 14 ml of gold and repeat the entire process again. The 3rd metallization stage gold beads can now be tested for stiffness measurement and conductivity measurement.

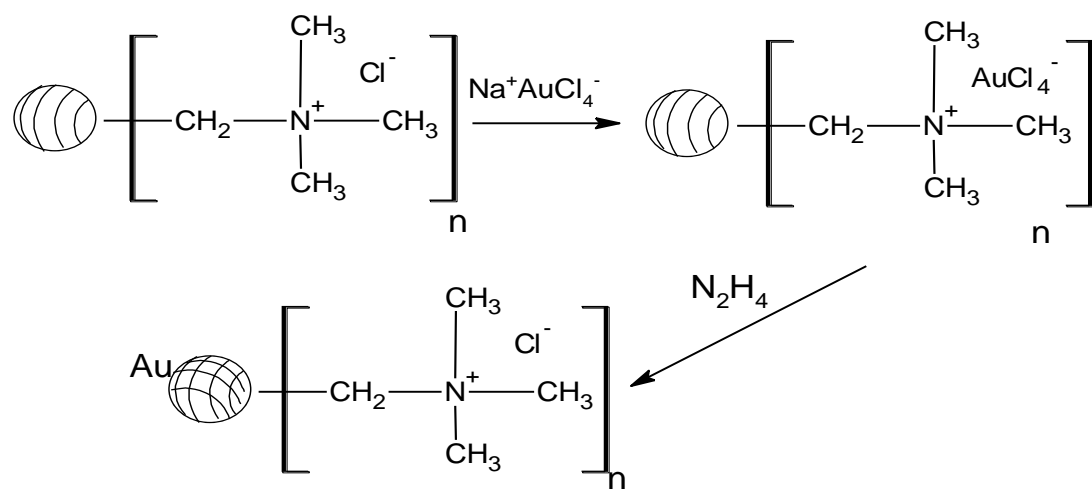


Figure 37 Chemical reactions for gold metallization process of IONAC A554 Cl⁻ form resins

Metallization of IONAC A554 Cl⁻ forms resins with gold salt NaAuCl_4 (Figure 37). When the salt solution is added to the IONAC A554 Cl⁻ resin beads, Cl⁻ ions are exchanged by AuCl_4^- and when Hydrazine is added to the solution gold ions are deposited inside the resin beads leaving nitrogen and heat outside.

Platinum beads were also synthesized using IONAC A554 Cl⁻ forms resins beads. This process is the same as described for gold metallization except $\text{NaAuCl}_4 \cdot 2\text{H}_2\text{O}$ was replaced by $\text{K}^+\text{PtCl}_6^-$. Metallization of IONAC A554 Cl⁻ form resins with platinum salt $\text{K}^+\text{PtCl}_6^-$ is shown in Figure 38.

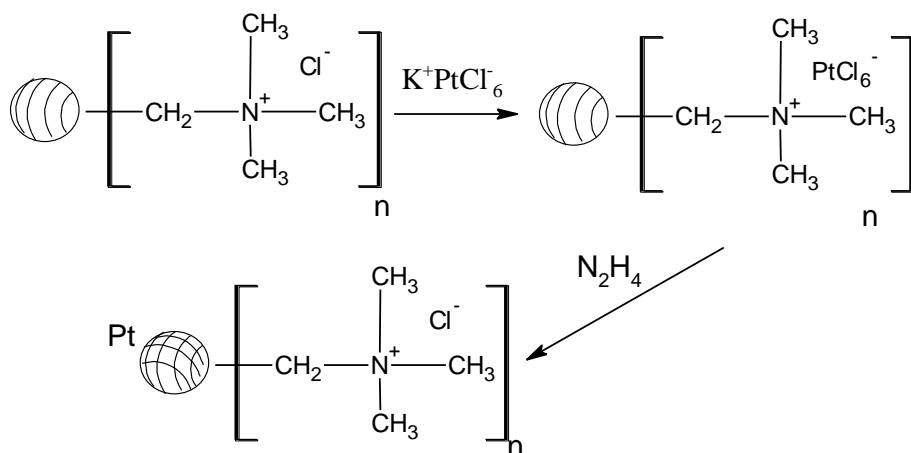


Figure 38 Chemical reactions for platinum metallization process of IONAC A554 Cl⁻ form resins

For metallization process, 0.25ml of IONAC A554 Cl⁻ form was stored in 22 ml distilled H₂O. Now, 0.25ml of IONAC A554 Cl⁻ form beads were treated in a test tube with 0.122 ml of K⁺PtCl₆⁻ (which is actually platinum salt). The test tube was vigorously shaken until all the Cl⁻ is replaced by the platinum salt K⁺PtCl₆⁻. The solution was washed and decanted using distilled water. When the salt solution is added to the IONAC A554 Cl⁻ resin beads, Cl⁻ ions are exchanged by PtCl₆⁻. Later, Hydrazine is added to the solution and due to chemical reaction platinum ions are deposited inside the resin beads leaving nitrogen and heat outside. After 15 mins, the solution was decanted and washed using distilled water until the solution was neutral in pH. Platinum metallized beads were used for testing their electromechanical properties.

With every stage of metallization, the beads become more conductive as the amount of gold is increased inside the resin. Stages of metallization can be increased until the desired conductivity is achieved. Apart from gold, platinum was also tested on the resin beads using the same procedure as mentioned above. The changes in conductivity and stiffness of different types of beads are discussed in the results and discussion section below.

Metallization of IL gel beads fabricated from the micro-reactor was performed after the metallization process was demonstrated on IONAC A554 Cl⁻ resin beads. IONAC A554 Cl⁻ ions metallization technique was used as a surrogacy technique to help us understand the metallization process. Before the metallization process, it was important to calculate the number of moles per mg of the IL in the gel beads. To calculate that, initially, we need to calculate the constant dry weight of the beads. To calculate the dry weight of the beads, few IL beads were weighed on a weighing scale to record the initial weight of the IL bead. These beads were then kept in a furnace which was maintained at 120⁰ C. Every 20 minutes, the IL beads were removed from the furnace and weighed until a constant dry weight was obtained. Using these data number of moles was calculated as following:

$$\text{No. of moles (n)} = \frac{x * y}{M}$$

Where, no. of moles = n, dry weight = x, molecular weight = M, and number of equivalent grams of beads = y

Now, since we know the number of moles present in the IL, we can now calculate the amount of gold salt solution, required to replace the IL by gold salt. Gold salt with sufficient molar quantity is mixed with the IL gel beads. The mixture is shaken vigorously until all the gold salt is deposited in the solution turning the solvent transparent in color. If the color of the solvent is still yellow, it suggests that all gold has been deposited in the resin beads and no extra gold salt can be further deposited. After metallization, the IL gel beads are decanted and washed in distilled water to remove any residual chemicals in the resin beads. Later, Hydrazine is added to the solution and Hydrazine reacts with gold deposited resin quickly reducing AuCl₄⁻ to Au⁰. The changes in conductivity and stiffness of different types of beads are discussed in the results and discussion section below.

4.0 RESULTS AND DISCUSSION

Results of this investigation are presented and discussed in this chapter. In order to determine the effect of chemical composition on the electromechanical properties, gel beads with/without IL were fabricated using the microreactor. Also, results show that using the microreactor, repeatability of beads with various chemical compositions can be synthesized. Experiments for mechanical properties such as stiffness and electrical properties such as dielectric constant and resistivity have been conducted and results are presented in the sections below. IL gel beads and IL resin beads have been metallized using anion exchange chemical process and their electromechanical properties have been tested and presented in the sections below.

4.1 Fabrication and Testing of gel beads without ionic liquid:

4.1.1 Polymer Gel Bead Synthesis and effects of flow rates on shape of the bead

The initial objective of PIL gel bead synthesis was to repeatedly create polymer gel beads in the microreactor facility. Previous works had demonstrated that the shape of droplets developed in microreactors was a function of flow rates of silicon oil and monomer solution[46], [56]. This involves creating monodispersed droplets of a monomer solution in an oil medium and polymerizing them with UV light. As such, a parametric study for bead synthesis without ionic

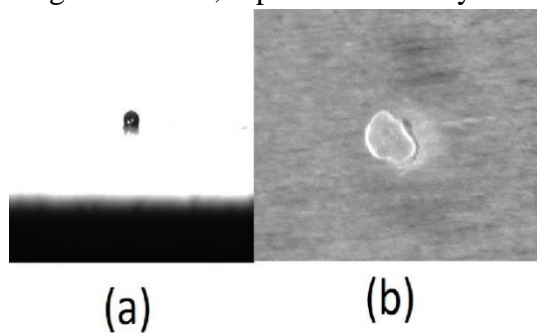


Figure 39(a) Front view of bead & (b) Top view of bead

liquids that varied flow rates and monomer composition was performed to determine to study the relation of flow rates of silicone oil and monomer solution to the shape of the PIL beads.

Fist we used colored water in oil to see that we could make monodispersed water droplets in immiscible silicon oil. The droplet formation is shown in Figure 20. Now, since we observed the dispersed formation of the water droplets, we modified the chemical composition from Rahman 2013 [46] by replacing IL by water as shown in Table 3. Droplets of the monomer solution were then polymerized by exposure to UV light in the microreactor to form polymerized beads. Polymerized gel beads obtained from the microreactor were irregular in shape, as shown in Figure 39. The time required to polymerize a normal polymer solution liquid was approximately 15 seconds. The time was recorded using a stopwatch which measured the time for a single emulsion droplet to convert from liquid state to solid state while traveling through the UV light exposed tube.

According to my hypothesis the shape of the beads will be affected due to two factors: (i) the aspect ratio of the beads as it is a function of the flow rates of the monomer and silicone oil [56], (ii) the chemical composition of the monomer solution which might be causing changes in the surface of the beads. To test this hypothesis, chemical composition of the beads was altered. In the updated chemical composition Tetramethylammonium chloride was added. Tetramethylammonium chloride is a type of salt. Also, the proportion of PEGDMA was increased. The new updated monomer composition is shown in Table 4.

Table 4 Updated monomer solution

Components	Quantity (%)
PEGDMA	73.4
Ionic Liquid	–
Water	18.3
Darocure 1173	6.5
Tetramethylammonium chloride	1.8

Due to the change in composition, the monomer solution polymerized extremely quickly as the proportion of photoinitiator was increased. The time required to polymerize the monomer solution was approximately 20 seconds and was measured using a stopwatch. The droplet will be transformed from transparent to translucent as it polymerizes into a gel bead. The monomer liquid polymerized at the early stage of the process, this resulted in the tubing to get a clog and hence this eventually resulted in blockage of the entire tubing and hence, the entire tubing was needed to be replaced. Crosslinker (PEGDMA) concentration in the monomer solution was increased in an effort to reduce the irregularity of the bead shape. The updated monomer solution is presented in Table 4. The increase in PEGDA concentration in the updated monomer solution resulted in a reduction in the polymerization time from approximately 20 s to 5 s. This rapid polymerization increased clogging in the tubing. When blockages were observed, the experiment would be ended and the tubing was replaced. Flow rates of the monomer and silicon oil were altered to avoid clogging (table 4).

Beads obtained from the microreactor were observed optically using a Ramé Hart system and it was observed that the beads obtained were smooth, but not spherical in shape. The effect of flow rates on bead aspect ratio was examined experimentally using the conditions listed in Table 5.

Table 5 Effect of flow rates on formation of beads

Flow Rate for Monomer ($\mu\text{L}/\text{min}$)	Flow Rate for silicone oil ($\mu\text{L}/\text{min}$)	Results
0.5	25	Irregular shape beads
1	25	Elongated shaped beads (Fig 38 (a))
5	30	Irregularity in shape of beads (Fig 38 (b))
8	35	Almost spherical but still irregular surface patterns of the beads (Fig 38 (c))
10	40	Clogging in some parts of the tube with spherical beads
10.5	50	Spherical beads were obtained (Fig 38 (d))

Horizontal and vertical images of the beads (Figure 40) show the polymerized gel beads formed as flow rates of monomer solution and silicon oil were altered. Flow rates of the continuous phase fluid (monomer solution) and dispersed fluid (silicon oil) have a significant effect on the ultimate shape of the polymerized bead. If the flow rate of the continuous phase fluid was higher than the dispersed phase then due to cross flow mechanism, elongated emulsions will be formed. Hence, considering the viscosity, capillary number, interfacial tension of the monomer solution, the flow rates should be maintained such that perfectly spherical emulsion are formed.

Images of the resultant polymer beads under a variety of different flow conditions are presented in Figure 40. Images in Figure 40 correspond to cases described in table 5. As the ratio of flow rates of monomer solution and silicon oil increases (Fig. 40 a-d), the shape of the bead changes from an elongated plug, to a spherical bead.

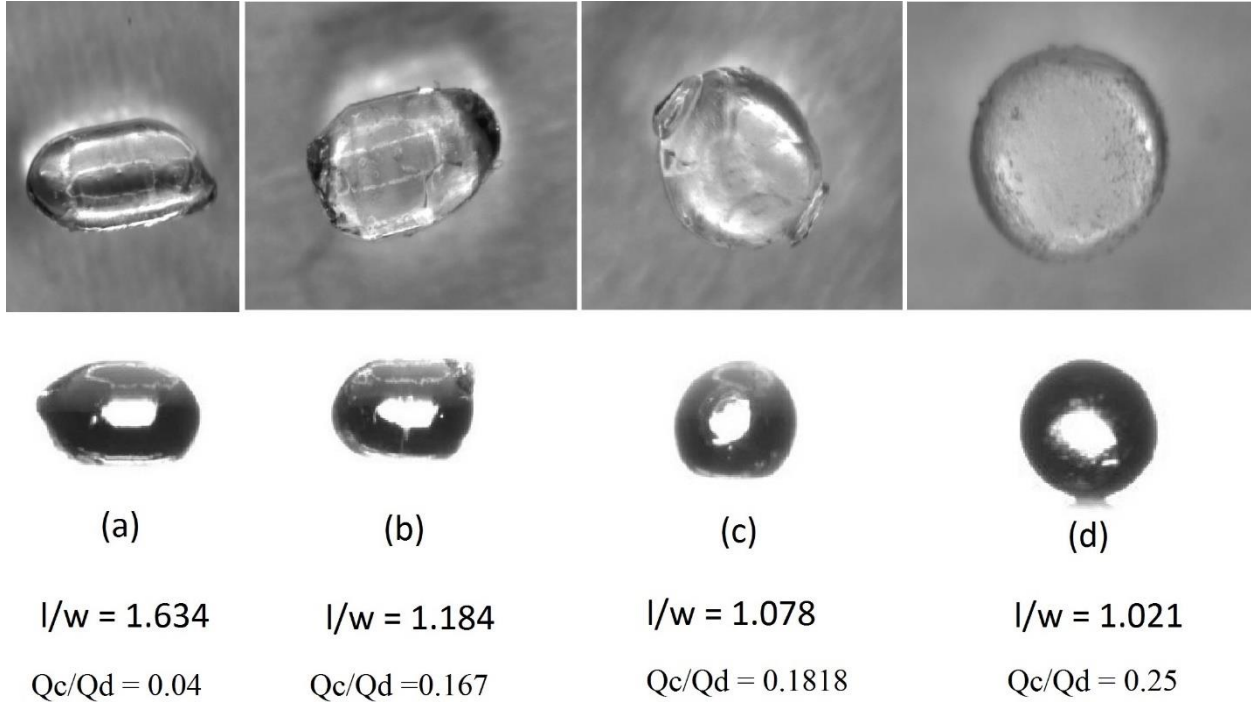


Figure 40 Images of the side and top view images from gel beads. Ratio of monomer to oil flow rate increases from (a) through (d).

Spherical beads were obtained by varying the flow rates of the syringe pumps of silicon oil and monomer solution. Emulsion stability criteria [56] was also used to analytically predict the length of the shape of the bead. This criterion predicts that,

$$\frac{l}{w} = k \left(\frac{Q_c}{Q_d} \right)^{-0.2} Ca^{-0.2},$$

Where,

$$Ca = \frac{\mu V}{\gamma}.$$

This suggests that an appropriate ratio of flow rates can be predicted by measuring the dynamic viscosity (μ) and surface tension between the two fluid phases (γ). The emulsion stability criteria were observed for the beads obtained shown in Figure 40. The graph of (l/w) vs (Q_c/Q_d) is shown in Figure 41.

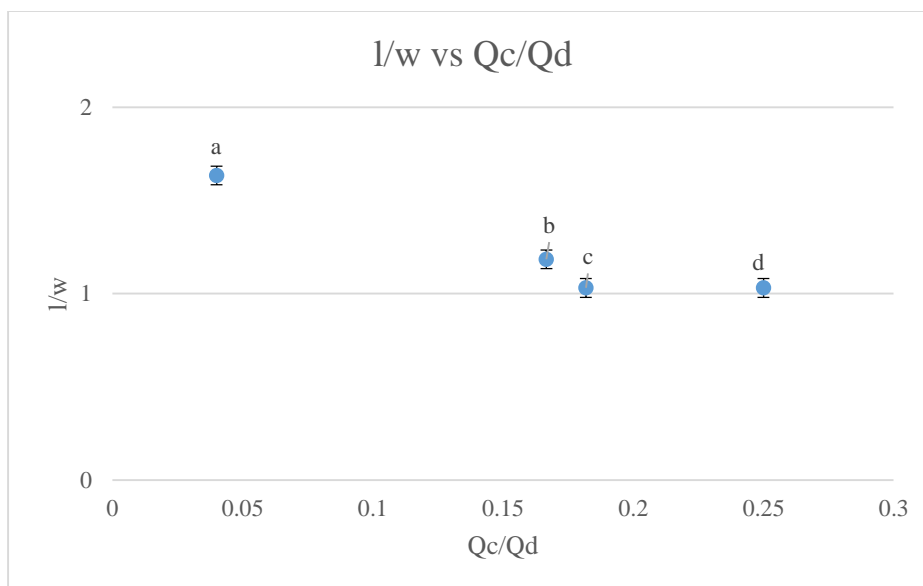


Figure 41 Graph for Bead aspect ratio (l/w) as a function of ratio of carrier and dispersed fluid flow rates (Q_c/Q_d). Circles represent aspect ratios of beads fabricated from Table 5

As shown in Figure 41, the ratio of Q_c/Q_d affects the shape of the bead. Hence, for non-IL gel beads it was observed that as the ratio of Q_c/Q_d was increased the shape of the bead of was more spherical as l/w tends to 1. Relative flow rates of the monomer/oil affect aspect ratio and target flow rates can be estimated based on the physical properties of the monomer & silicon oil. Since the scaling seems similar in the experiment as compared to the Rahman 2013 [46] and Tan 2008 [56]. The coefficient of emulsion stability is calculated using experimental data. As shown in Figure 41, using the values of flow rates of the spherical shape bead, the known values were inserted in the equation for emulsion stability. Hence, from this equation we get the coefficient for emulsion stability as 0.22. Using the formula for emulsion stability, we were able to calculate the flow rates of monomer solution and silicon oil for spherical emulsions. Further research can be done in the future to evaluate the effects of each chemical composition on the size of the beads and could be check by using the formula.

4.1.2 Polymer Gel Bead Synthesis and effects of chemical composition on the electromechanical properties of the bead

Photoinitiator and crosslinker are used in every monomer chemical composition as per [46] as they are required to polymerize and cross-link the monomer solution respectively. Hence, it was important to study the effects of varying percentage of Photoinitiator and crosslinker in the monomer solution on electro-mechanical properties such as stiffness, resistivity and dielectric constant. Gel beads could be an attractive proof mass in a variety of energy harvesting devices. In each device type, higher efficiencies can be attained by improving the physical properties of the proof mass such as resistivity, stiffness and dielectric constant. Microfluidically synthesized PIL beads may prove to be an attractive choice for a variety of energy harvesting devices because they are relatively easy to fabricate and the various properties of the beads should be a function of the chemical composition of the IL monomer. This work is particularly interested in electromechanical properties such as elasticity, resistivity, and dielectric constant IL gel beads. Hence, it is important to understand which component of the monomer solution will affect the properties mentioned earlier.

In order to study the effects of varying composition, we looked at beads without IL to (i) examine the effects of non-IL components like the crosslinker and (ii) to prove out the characterization method. Polymerized non-IL gel beads were fabricated as per different chemical compositions, shown in Table 6.

Table 6 Composition of non-IL gel beads

Monomer Solution	Components	Quantity (Mass Fraction %)	Recipe for 5 ml of monomer solution
A	PEGDMA Di-vinyl monomer	18 %	0.9 ml
	Ionic Liquid Monomer	0%	0.00 ml
	Milli-Q Water	75%	3.75 ml
	Darocur 1173	7%	0.35 ml
B	PEGDMA Di-vinyl monomer	74%	3.608 ml
	Ionic Liquid Monomer	0%	0.000 ml
	Milli-Q Water	19%	1.038 ml
	Darocur 1173	7%	0.354 ml
C	PEGDMA Di-vinyl monomer	7%	0.341 ml
	Ionic Liquid Monomer	0%	0.000 ml
	Milli-Q Water	19%	1.038 ml
	Darocur 1173	74%	3.742 ml
D	PEGDMA Di-vinyl monomer	30%	1.463 ml
	Ionic Liquid Monomer	0%	0.000 ml
	Milli-Q Water	60%	3.277 ml
	Darocur 1173	10%	0.506 ml
E	PEGDMA Di-vinyl monomer	55%	2.682 ml
	Ionic Liquid Monomer	0%	0.000 ml
	Milli-Q Water	37%	2.021 ml
	Darocur 1173	8%	0.405 ml

Beads A, B, C, D, and E were fabricated in the microreactor and characterized in the stiffness measurement and the impedance analyzer.

Initially, gel beads of monomer A was placed on a glass plate and compressed at 5%, 10%, 15% and 20%. The experiment was conducted and results were obtained as per the formula:

Stiffness = Load or Force acting on the bead / Deformation of the bead [57].

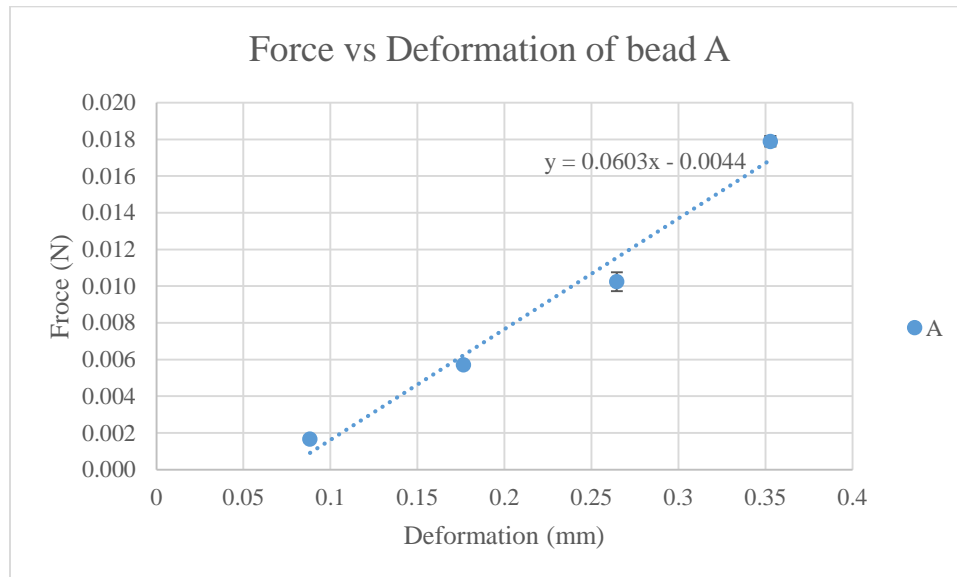


Figure 42 Graph of force vs deformation of bead A

As shown in Figure 42, it was observed that as the rate of deformation increased, the force acting on the bead also increased. From Figure 42, we can conclude that, the stiffness of the bead increases as it is more compressed. In accordance to Hook's law, the slope of graph is the spring constant of the bead A which is 0.0603.

With reference to above procedure, the spring constant of beads B, C, D, and E were calculated. The spring constant of beads A, B, C, D and E is shown in Figure 43. As shown in Figure 43, the spring constant of B and E is greater than compared to A, C, and D. Also, as seen from the Figure 43, the beads B and E have higher di-vinyl monomer percentage than beads A, C and D.

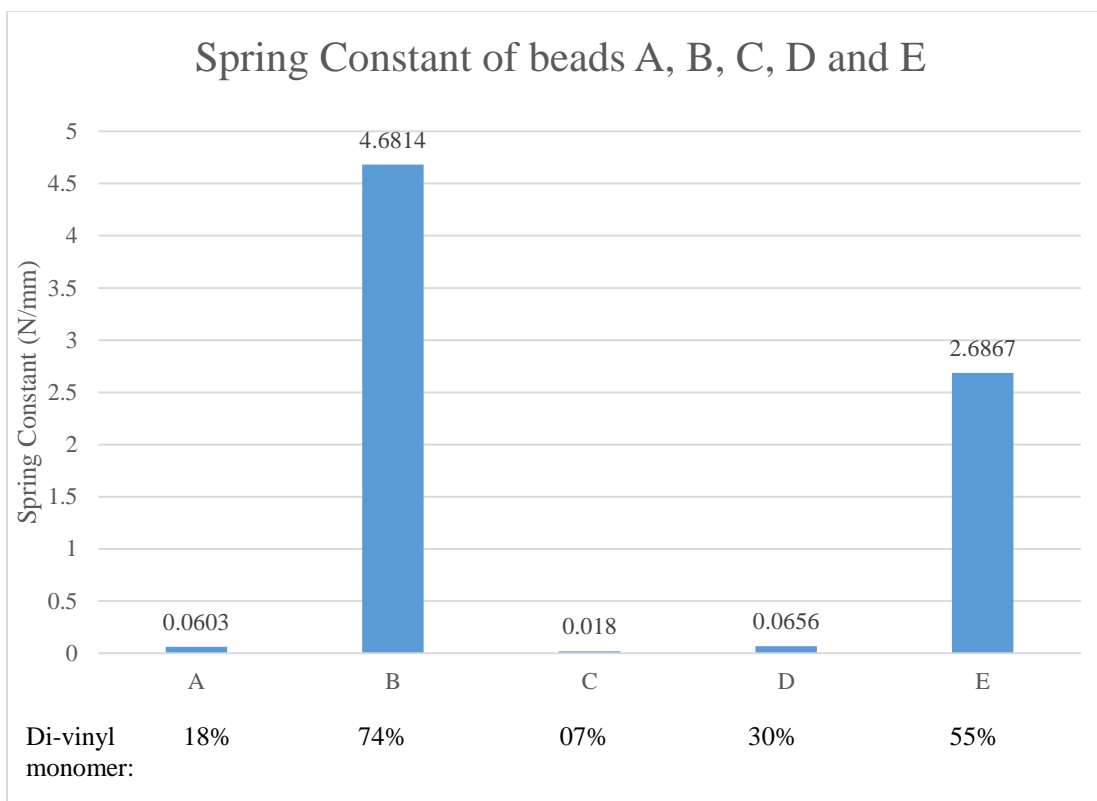


Figure 43 Spring Constant of Beads A, B, C, D and E. di-vinyl monomer percentage of beads A, B, C, D and E is shown.

The graph of stiffness vs compression of all beads namely, A, B, C, D and E are shown in Figure 44 and Figure 45. Comparing the above graph and the chemical composition of the beads A-E, it has been observed that for beads with a higher percentage of crosslinker and a low percentage of Photoinitiator have higher stiffness. As a crosslinker helps in joining two or more molecules by a covalent bond in the monomer solution [59], it helps in improving the stiffness of the gel bead.

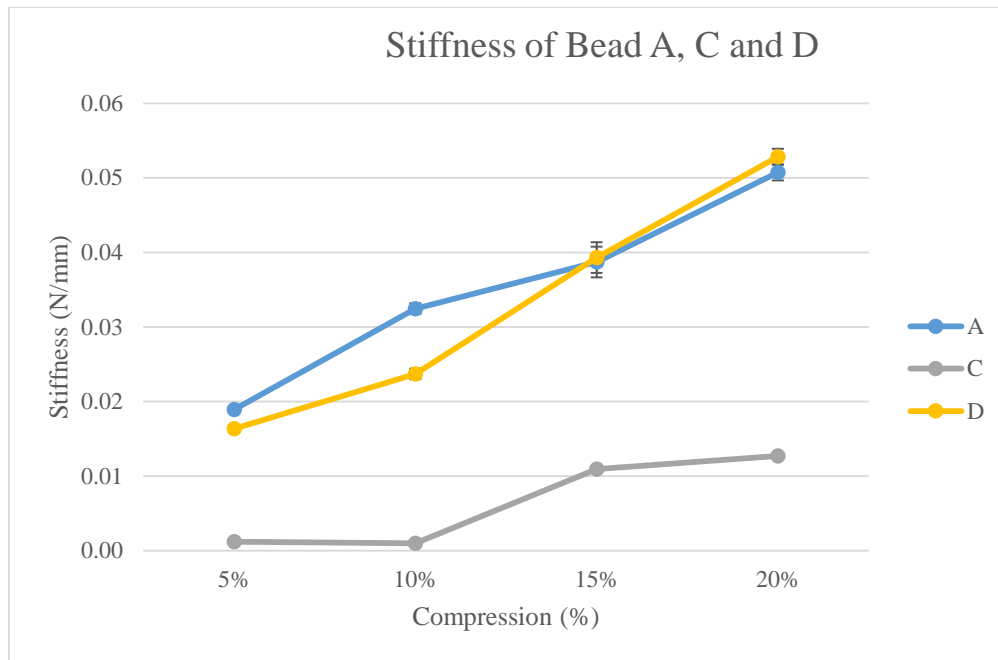


Figure 44 Graph of stiffness vs compression for bead A, C, and D

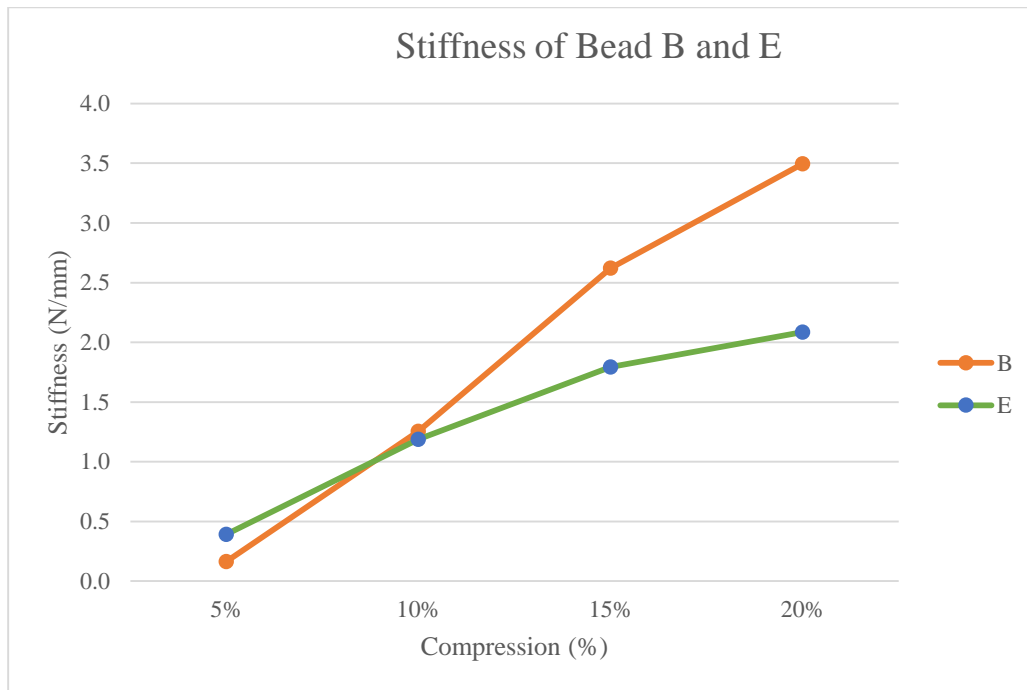


Figure 45 Graph of stiffness vs compression of beads B and E

Characterization of the conductivity and dielectric coefficient of polymer gel beads were made using the impedance analyzer as described in section 3.3. From the impedance analyzer, various properties of bead A were evaluated such as impedance, capacitance, admittance, etc.

Dielectric constant and resistivity were calculated using the data from the impedance analyzer as explained in the experimental methodology section 3.3. As the gel bead A is compressed from 5% to 20%, the contact area of the gel bead increases. The contact area of a single bead was observed as compression of the bead was increased from 5% to 20%, is shown in Figure 46.

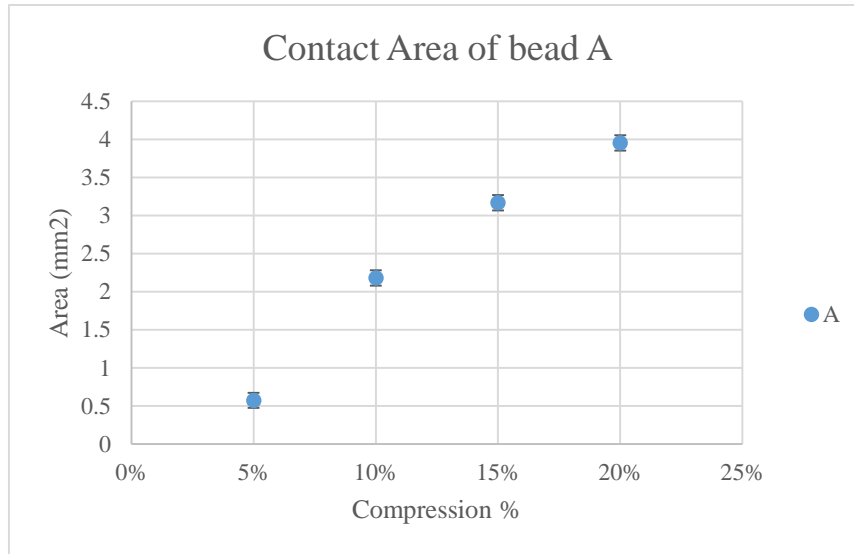


Figure 46 Graph showing increase in contact area of a single bead A with increase in compression from 5% to 20%.

As explained in section 3.3, the dielectric constant and resistivity is a function of the contact area of the gel bead. Hence, as the contact area increases, the properties of the gel beads also change accordingly. As discussed in section 3.3, for all energy harvesting applications, more than one beads are packed in a small confined area. Hence, the dielectric constant and resistivity observed from these multiple packed beads is actually total effective dielectric constant and effective resistivity of these beads.

The graph of capacitance vs compression is shown in Figure 47. As shown in Figure 47, the capacitance of the bead increased by 47% when compressed from 5% to 20%.

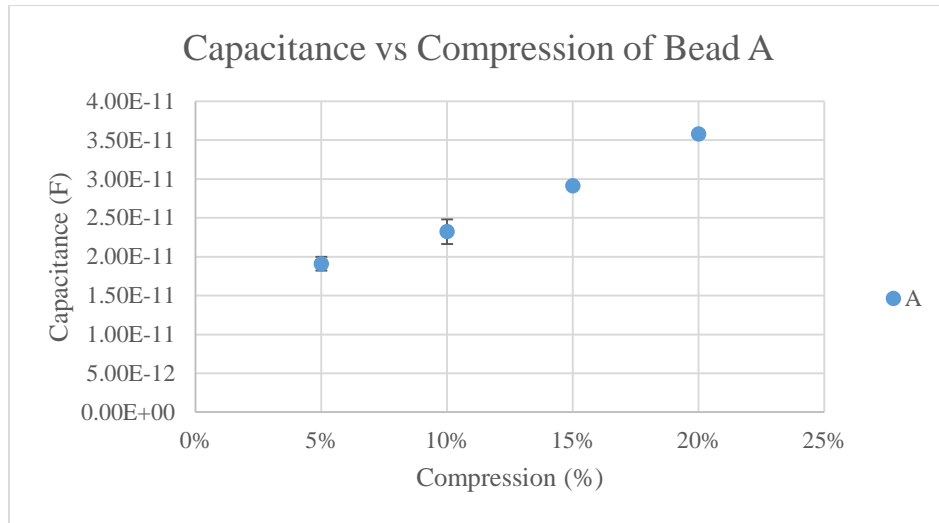


Figure 47 Graph showing increase in Capacitance as beads A are compressed from 5% to 20%

Since, we know the capacitance and contact area of bead A at compression from 5% to 20%, we can now calculate dielectric constant. The graph of dielectric constant vs compression of bead A is shown in Figure 48. As shown in Figure 48, the dielectric constant of the bead A increases from 60.95 to 96.17 as the bead is compressed from 5% to 20%. The increase in dielectric constant is monotonic and appears to be linear. As the beads are compressed the contact area of the beads increase resulting in an increase in dielectric constant.

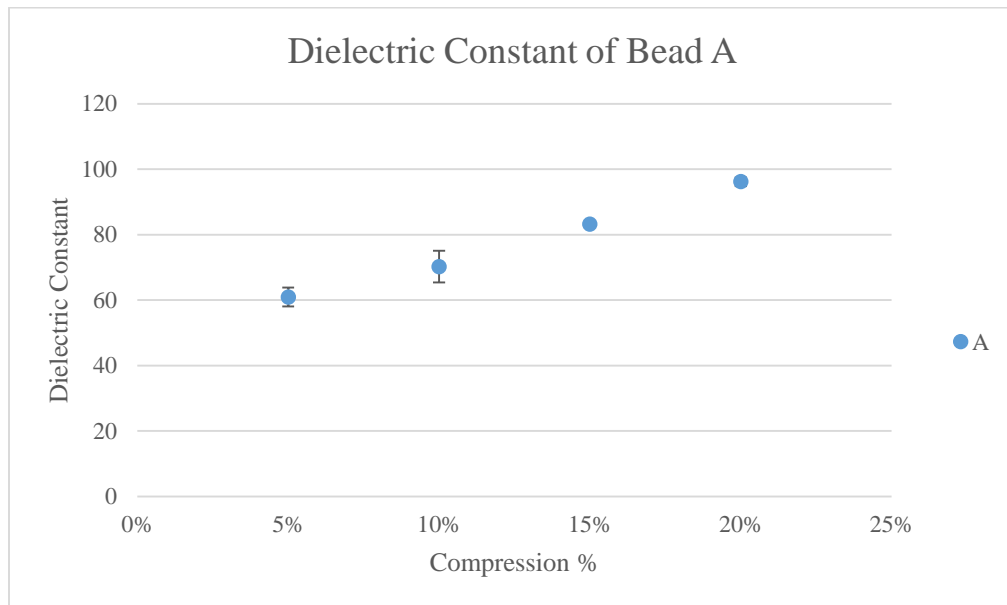


Figure 48 Graph showing increase in dielectric constant as beads A are compressed from 5% to 20%

With reference to above procedure, the dielectric constant of beads B, C, D, and E was calculated. The graph of dielectric constant vs compression of all beads namely, A, B, C, D and E are shown in Figure 49. As shown in Figure 49, the dielectric constant of bead A and E is highest as compared to D, B, and C. It is observed that for higher dielectric constant, high amount of liquid monomer and low amount of photoinitiator was required.

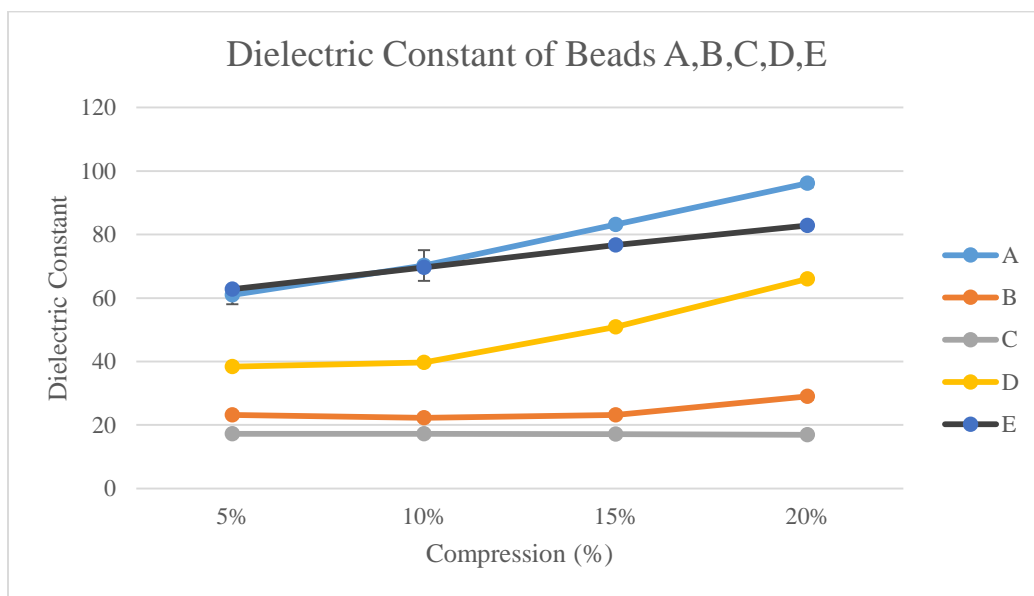


Figure 49 Graph of dielectric constant vs compression of beads A, B, C, D and E

Now using the data from the impedance analyzer and formula for resistivity mentioned in the experimental methodology section, these properties were calculated as explained in the experimental methodology section 3.3. As discussed in section 3.3, the impedance of beads can be observed using the impedance analyzer. The effect of impedance is observed as the bead is compressed from 5% to 20% of original size. The change in impedance of the bead A, is shown in Figure 50. As shown in Figure 50, the impedance decreases as the bead is compressed from 5% to 20%. The impedance decreases by 49% as the gel beads are compressed from 5% to 20% of its original size.

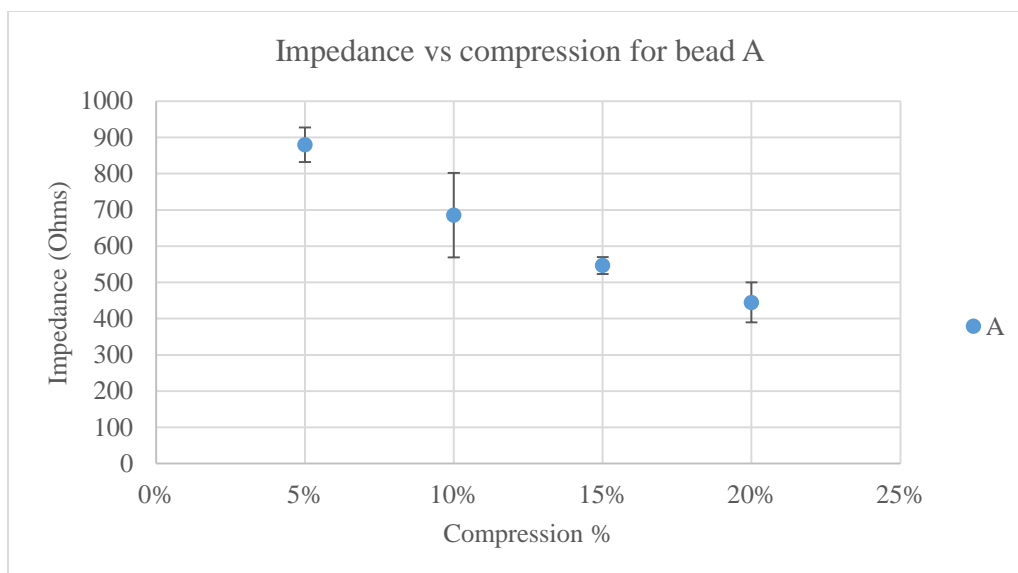


Figure 50 Graph showing decrease in impedance as beads A are compressed from 5% to 20%

Now, since, we know the value of impedance when beads were compressed from 5% to 20%, we can now calculate the resistivity of these beads. The graph of resistivity vs compression of bead A is shown in Figure 51. As shown in Figure 51, as the beads were compressed, the resistivity of the beads decreased. As shown in Figure 46, the contact area of the beads increased as they were compressed from 5% to 20% of original size. Hence, from the formula discussed in section 3.3, it has been observed that the as contact area increases, resistivity decreases. With reference to above procedure, the resistivity of beads B, C, D, and E was calculated. The graph of resistivity vs compression of all beads namely, A, B, C, D and E are shown in Figure 52.

As shown in Figure 52, the resistivity of A and E is lowest as compared to D, B, and C similar to the dielectric constant results. The resistivity of A and E was $0.187 \Omega \cdot m$ and $0.217 \Omega \cdot m$ respectively. Hence, we can state that for lower resistivity high proportion conductivity medium must be present in the monomer solution as compared to the crosslinker and Photoinitiator. If more proportion of conductivity medium is present in the gel beads, there will more ions present, making the beads with higher dielectric constant and lower resistivity.

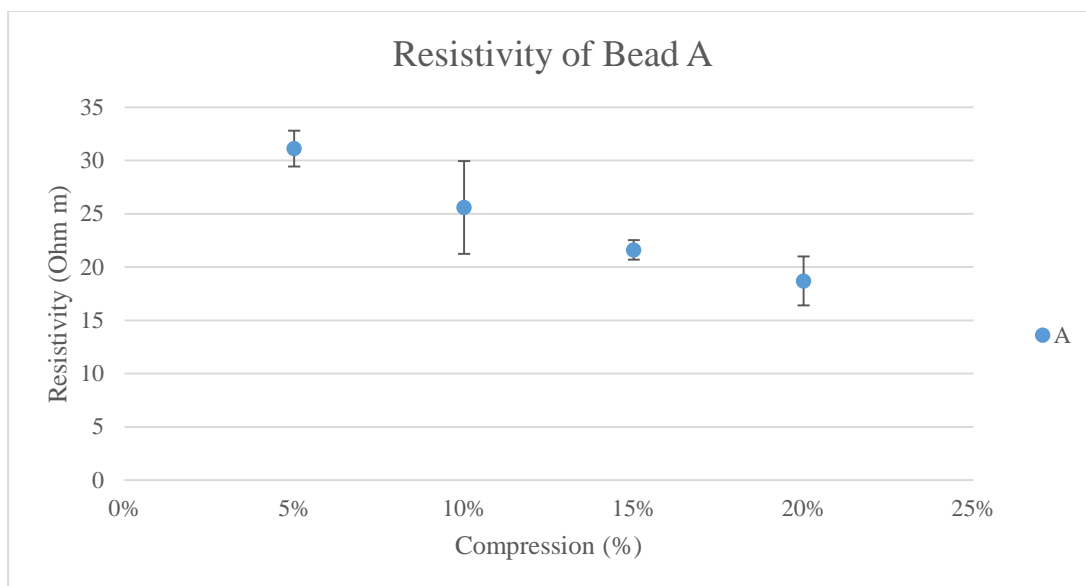


Figure 51 Graph of resistivity vs compression of bead A

Evaluating the graphs, it has been observed that by varying the chemical composition of a monomer solution its properties could alter as per requirement. But, since the gel bead had no IL or any conductive liquid in its solution, and IL was added to the monomer solution.

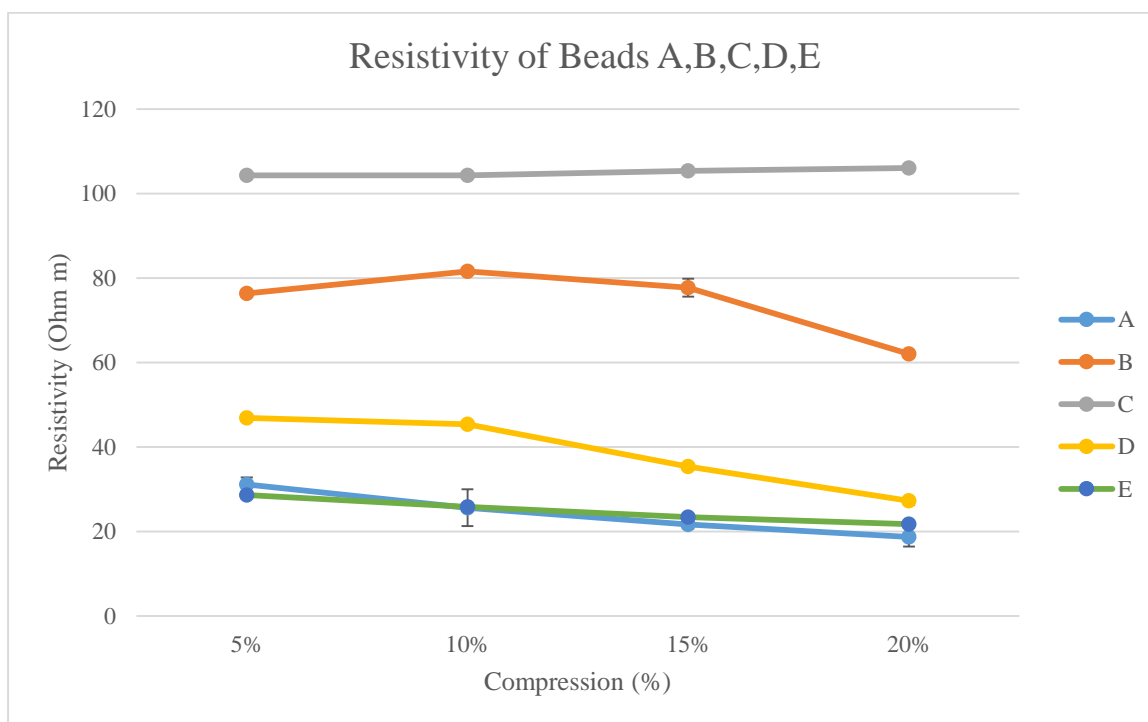


Figure 52 Graph of resistivity vs compression of beads A, B, C, D and E

4.1.3 Fabrication and testing of gel beads with Ionic liquid:

With the help of Dr. Smith, an IL was procured and was used in the chemical composition of the monomer solution. The IL solution was selected to have free ions which would make the ionic liquid more ionically charged, thus making it more conductive. [2-(Methacryloyloxy) ethyl] trimethylammonium chloride solution was selected as an Ionic Liquid, as it contained similar acrylic group. The initial chemical composition of the gel bead monomer solution is shown in Table 7

Table 7 Monomer solution for gel bead with 45% IL

Monomer Solution	Components	Quantity (Mass Fraction %)	Recipe for 5 ml of monomer solution
IL 45%	PEGDMA Di-vinyl monomer	10 %	0.50 ml
	Ionic Liquid Monomer	45%	2.25 ml
	Milli-Q Water	5%	0.25 ml
	Darocur 1173 Photoinitiator	40%	2.00 ml

As shown in Table 7, the monomer solution had a low quantity of crosslinker while the proportion of IL and photoinitiator was high. The beads were fabricated using this chemical



Figure 53 Swollen gel beads with 45% IL

composition. As shown in Figure 53, due to the high proportion of IL, beads when stored in the water got swollen and lost their original spherical shape. Due to which, these beads were extremely

elastic and had high rolling resistant due to which they would rupture when rolled on any surface.

Mechanical property such as stiffness of the gel beads with 45% IL was measured using stiffness measurement facility as discussed in earlier sections. The effect of force acting on the IL gel beads is compared with the non-IL gel beads. The result of compression of IL beads from 5% to 20% of their original size, is shown in Figure 54.

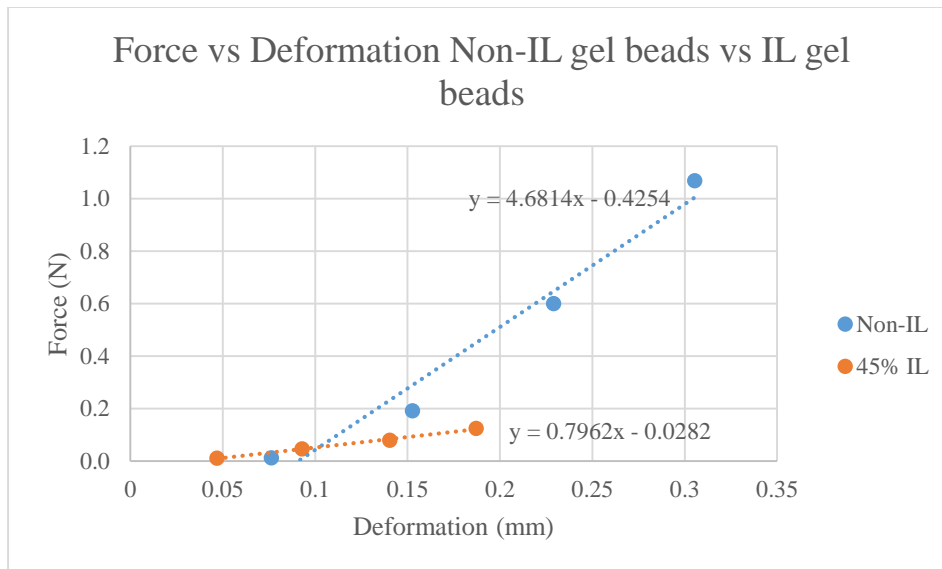


Figure 54 Comparison of force acting on the IL at 45% and on non-IL gel bead at compression ranging from 5% to 20% of the original size of the gel beads.

As shown in the Figure 54, the spring constant can be calculated from the slope of the linear graphs of IL and non-IL gel beads. It can be observed that the spring constant of gel beads with 45% IL was 0.745, while spring constant for non-IL was 7.148. Hence, the spring constant of gel beads with 45% IL was almost an order less in magnitude as compared to non-IL.

As shown in Figure 55, the stiffness of the IL gel beads was also poor as compared to the non-IL gel beads. It was observed as the proportion of IL was increased, the stiffness of the gel beads decreased. Also, the IL gel bead had a lower proportion of crosslinker in its chemical composition. As seen from observations before, the stiffness of a bead can be increased by increasing the crosslinker proportion in the chemical composition of the gel beads.

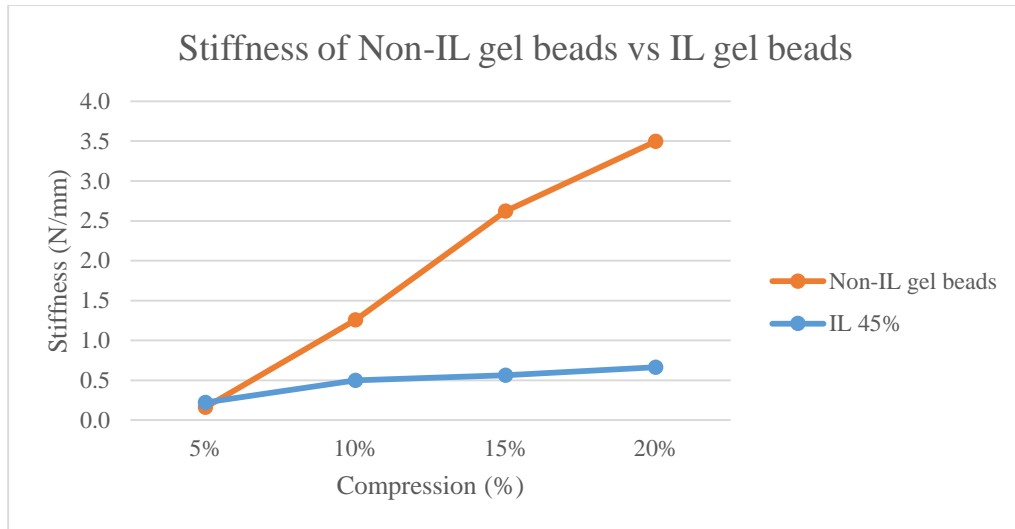


Figure 55 Graph of stiffness of non-IL gel beads vs. IL gel beads w.r.t. compression ranging from 5% to 20%.

The IL gel beads were tested for electrical properties using the impedance analyzer as discussed in the section 3.3. As shown in Figure 56, the dielectric constant of the gel beads increases due to the addition of IL in the gel beads. As shown in Figure 56, the dielectric constant

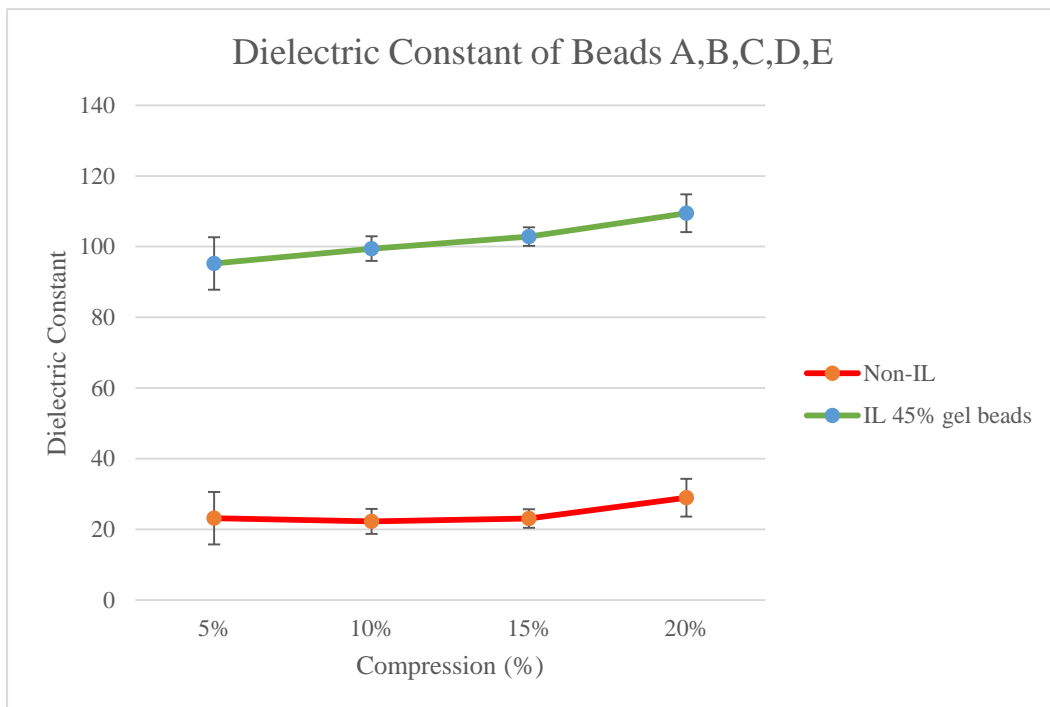


Figure 56 Graph of dielectric constant of Non-IL gel beads vs IL gel beads

increased by almost 73%. Due to increased dielectric constant, the capability of the gel beads to store more charge, is increased. Also, the IL gel beads have more number of free ions as

compared to that of non-IL gel beads, hence, IL gel beads have more capacity to store more electric charges.

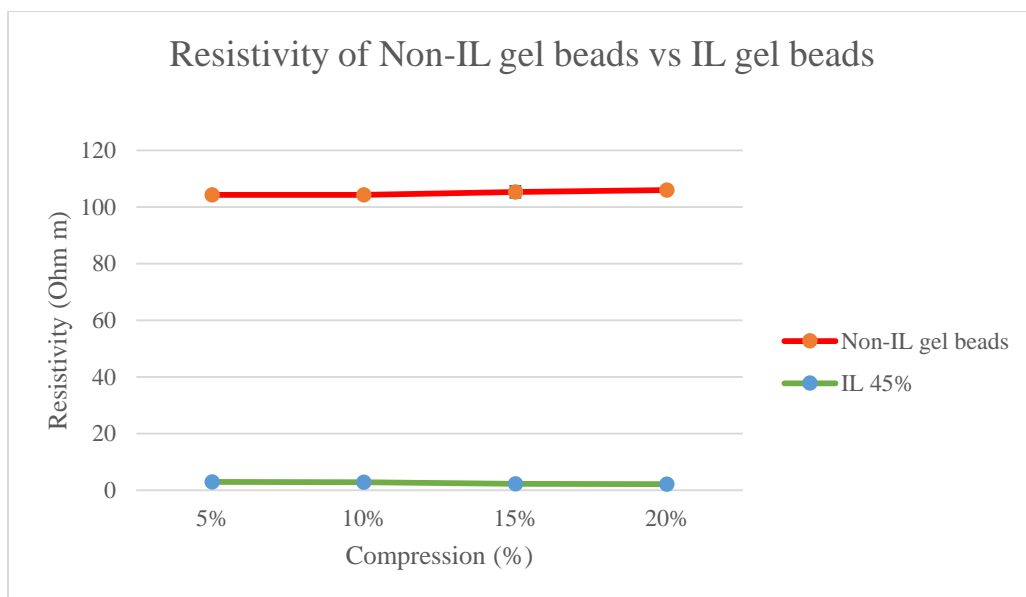


Figure 57 Graph of resistivity of non-IL gel beads vs IL gel beads

Apart from dielectric constant, resistivity was also measured for the IL gel beads. It was observed that the resistivity of the gel decreased considerably as IL was added to the monomer solution. As shown in Figure 57, the resistivity of IL gel beads is lower than non-IL gel beads. The resistivity of gel beads with 45%IL is less by almost 96%, as compared to non-IL gel beads. Resistivity of IL gel beads is low because of the presence of more electrically active ions in them as compared to Non-IL gel beads. IL gel beads had a higher proportion of IL making them less resistive and with a high dielectric constant. Since the IL gel beads had a lower quantity of di-vinyl monomer, the IL gel beads are more elastic in nature.

To study the effect of varying IL composition in the monomer solution on the electromechanical properties, beads with chemical compositions shown in Table 8 were synthesized and characterized.

Table 8 Chemical Composition with varying proportions of IL monomers

Monomer Solution	Components	Quantity (Mass Fraction %)	Recipe for 5 ml of monomer solution
IL 10%	PEGDMA Crosslinker	36%	1.80 ml
	Ionic Liquid Monomer	4%	0.20 ml
	Milli-Q Water	5%	2.50 ml
	Darocur 1173	10%	0.50 ml
IL 5%	PEGDMA Crosslinker	38%	1.90 ml
	Ionic Liquid Monomer	2%	0.1 ml
	Milli-Q Water	50%	2.50 ml
	Darocur 1173	10%	0.50 ml
IL 2.5%	PEGDMA Di-vinyl monomer	39%	1.95 ml
	Ionic Liquid Monomer	1%	0.05 ml
	Milli-Q Water	50%	2.50 ml
	Darocur 1173	10%	0.50 ml

The beads obtained from the microreactor were tested using impedance analyzer and stiffness measurement facilities. The results obtained are shown in Figure 58, Figure 59, Figure 60 and Figure 61.

As shown in Figure 58, the dielectric constant of IL gel beads decreased as the proportion of IL decreased in the monomer solution. The dielectric constant of IL gel beads dropped by almost 15% when the IL was reduced by half in proportion from 10% IL to 5% IL and to 2.5% IL. As the percentage of IL in the bead is decreased, its ability to store charge or energy also reduced. This is reflected in the reduction in the dielectric coefficient.

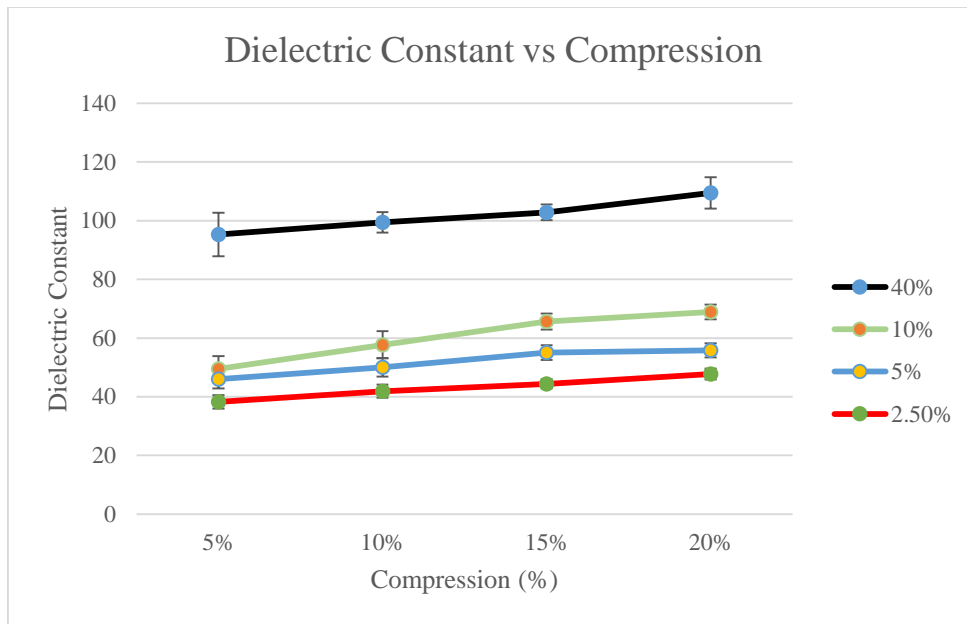


Figure 58 Graph of dielectric constant vs compression of IL gel beads

The resistivity of the gel beads also calculated for IL gel beads. As observed from Figure 59, the resistivity of gel beads decreased as the proportion of IL was decreased in the gel beads. As the IL percentage was dropped from 40% to 10% the resistivity increased by almost 50%. Hence, as the percentage of IL in the bead is decreased, the number of free charges in the bead is also reduced. This ultimately reduces its conductivity.

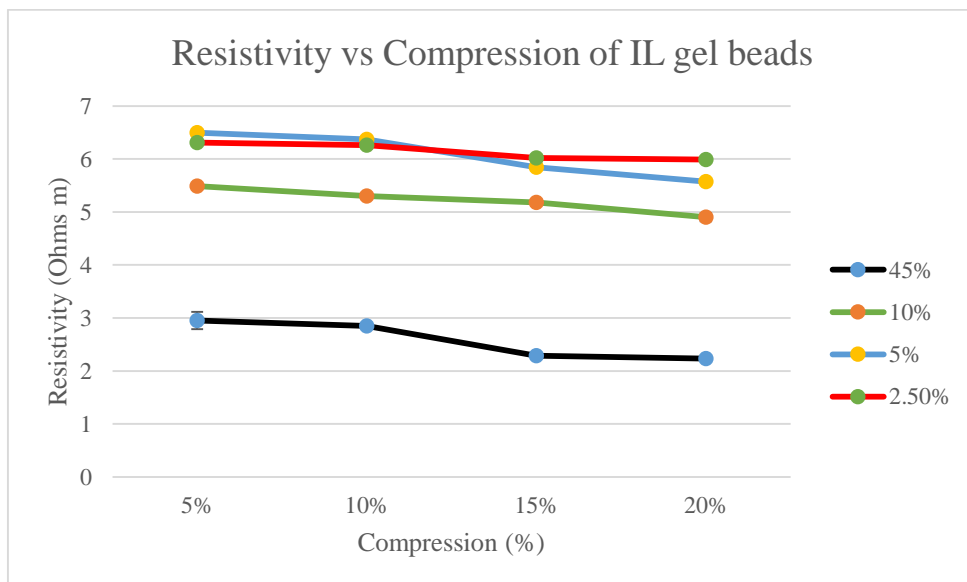


Figure 59 Graph of resistivity vs compression of IL beads

The effect of ionic liquid concentration on mechanical stiffness was examined using the stiffness measurement facility. The spring constant was calculated by plotting the graphs of force vs compression. As shown in Figure 60, the spring constant of IL beads is observed from the equation of the slopes of force vs compression.

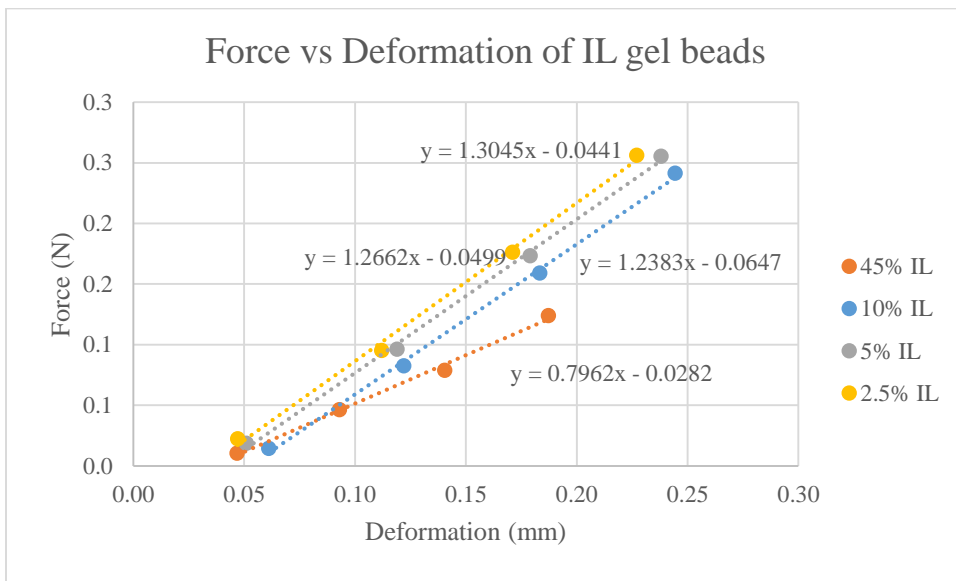


Figure 60 Graph of Force acting on IL gel beads when compressed from 5% to 20% of original size.

From Figure 60, it can be observed that, as the IL concentration decreases from 45% to 10%, the spring constant of the gel beads increases from 0.7458 to 1.5143. Also, as the IL concentration further decreases from 10% to 5%, the spring constant only increases from 1.5143 to 1.5646. When the gel bead with IL 2.5% is observed in Figure 60, the spring constant has only increased by a small amount from 1.5646 to 1.5758. We can say that, as IL concentration decreases the gel beads become stiffer, but as the IL concentration decreases than 10%, there is no major change in stiffness of the gel beads.

As shown in Figure 61, the stiffness of the gel beads increased as the proportion of IL was reduced. As the IL percentage was dropped from 45% to 10%, the stiffness of the beads increased by 32%. As the IL percentage dropped from 10% to 5% the stiffness of the beads increased by just

approximately 8%. But, as the IL percentage dropped from 5% to 2.5% the stiffness of the beads increased by only 5%. As shown in Figure 58 and Figure 59, as the proportion of IL was increased to 40% the conductivity of the gel bead increased but compromising the physical properties such as stiffness as shown in Figure 61. As the IL proportion in the beads decreased and proportion of crosslinker increased resulting in increasing stiffness of the bead.

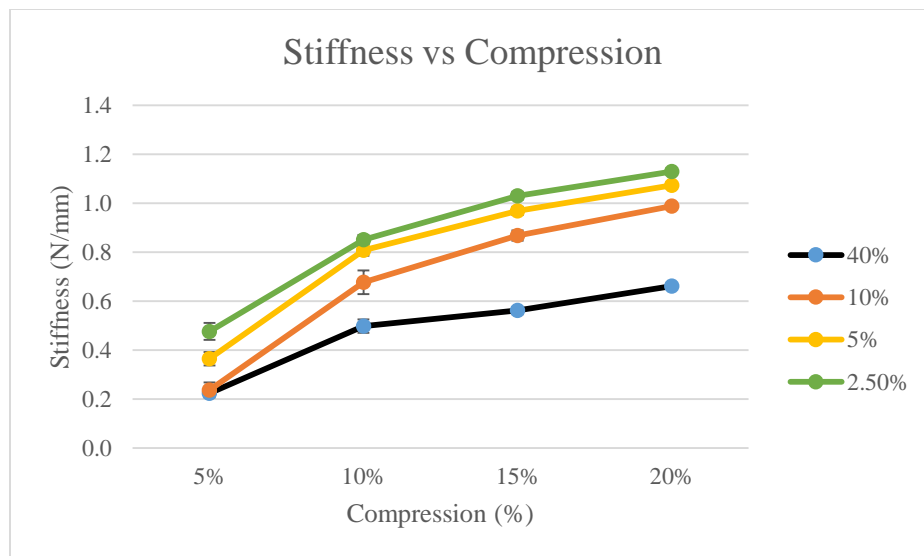


Figure 61 Graph of stiffness vs compression of IL beads

With the help of Dr. Smith, we could evaluate that, to improve the conductivity of the IL gel beads without compromising the elasticity of the bead, beads could be metallized with a conductive metal such as gold or platinum.

4.2 Metallization process

4.2.1 Metallization and testing of IONAC A554 Cl⁻ resin

Metallization of gel beads is another potential method to improve electrical properties [58]. A metallization process based on Warshawsky 1989 [58] was developed with the help of Dr. Smith. To study the effects of metallization process, IL resin beads were tested initially in the impedance analyzer and stiffness measurement facility to get a reference data to compare with metallized beads. IONAC A554 Cl⁻ resin beads were used for bead exchange process for

metallization. Platinum was used initially for metallization. Components required for metallization of IONAC A554 Cl⁻ resin with platinum, are shown in Table 9.

Table 9 Metallization composition of IONAC A554 Cl⁻ resin beads with platinum

	Materials	Quantity	Moles (m moles)	Molecular Weight
I	IONAC A554 Cl ⁻ form in 22ml of distilled H ₂ O	0.25 ml	0.350	1.4 meq/ml
II	Aqueous solution of K ⁺ PtCl ₆ ⁻ dissolved in 5ml of distilled water	0.122 ml	0.251	486 g/mol
III	Distilled H ₂ O	10 ml		
IV	10% Aqueous N ₂ H ₄	Excess		

The metallization process used for gold and platinum beads is described in section 3.4.

Gold was also used for metallization of resin beads. Components required for gold metallization are shown in table 10.

Table 10 Metallization composition of IONAC A554 Cl⁻ with Gold salt NaAuCl₄*2H₂O

	Materials	Quantity	Moles (m moles)	Molecular Weight
I	IONAC A554 Cl ⁻ form	3 eq ml	4.2	1.4 meq/ml
II	Aqueous solution of NaAuCl ₄ *2H ₂ O 10 th molar solution	42 ml	4.2	397.8 g/mol
III	Distilled H ₂ O	10 ml		
IV	Hydrazine (N ₂ H ₄)	0.8g dissolved in 20ml distilled H ₂ O	31	32

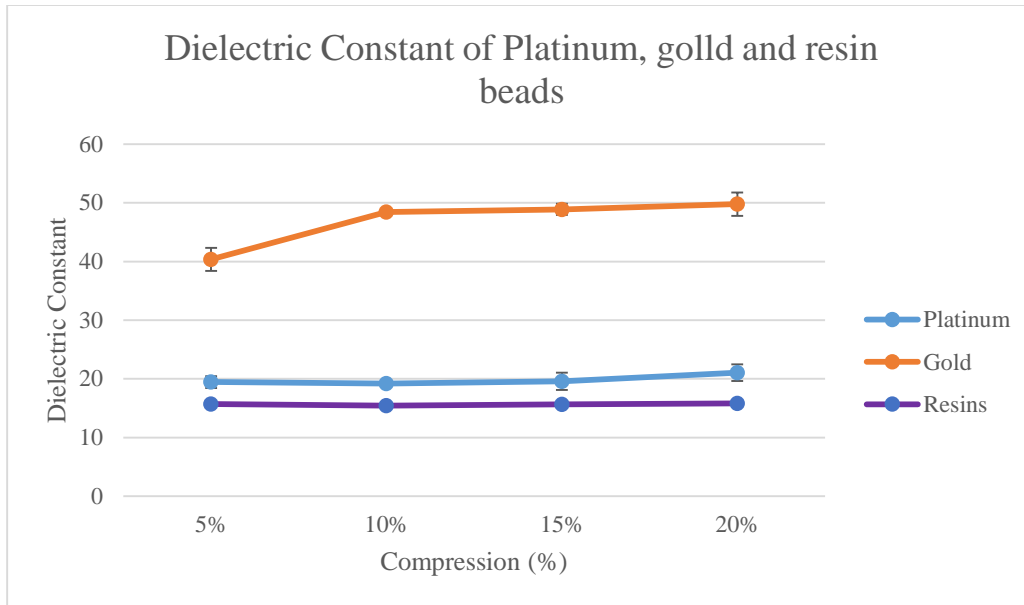


Figure 62 Graph of dielectric constant vs compression of resin, Platinum and gold metallized beads

Results obtained from metallization from resins with no metallization, resins with gold metallization and resins with platinum metallization were observed.

Electrical characterization of gold and platinum beads was used to determine which metal would provide better properties. Metallization with either metal was found to increase the dielectric constant of the resin beads (Fig 62). However, it was observed that the dielectric constant of the gold coated resins was more by almost twice than compared to the dielectric constant of platinum coated resin beads. As gold is more conductive than platinum [60], gold has more charged ions and hence has a higher dielectric constant as compared to platinum.

As shown in Figure 63, the resistivity of the resin beads was improved due to the addition of gold and platinum in the chemical composition of the resin beads respectively. But, it was observed that the resistivity of the gold metallized resins was better than platinum metallized resin beads. The resistivity of gold was almost half of that of platinum as gold is more conductive than platinum [60], gold has more charged ions and hence has a higher dielectric constant as compared to platinum.

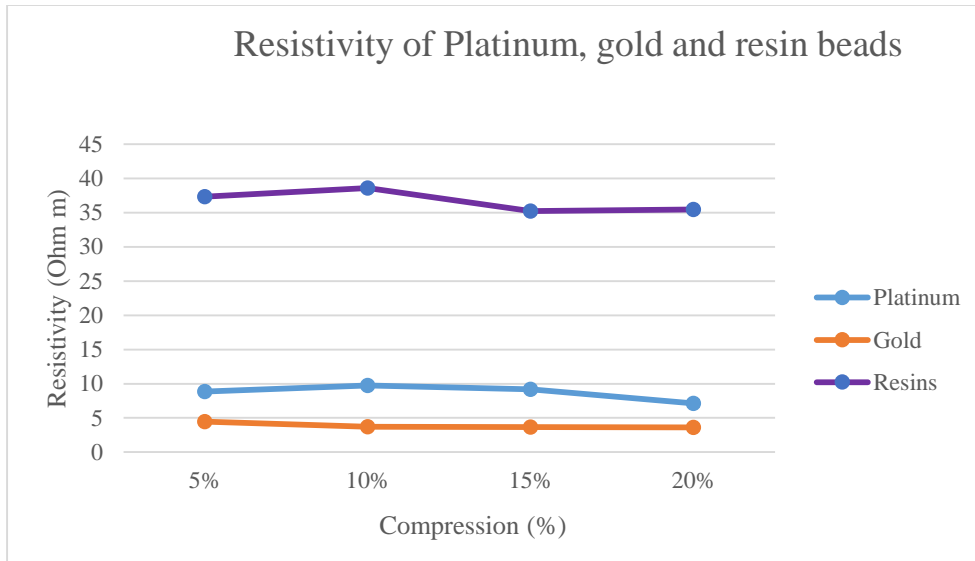


Figure 63 Graph of resistivity vs compression of resin, platinum resins and gold metallized resin beads

Mechanical property such as stiffness was calculated using the stiffness measurement facility as discussed in the experimental methodology section earlier. As shown in Figure 64, it was observed that stiffness of the resin beads increased as the resin beads were metallized using platinum and gold.

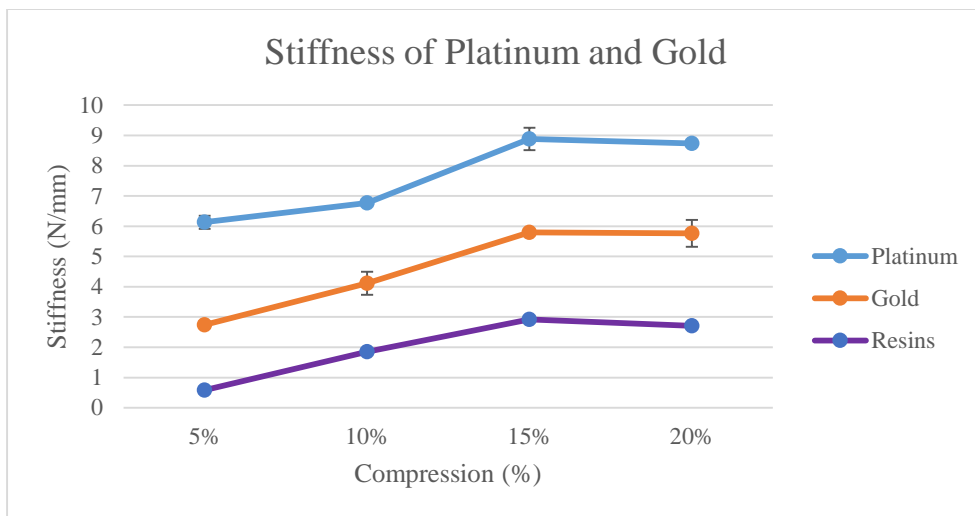


Figure 64 Graph of stiffness vs compression of resin, platinum resins and gold metallized resin beads

As shown in Figure 64, the stiffness of the resin beads almost doubled when gold was added and the stiffness of the resin beads almost quadrupled when platinum was added to the resin beads.

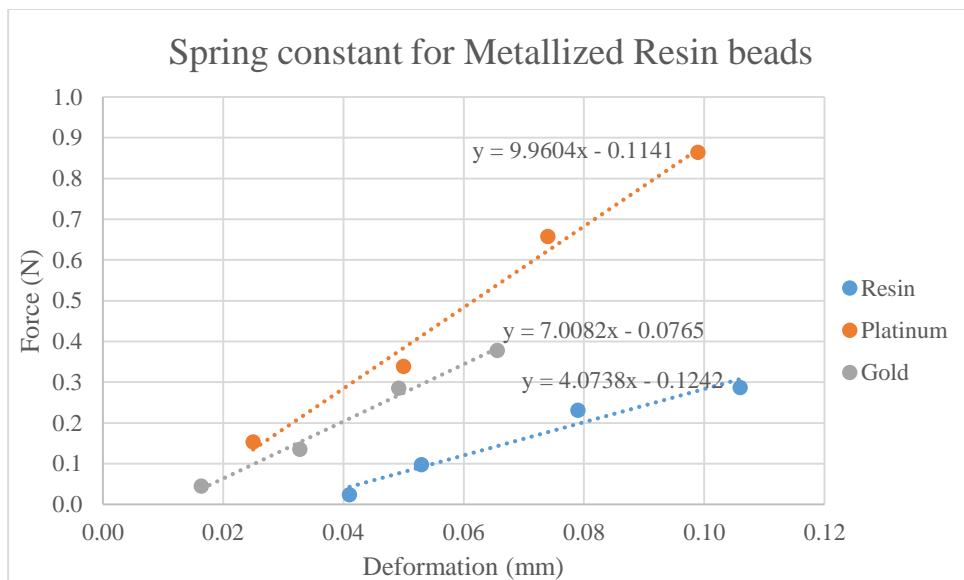


Figure 65 Graph of force vs compression to calculate spring constant of resin, platinum coated resins and gold coated resins.

Also, the spring constant for metallization of resin beads was calculated from the graph of force vs compression, as shown in Figure 65. As shown in Figure 65, the spring constant for resin beads was low. Due to gold metallization process, the spring constant of the resin beads increased from 1.844 to 2.2987. Whereas, due to platinum metallization process, the spring constant of the resin beads increased from 1.844 to 4.9048. It was observed that platinum was stiffer than gold. Considering the results obtained from Figure 62, Figure 63, Figure 64 and Figure 65, it can be observed that platinum improves the stiffness of the beads but gold improves the electrical properties of the gel beads making them more conductive. Hence, gold was preferred than platinum as it had better electrical properties with fairly good physical properties.

To observe the effects of a various number of stages of metallization on the resin beads gold was metallized multiple times on the resin beads. Gold $\text{NaAuCl}_4 \cdot 2\text{H}_2\text{O}$ salt was used for metallization process. Three stages of gold deposition processes were undertaken and are shown in Table 11. The gold deposited beads were obtained from each stage and tested for electromechanical properties using the impedance analyzer and stiffness measurement experimental facilities.

Table 11 Metallization composition of IONAC A554 Cl⁻ with 3 stages of Gold salt NaAuCl₄*2H₂O

Materials		Quantity	Moles (m moles)	Molecular Weight
Stage I				
I	IONAC A554 Cl ⁻ form	3 eq ml	4.2	1.4 meq/ml
II	Aqueous solution of NaAuCl ₄ *2H ₂ O 10 th molar solution	42 ml	4.2	397.8 g/mol
III	Distilled H ₂ O	10 ml		
IV	Hydrazine (N ₂ H ₄)	0.8g dissolved in 20ml distilled H ₂ O	31	32
Stage II				
I	IONAC A554 Cl ⁻ form	2 eq ml	2.8	1.4 meq/ml
II	Aqueous solution of NaAuCl ₄ *2H ₂ O 10 th molar solution	28 ml	2.8	397.8 g/mol
III	Distilled H ₂ O	10 ml		
IV	Hydrazine (N ₂ H ₄)	0.8g dissolved in 20ml distilled H ₂ O	31	32
Stage III				
I	IONAC A554 Cl ⁻ form	1 eq ml	1.4	1.4 meq/ml
II	Aqueous solution of NaAuCl ₄ *2H ₂ O 10 th molar solution	14 ml	1.4	397.8 g/mol
III	Distilled H ₂ O	10 ml		
IV	Hydrazine (N ₂ H ₄)	0.8g dissolved in 20ml distilled H ₂ O	31	32

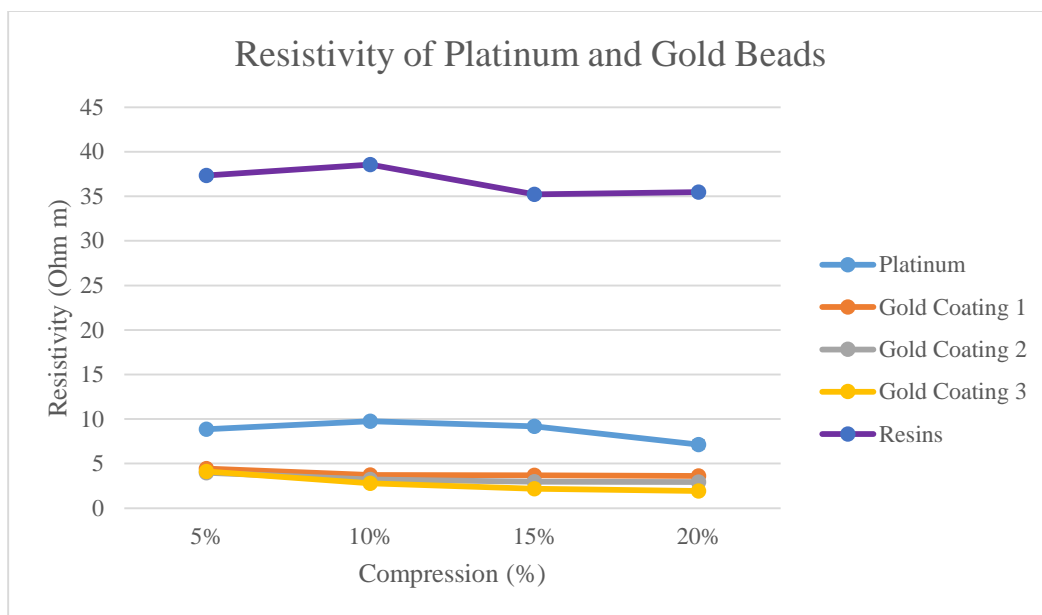


Figure 66 Graph of Resistivity of platinum and metallization stages of gold beads vs compression

The metallized beads obtained from each metallization stage were tested for electrical properties in the impedance analyzer. As shown in Figure 66, the resistivity of platinum and gold was lower than original resin beads. But as the metallization stages for gold were incremented, the resistivity of these beads reduced. The resistivity was reduced by 20% with 2nd metallization coating and was further reduced by 34% after 3rd metallization coating. Also from the Figure 66, it can be observed that the change in resistivity is observed more at higher compression. Also, as we increase the gold metallization stages, the gold concentration increases, eventually leading to more conductive gel beads.

As shown in Figure 67, the dielectric constant of resin beads increased as the number of metallization coating were increased. The dielectric constant was increased by 44% after 2nd gold metallization coating but, the dielectric constant was increased by only 5% after 3rd metallization coating, for beads at 20% compression.

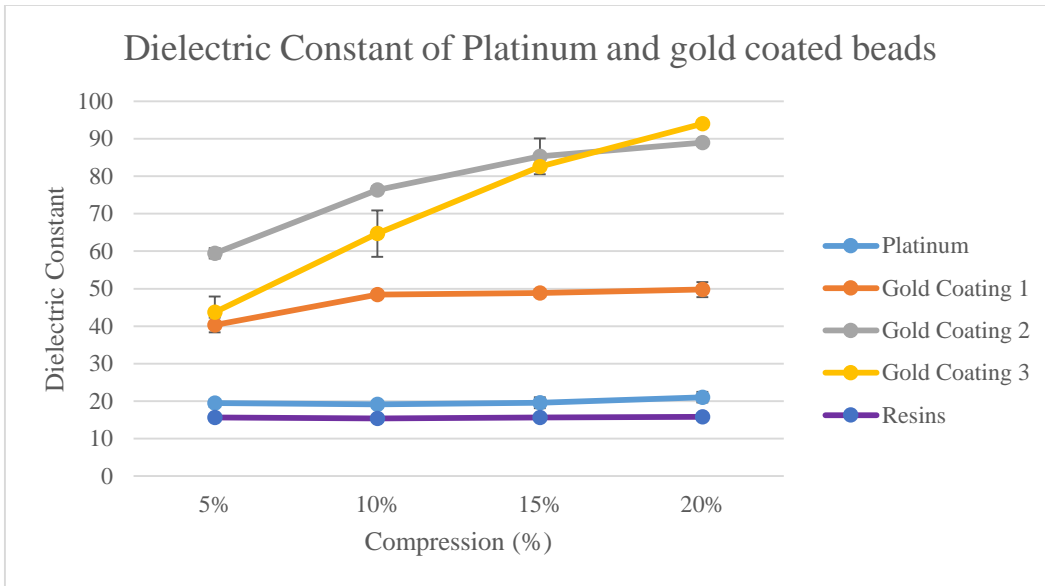


Figure 67 Graph of dielectric constant of platinum and metallization stages of gold beads vs compression

It is observed that as the metallization stages increased, the capability to store charge increased in resin beads as more amount of metal beads were present in the bead. Hence, increasing the number of metallization coating increases the electrical properties of resin IL beads.

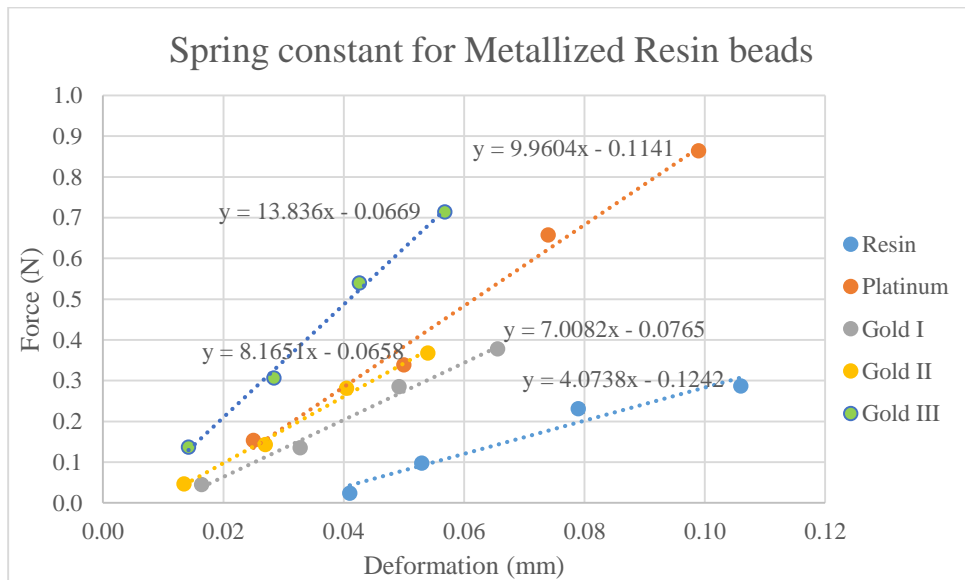


Figure 68 Graph of force vs compression to calculate spring constant of metallization stages of gold coated resins.

Also, the spring constant for metallization of resin beads was calculated from the graph of force vs compression, as shown in Figure 68. As shown in Figure 68, the spring constant for resin

beads was low. Due to gold metallization process, the spring constant of the resin beads increased from 4.0738 to 7.0082 for first gold coating, to 8.1651 after 2nd metallization coating and increased to 13.836 for 3rd metallization coating.

The stiffness of beads obtained from each metallization stage was also calculated. The results obtained from stiffness calculation are shown in Figure 68. The stiffness was increased by 15% after 2nd gold metallization coating but, the stiffness was increased by 45% after 3rd metallization coating, for beads at 20% compression.

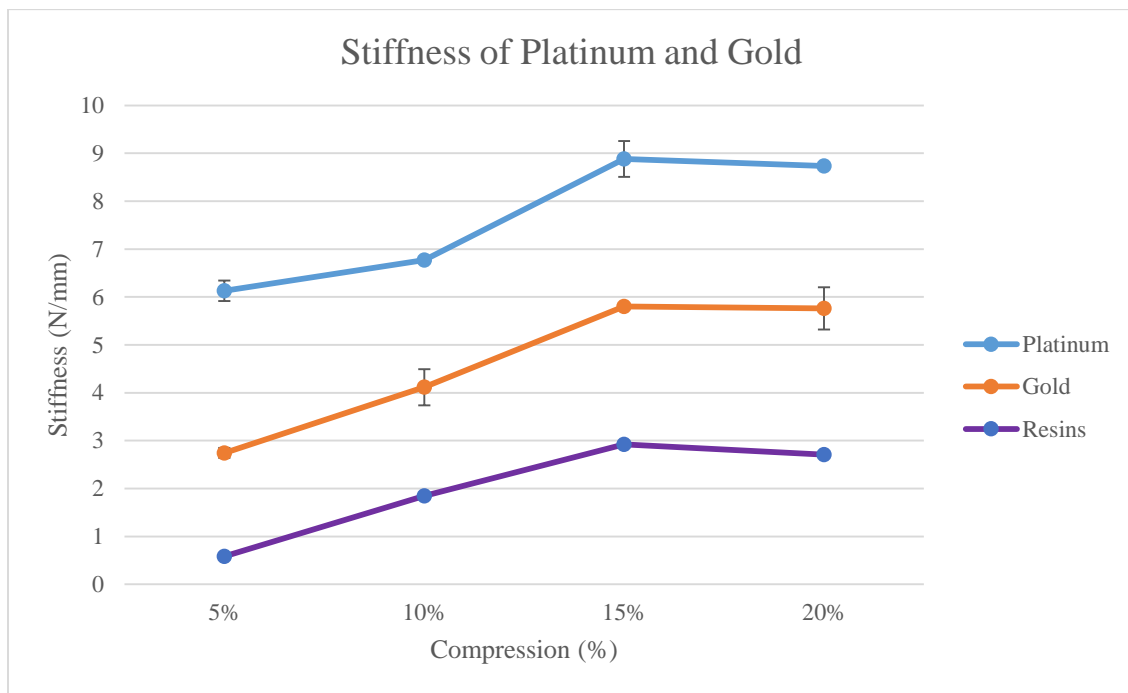


Figure 69 Graph of Stiffness of platinum and gold beads vs compression

As per results are shown in Figure 69, we can say that as the metallization stage was incremented, more gold was deposited in the resin bead, thereby increasing the stiffness of the beads. Hence, it is observed that by increasing metallization coatings increasing the stiffness of the resin beads.

4.2.2 Metallization and testing of IL gel beads:

Metallization of IL gel beads fabricated from the micro-reactor was performed after the metallization process was demonstrated on IONAC A554 Cl⁻ resin beads.

Initially, the IL gel bead with 45% IL was used for metallization process. IL with 45% is selected to check the effect on metallization on a gel bead with a higher amount of IL. The components required for metallization process of IL bead are shown in Table 11.

Table 12 Metallization composition of IL beads with 45% IL monomer

	Materials	Quantity	Moles (m moles)	Molecular Weight
I	IL gel beads	1 g	0.312	207.7 meq/ml
	13% solid gel beads	(0.13 g)		
II	Aqueous solution of NaAuCl ₄ *2H ₂ O 10 th molar solution	3.12 mL	0.321	397.8 g/mol
III	Distilled H ₂ O	10 ml	Excess	
IV	Hydrazine (N ₂ H ₄)	0.5 ml (excess)	31	32

The metallization of the IL beads with 45% IL monomer was performed as described in section 3.4. Unfortunately, the gel beads ruptured completely after the metallization process (Figure 63). The beads obtained after metallization were gel beads with very weak physical structure. Since these beads have a high concentration of IL, they contain a higher proportion of free ions which would be replaced by gold ions. Hence, a higher proportion of gold was deposited in the gel bead. The high concentration of IL also results in a lower proportion of crosslinker, which binds the gel beads in their original shape. Hence, it was assumed that the metallized beads ruptured due to a lower proportion of crosslinker for a higher proportion of gold exchanged in the IL gel bead. The ruptured beads are shown in Figure 70. This assumption was tested by

synthesizing beads with lower IL concentration and more di-vinyl monomer.



Figure 70 Ruptured beads with 45% IL composition

To avoid rupturing of IL beads, beads with 10% IL composition were selected for metallization process. The chemical compositions for metallization process of IL beads with 10% IL composition of monomer solution, is shown in Table 13.

Table 13 Metallization composition of IL beads with 10% IL monomer

	Materials	Quantity	Moles (m moles)	Molecular Weight
I	IL gel beads	1 g	0.0625	207.7 meq/ml
	26% solid gel beads	(0.26 g)		
II	Aqueous solution of NaAuCl ₄ *2H ₂ O 10 th molar solution	0.625 ml	0.0625	397.8 g/mol
III	Distilled H ₂ O	10 ml		
IV	Hydrazine (N ₂ H ₄)	0.5 ml (excess)	31	32

Gel beads with 10% IL monomer were metallized using a similar procedure as explained in the earlier sections. These beads were tested for stiffness, resistivity, and dielectric measurement. But unfortunately, beads with 10% IL monomer composition ruptured after the

electro-mechanical measurements (Figure 71). This result supports the hypothesis that low di-



Figure 71 Ruptured beads with 10% IL composition

vinyl monomer concentration results in rupture. Beads were more stable after lowering IL proportion from 45% to 10%, but they still ruptured when they were compressed. While they might be suitable for some applications, they would not survive long in vibrational harvesters.

Beads with 5% IL concentration were synthesized to further examine the effect of di-vinyl monomer concentration on bead stability. The chemical compositions for metallization process of IL beads with 5% IL composition of monomer solution, is shown in Table 14.

Table 14 Metallization composition of IL beads with 5% IL monomer

	Materials	Quantity	Moles (m moles)	Molecular Weight
Stage I				
I	IL gel beads 23% solid gel beads	1 g (0.23 g)	0.0553	207.7 meq/ml
II	Aqueous solution of NaAuCl ₄ *2H ₂ O 10 th molar solution	0.553 ml	0.0553	397.8 g/mol
III	Distilled H ₂ O	10 ml		
IV	Hydrazine (N ₂ H ₄)	0.5 ml (excess)	31	32
Stage II				
I	IL gel beads 23% solid gel beads	0.5 g (0.115 g)	0.0276	207.7 meq/ml
II	Aqueous solution of NaAuCl ₄ *2H ₂ O 10 th molar solution	0.276 ml	0.0276	397.8 g/mol
III	Distilled H ₂ O	10 ml		
IV	Hydrazine (N ₂ H ₄)	0.25 ml (excess)	31	32

A gold metallized IL liquid beads were formed after this process and were stable in structure. The beads obtained were termed as 1st stage beads and half of them were tested for electro-mechanical properties. The metallization was carried again with half of beads from 1st stage of metallization process. Stage II of metallization process was carried out as per the chemical composition is shown in Table 14. But, after Stage II of metallization process, the beads ruptured completely. This result, along with those from the 45% and 10% beads suggests that reduction of the IL concentration increases the amount of metal that can be absorbed by the beads for stable compression.

To further examine the effect of IL concentration on stability and performance of PIL gel beads, IL beads with 2.5% were used for metallization process. The chemical compositions for

metallization process of IL beads with 5% IL composition of monomer solution, is shown in Table 14.

Table 15 Metallization composition of IL beads with 2.5% IL monomer

	Materials	Quantity	Moles (m moles)	Molecular Weight
Stage I				
I	IL gel beads 18% solid gel beads	1 g (0.18 g)	0.0216	207.7 meq/ml
II	Aqueous solution of NaAuCl ₄ *2H ₂ O 10 th molar solution	0.216 ml	0.0216	397.8 g/mol
III	Distilled H ₂ O	10 ml		
IV	Hydrazine (N ₂ H ₄)	0.5 ml (excess)	31	32
Stage II				
I	IL gel beads 18% solid gel beads	0.66 g (0.1188 g)	0.0143	207.7 meq/ml
II	Aqueous solution of NaAuCl ₄ *2H ₂ O 10 th molar solution	0.143 ml	0.0143	397.8 g/mol
III	Distilled H ₂ O	10 ml		
IV	Hydrazine (N ₂ H ₄)	0.33 ml (excess)	31	32
Stage III				
I	IL gel beads 18% solid gel beads	0.33 g (0.0594 g)	0.00715	207.7 meq/ml
II	Aqueous solution of NaAuCl ₄ *2H ₂ O 10 th molar solution	0.0715 ml	0.00715	397.8 g/mol
III	Distilled H ₂ O	10 ml		
IV	Hydrazine (N ₂ H ₄)	0.15 ml (excess)	31	32

The metallization of the IL beads with 2.5% IL monomer was followed using the metallization procedure similar to that explained in the earlier sections. Gold metallized IL liquid beads were formed after this process and were stable in structure. The beads obtained were termed as 1st stage beads and 1/3rd of them were tested for electro-mechanical properties while rest 2/3rd



Figure 72 Heat treatment for metallization process

of them were forwarded to the stage II of metallization process. In the metallization process for stage II, gold salt was reacting slowly. Hence, to increase the reaction speed, the metallization process was heated as shown in Figure 72. As shown in Figure 72, the test tube with gold salt 1/10th molar solution and IL beads obtained from stage I was placed in a beaker filled with water. The beaker was heated for 10 mins at 80^o C and this resulted in the quick reaction of the gold salt solution with the 1st stage IL beads. The metallization process was completed using the standard procedure as described in the earlier section. Beads obtained from this metallization process were termed as stage II gold metallized beads and 1/3rd of these were tested for electro-mechanical

properties while rest 1/3rd of them were forwarded to the stage III of metallization process. The chemical composition for metallization of stage III is shown in Table 15. The metallization process for stage III completed as per the procedure described in earlier section. The metallized beads



Figure 73 Metallized stage III IL beads

obtained from this stage III were stable in structure. Stage III metallized beads were tested for electro-mechanical properties. The beads after stage III are shown in Figure 73.

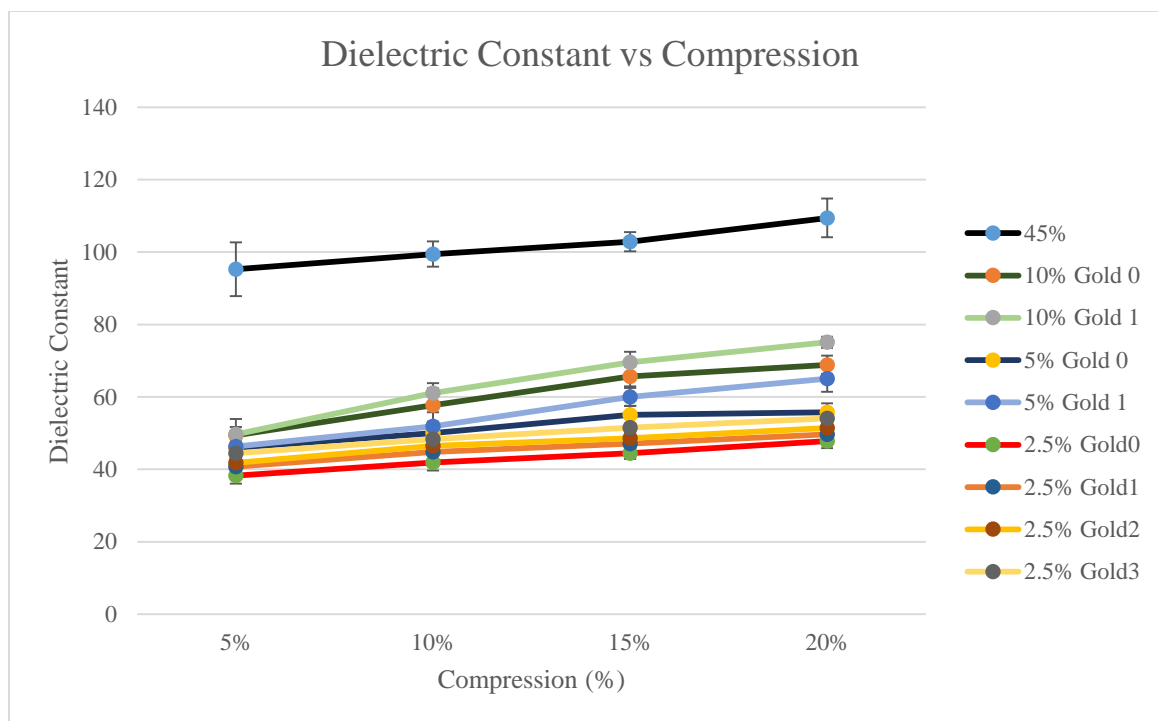


Figure 74 Graph of dielectric constant vs compression of metallized IL beads

Electrical measurements were done to calculate dielectric constant and resistivity as described in the experimental methodology section. Results of dielectric constant were obtained from the data obtained from the impedance analyzer. The dielectric constant for gel beads with 10% IL was increased by 9% after 1st gold metallization coating. The dielectric constant for gel beads with 5% IL was increased by 8% after 1st gold metallization coating. The dielectric constant for gel beads with 2.5% IL was increased by 4% after each gold metallization coating. It was observed that dielectric constant of the beads increased as the number of metallization coatings increased. The graph of dielectric constant vs compression of metallized IL beads is shown in Figure 74.

From the data obtained from the impedance analyzer, the resistivity was also calculated. The resistivity for gel beads with 10% IL was decreased by 8% after 1st gold metallization coating. The resistivity for gel beads with 5% IL was decreased by 7% after 1st gold metallization coating. The resistivity for gel beads with 2.5% IL was decreased by 3% after each gold metallization

coating.

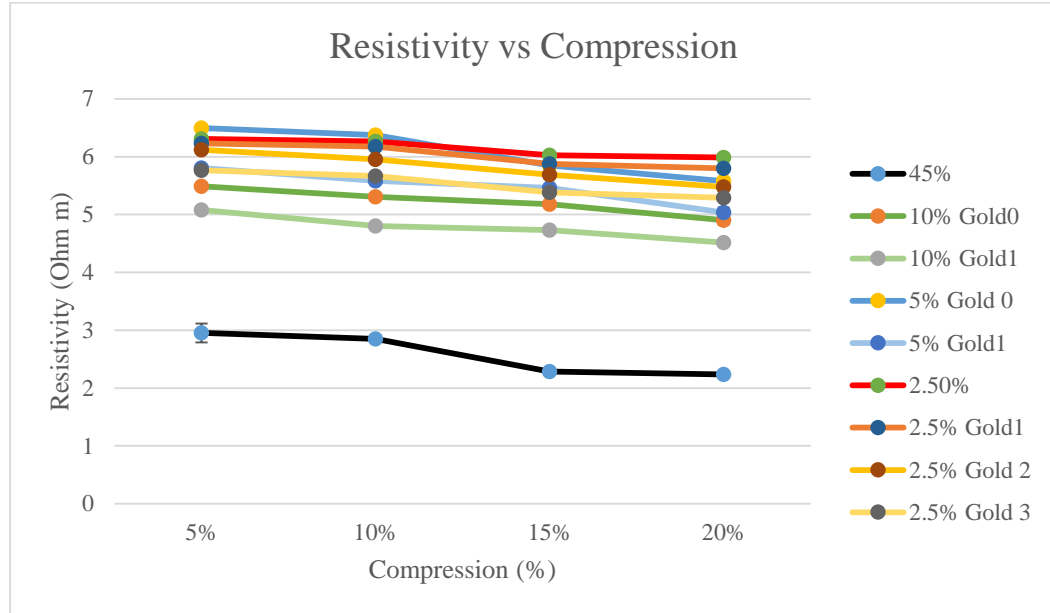


Figure 75 Graph of resistivity vs compression of metallized IL beads

It was observed that as metallization coatings were increased for IL gel beads, the resistivity of the beads decreased and hence became more conductive. The graph of resistivity vs compression of metallized IL beads is shown in Figure 75.

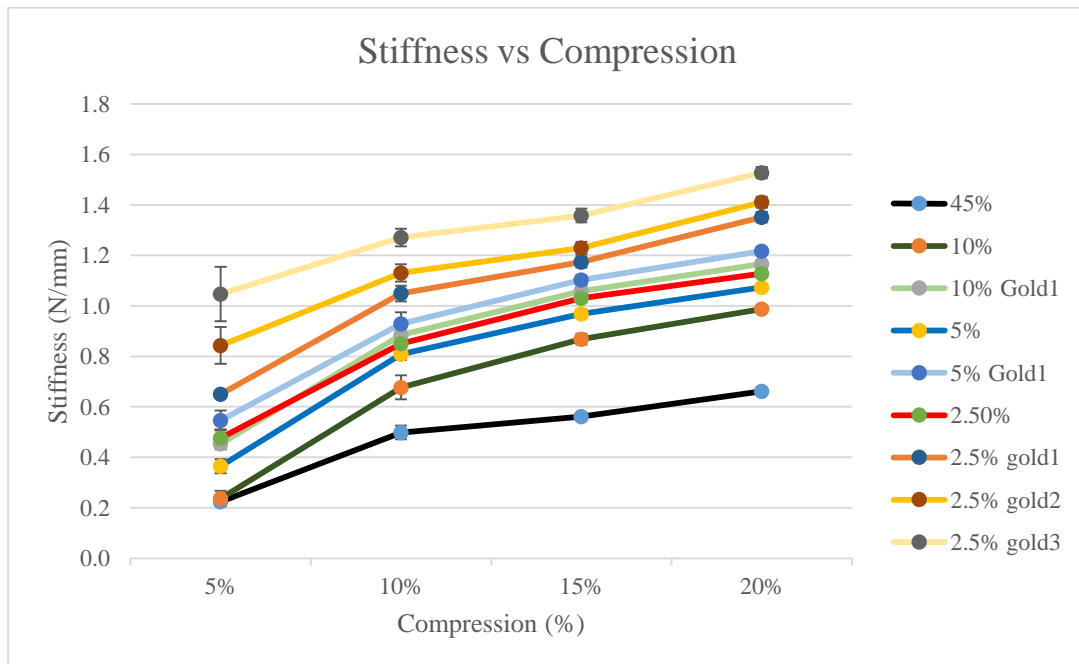


Figure 76 Graph of stiffness vs compression of metallized IL beads

Mechanical measurements on the metallized IL beads were done using stiffness measurement facility. The results of stiffness vs compression are shown in Figure 76. The stiffness for gel beads with 10% IL was increased by 15% after 1st gold metallization coating. The dielectric constant for gel beads with 5% IL was increased by 11% after 1st gold metallization coating. The dielectric constant for gel beads with 2.5% IL was increased by 10% after 1st gold metallization coating and was increased by 7% after 2nd gold metallization coating and was increased 4% after 3rd gold metallization coating. As per the graph is shown in Figure 76, it can be observed that as IL percentage in the gel bead increased, the gel beads were more elastic. Also, the spring constant was calculated for each IL gel beads, is shown in Figure 77.

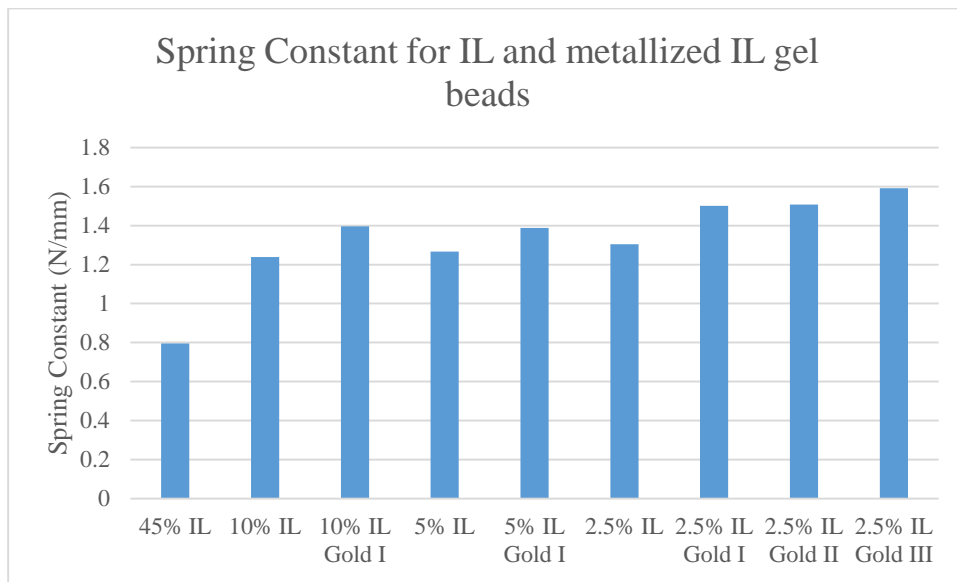


Figure 77 Spring constant of IL gel beads and metallized IL gel beads

From Figure 77, it can be observed that, the spring constant was high for gel beads with low IL percentage. Although, metallization of IL, increased the stiffness of the gel beads, but not with a significant value. The spring constant of 10% IL gel beads increased by 15%, while spring constant for 5% IL gel beads increased by only 11% and for 2.5% IL gel beads, the spring constant increased by only 8%. Hence, we can now say that, due to metallization process, the IL gel beads become stiffer than the IL gel beads without metallization process.

But, from the experiments, it can be observed that for gel beads with IL percentage higher than 10% beads, would rupture after the second metallization coating. This occurred due to a higher proportion of gold deposited in the monomer solution and not sufficient crosslinker to bind the structure of such high amount of gold present in the gel beads. Also, as the IL percentage was decreased from 5% to 2.5% from the beads chemical composition, the metallized beads were more physically stable and would be used for energy harvesting applications.

4.3 Characterization of gel beads:

To characterize the experiments done of resins, IL gel beads, and metallization process, we compared the data of selected beads such as;

1. IONAC C¹⁻ A544 Resin beads
2. Platinum metallized resin beads
3. Stage I gold metallized resins (Gold I),
4. Stage II gold metallized resins (Gold II),
5. Stage III gold metallized resins (Gold III),
6. IL gel beads with IL 45% by proportion (IL 45),
7. IL gel beads with IL 10% by proportion (IL10),
8. Gold metallized IL gel beads with IL 10% by proportion (IL10 Gold I)
9. IL gel beads with IL 5% by proportion (IL 5),
10. Gold metallized IL gel beads with IL 5% by proportion (IL5 Gold I)
11. IL gel beads with IL 2.5% by proportion (IL2.5),
12. Stage I gold metallized IL gel beads with IL 2.5% by proportion (IL2.5 Gold I).
13. Stage II gold metallized IL gel beads with IL 2.5% by proportion (IL2.5 Gold II).
14. Stage III gold metallized IL gel beads with IL 2.5% by proportion (IL2.5 Gold III).

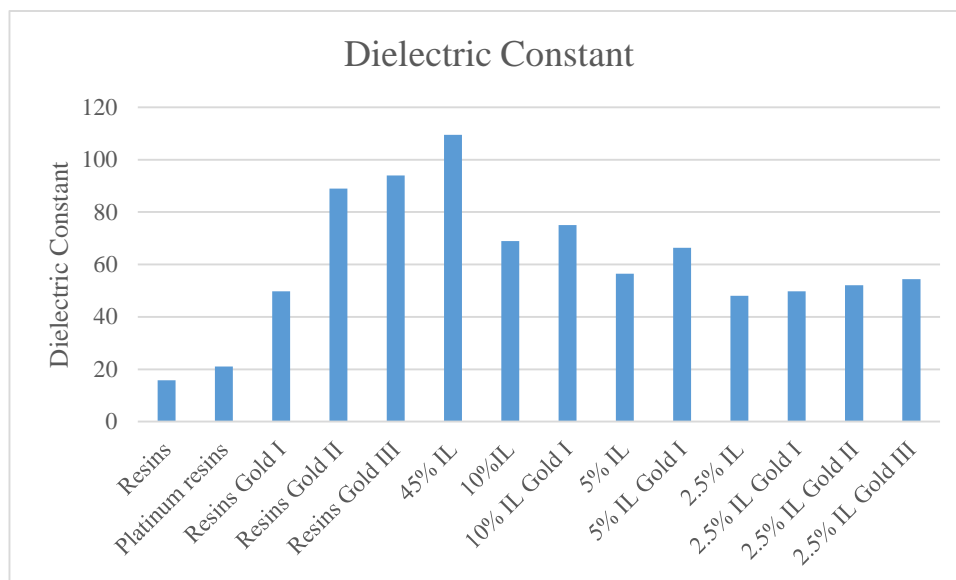


Figure 78 Dielectric constant at 20% compression

Values of dielectric constant at 20% compression of these beads was evaluated and is shown in Figure 78. As shown in Figure 78, it is observed that IL gel beads with 45% proportion of IL have highest dielectric constant and hence have the highest capability of storing charge. But from Figure 78, it can be observed that dielectric constant of IL with 2.5% proportion of IL has a lowest dielectric constant as it has lowest number of free ions.

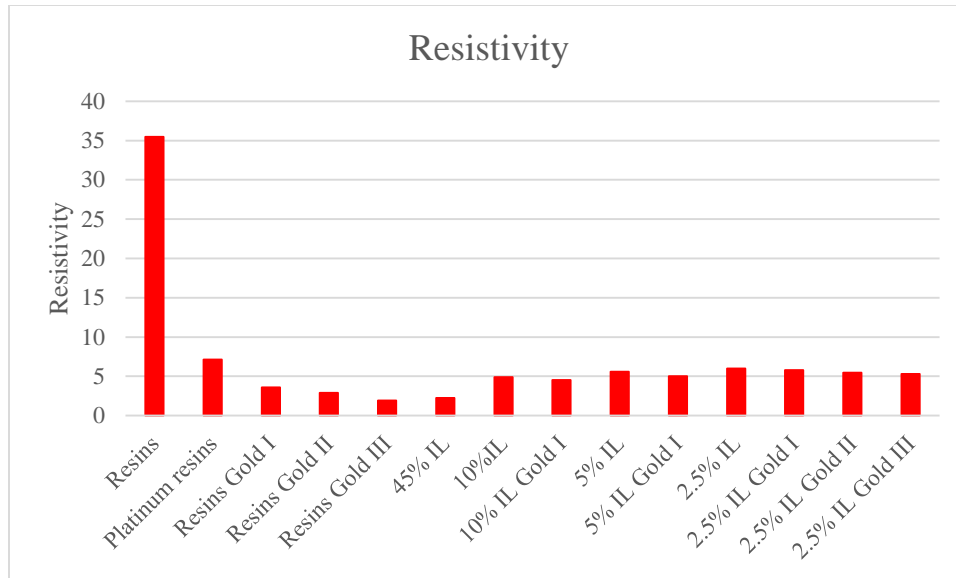


Figure 79 Resistivity of polymerized gel beads at 20% compression

The resistivity of these IL beads at 20% compression was also evaluated and is shown in Figure 79. As shown in Figure 79, it can be observed that resistivity of stage III of resin beads was lowest followed by IL gel bead with 45% IL proportion. While the gel beads with IL 2.5% has the highest resistivity and hence is less conductive.

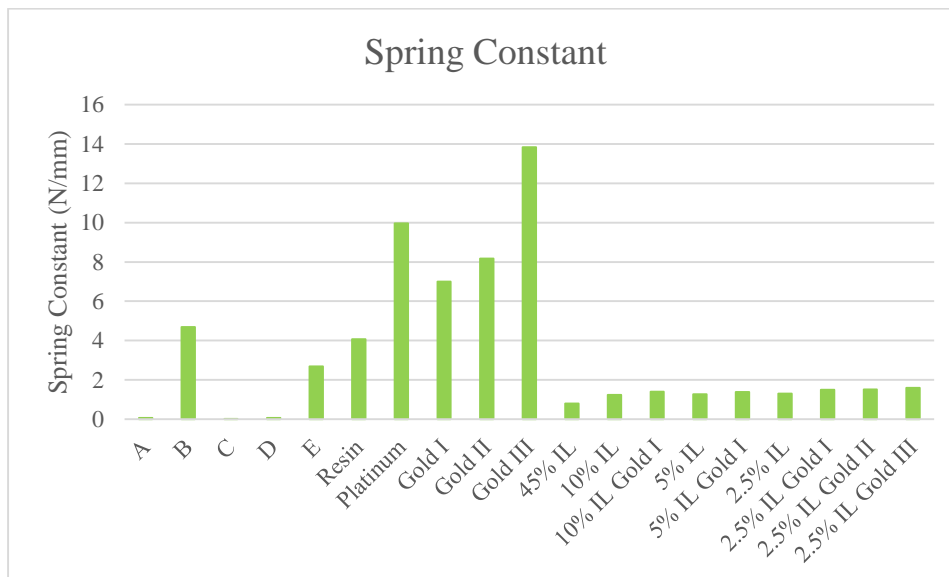


Figure 80 Spring constant of IL beads at 20% compression

The spring constant of these IL beads at 20% compression was also evaluated and is shown in Figure 80. As shown in Figure 80, it can be observed that stiffness of stage III of resin beads was highest while the stiffness of IL gel bead with 45% IL proportion was lowest.

From graphs shown in Figure 78, Figure 79 and Figure 80 we can evaluate that IL gel beads with a higher percentage of IL have good electrical properties but are more elastic in nature. Hence, if the physical properties of these gel beads with a higher proportion of IL can be improved by improvising the chemical composition, these IL gel beads will prove efficient for various energy harvesting applications.

Hence updating table 2 we can suggest the IL gel bead fabricated from the above experimental methods for few of the energy harvesting applications. The IL gel beads for energy harvesting applications are shown in Table 16.

Table 16 Suggested IL gel beads for energy harvesting applications

	Electrostatic Energy Harvester	Vibrational based Energy Harvester
Dielectric Constant	High [1.007(Hg)][50]	High [1.007(Hg)][50]
Resistivity	Low [9.8*10 ⁻⁷ ohm m (Hg)] [51]	Low [9.8*10 ⁻⁷ ohm m (Hg)] [51]
Rolling Resistance (Data N/A)	Low	High
Stiffness	High	Low
Suggested IL gel beads	Stage III of gold metallized IONAC resin beads	IL gel bead with 45% proportion of IL without metallization

As shown in Table 16, we can observe that, for electrostatic energy harvester, IL gel beads are required with low dielectric constant and low resistivity for more conductivity of the energy harvester; should contain high stiffness to roll on the dielectric plate. Hence, according to the results obtained from the characterization of beads we can say that Stage II of gold metallized IONAC resin beads are a most eligible choice. For Vibrational based energy harvester and Dye-sensitized solar cell, IL gel beads are required with high dielectric constant and low resistivity for more conductivity of the energy harvester; should contain low stiffness so that they can be more elastic in nature and can be compressed under vibrations. Future work can focus on these different applications and work on optimizing bead size / composition for each type.

5.0 CONCLUSIONS

5.1 Fabrication of non-IL gel beads using the microreactor

The process of fabricating beads with different chemical compositions has been studied resulting in successful fabricating beads with microreactor. Various different chemical compositions were created and gel beads were fabricated using the microreactor. Comparing the results of electromechanical experiments, it can conclude that for beads with a higher percentage of crosslinker has higher stiffness and for beads with a high amount of liquid monomer have high dielectric constant and low resistivity making them more conductive.

5.2 Fabrication of IL gel beads using the microreactor

The beads fabricated with non-IL chemical composition were not conductive since they did not have any conductive solution in their chemical composition. Hence, to increase the conductivity of the beads, [2-(Methacryloyloxy) ethyl] trimethylammonium chloride solution was selected as an IL. The proportion of IL in the monomer solution was fixed at 45% but the physical structure of the beads was very elastic. The proportion of IL in the monomer solution was updated to 10%, 5%, and 2.5% and the beads were tested for electromechanical properties. As seen from results section we can conclude that as the proportion of IL decreased the bead became more physically stronger but due to less amount of IL present in them, they were less conductive.

5.3 Metallization of IL gel beads and resin

The beads fabricated with IL using microreactor were conductive but lacked physical properties, hence, metallization process was developed to increase the conductivity of beads with a low amount of IL percentage in their composition resulting in increased conductivity and physical properties. Metallization process was initially done on commercially available resin

beads, IONAC A554 Cl⁻ from IL beads. These resin beads were tested for electromechanical properties. These beads were metallized using platinum and gold metals salts. The metallized platinum and gold resin beads were tested for electromechanical properties and it was concluded that gold is more conductive than platinum. Various stages of gold metallization were done to conclude that, with every increment of metallization stage, the conductivity of the resin beads increased.

The IL beads fabricated from the microreactor were metallized using gold salt solution. IL gel beads with varying composition 45%, 10%, 5% and 2.5% were metallized using gold salt solution. As shown from the results section, it can be concluded that as the percentage of IL is decreased from initial chemical composition the resultant metallized beads were less conductive but with better structural properties. Hence, it can conclude that, when the IL percentage is less than 5% in the monomer solution, the resultant metallized beads had better physical properties.

4.4 Contributions of my thesis

In my thesis, I was able to achieve following contributions:

- 1) Commissioned microreactor facility.
- 2) Commissioned facility for mechanical characterization.
- 3) Developed a methodology for electrical characterization in the impedance analyzer.
- 4) Examined the effect of relative flow rate on the shape of PIL beads.
- 5) Examined the effect of IL% on the electromechanical properties of PIL beads.
- 6) Examined the effect of metallization of PIL gel beads on electro-mechanical characteristics.

6.0 FUTURE WORK

Future work will focus on various focusing areas such as:

- 1) Develop a more efficient methodology to enhance the shape of the polymerized gel beads.
- 2) Improve the physical properties of gel beads with a higher percentage of IL present in their monomer solution.
- 3) Improve the chemical composition of the monomer solution of IL gel beads.
- 4) Develop the formula for emulsion stability to calculate flow rates of silicon oil and monomer solution to get perfect dispersed emulsions.
- 5) Improve the metallization process to get metallized IL gel beads with good electrical as well as physical properties.
- 6) Test the IL gel beads on any energy harvester and characterize the data obtained for the harvester.

REFERENCES

- [1] I. E. A. IEA, “World Energy Outlook 2011,” *Int. Energy Agency*, p. 666, 2011.
- [2] A. A. Rafindadi, Z. Yusof, K. Zaman, P. Kyophilavong, and G. Akhmat, “The relationship between air pollution, fossil fuel energy consumption, and water resources in the panel of selected Asia-Pacific countries,” *Environ. Sci. Pollut. Res.*, vol. 21, no. 19, pp. 11395–11400, 2014.
- [3] S. Chu and A. Majumdar, “Opportunities and challenges for a sustainable energy future,” *Nature*, vol. 488, no. 7411, pp. 294–303, 2012.
- [4] E. Roldán, M. Gómez, M. R. Pino, J. Pórtoles, C. Linares, and J. Díaz, “The effect of climate-change-related heat waves on mortality in Spain: uncertainties in health on a local scale,” *Stoch. Environ. Res. Risk Assess.*, 2015.
- [5] R. a Silva *et al.*, “Global premature mortality due to anthropogenic outdoor air pollution and the contribution of past climate change,” *Environ. Res. Lett.*, vol. 8, no. 3, p. 34005, 2013.
- [6] S. Solomon, G.-K. Plattner, R. Knutti, and P. Friedlingstein, “Irreversible climate change due to carbon dioxide emissions.,” *Proc. Natl. Acad. Sci. U. S. A.*, vol. 106, no. 6, pp. 1704–9, 2009.
- [7] J. Kronenberg and R. Winkler, “Wasted waste: An evolutionary perspective on industrial by-products,” *Ecological Economics*, vol. 68, no. 12. pp. 3026–3033, 2009.
- [8] A. T. Submitted *et al.*, “Vibration-based Electromagnetic Energy Harvesters for MEMS Applications,” no. April, 2011.
- [9] R. Bogue, “Energy harvesting: a review of recent developments,” *Sens. Rev.*, vol. 35, no.

- 1, pp. 1–5, 2015.
- [10] O. Dzioubinski and R. Chipman, “Trends in Consumption and Production-Selected Minerals,” no. 5, 1999.
- [11] J. C. Herrera, D. B. Work, R. Herring, X. Ban, Q. Jacobson, and A. M. Bayen, “Evaluation of traffic data obtained via GPS-enabled mobile phones: The Mobile Century field experiment,” *Transp. Res. Part C Emerg. Technol.*, vol. 18, no. 4, pp. 568–583, 2010.
- [12] S. C. W. Krauter, *Solar Electric Power Generation*. 2006.
- [13] P. Effects, “Seebeck and Peltier Effects Introduction,” *Seebeck Peltier Eff. Introd.*, pp. 1–8, 2003.
- [14] “Gregersen, Erik, ed. Britannica Guide to Electricity and Magnetism. Chicago, IL, USA: Encyclopaedia Britannica, Inc., 2011. ProQuest ebrary. Web. 4 November 2015. Copyright © 2011. Encyclopaedia Britannica, Inc.. All rights reserved.,” no. November, 2015.
- [15] S. P. Beeby *et al.*, “A micro electromagnetic generator for vibration energy harvesting,” *J. Micromechanics Microengineering*, vol. 17, no. 7, pp. 1257–1265, 2007.
- [16] S. Cheng, N. Wang, and D. P. Arnold, “Modeling of magnetic vibrational energy harvesters using equivalent circuit representations,” *J. Micromechanics Microengineering*, vol. 17, no. 11, pp. 2328–2335, 2007.
- [17] C. K. LEE, Y. H. HSU, W. H. HSIAO, and J. W. J. WU, “Electrical and mechanical field interactions of piezoelectric systems: foundation of smart structures-based piezoelectric sensors and actuators, and free-fall sensors,” *Smart Mater. Struct.*, vol. 13, no. 5, pp. 1090–1109, 2004.

- [18] K. Nakano, S. J. Elliott, and E. Rustighi, "A unified approach to optimal conditions of power harvesting using electromagnetic and piezoelectric transducers," vol. 16, pp. 948–958, 2007.
- [19] S. Roundy and P. K. Wright, "A piezoelectric vibration based generator for wireless electronics," *Smart Mater. Struct.*, vol. 13, no. 5, pp. 1131–1142, 2004.
- [20] "Analysis of a Micro-Electric Generator for Microsystems.pdf." .
- [21] S. Priya and D. J. Inman, *Energy harvesting technologies*. 2008.
- [22] "Aurivillius-type ceramics, a class of high temperature piezoelectric materials.pdf." .
- [23] R. Ribichini, "Modelling of electromagnetic acoustic transducers," *A thesis Submitt. to Imp. Coll. London degree Dr. Philos.*, no. February, 2011.
- [24] G. Reyne, "Electromagnetic actuation for MOEMS, examples, advantages and drawbacks of MAGMAS," *J. Magn. Magn. Mater.*, vol. 242–245, pp. 1119–1125, 2002.
- [25] N. D. Khupse and A. Kumar, "Ionic liquids: New materials with wide applications," *Indian J. Chem. - Sect. A Inorganic, Phys. Theor. Anal. Chem.*, vol. 49, no. 5–6, pp. 635–648, 2010.
- [26] J. Wilkes, "Properties of ionic liquid solvents for catalysis," *J. Mol. Catal. A Chem.*, vol. 214, no. 1, pp. 11–17, 2004.
- [27] Y. Huang, X. Zhang, Y. Zhao, S. Zeng, H. Dong, and S. Zhang, "New models for predicting thermophysical properties of ionic liquid mixtures," *Phys. Chem. Chem. Phys.*, vol. 17, no. 40, pp. 26918–26929, 2015.
- [28] T. Welton, "Room-temperature ionic liquids. Solvent for synthesis and catalysis," *Chem.Rev*, vol. 99, no. 8, pp. 2071–2083, 1999.
- [29] D. Robin and R. Kenneth, "Ionic liquids-solvents of the future ?," 2003.

- [30] M. Uerdingen, C. Treber, M. Balsler, G. Schmitt, and C. Werner, "Corrosion behaviour of ionic liquids," *Green Chem.*, vol. 7, no. 5, p. 321, 2005.
- [31] A. Hagfeldt, G. Boschloo, L. Sun, L. Kloo, and H. Pettersson, "Dye-sensitized solar cells.," *Chem. Rev.*, vol. 110, pp. 6595–6663, 2010.
- [32] O. Winther-Jensen, V. Armel, M. Forsyth, and D. R. MacFarlane, "In situ photopolymerization of a gel ionic liquid electrolyte in the presence of iodine and its use in dye sensitized solar cells," *Macromol. Rapid Commun.*, vol. 31, no. 5, pp. 479–483, 2010.
- [33] M. S. Su, M. Y. A. Rahman, and A. Ahmad, "ScienceDirect Review on polymer electrolyte in dye-sensitized solar cells (DSSCs)," vol. 115, pp. 452–470, 2015.
- [34] P. M. Sommeling, M. Späth, H. J. P. Smit, N. J. Bakker, and J. M. Kroon, "Long-term stability testing of dye-sensitized solar cells," *J. Photochem. Photobiol. A Chem.*, vol. 164, no. 1–3, pp. 137–144, 2004.
- [35] S. Kanchi and D. Sharma, "Dye Sensitized Solar Cells: Tool to Overcome the Future Energy Crisis," *J. Environ. Anal. Chem.*, vol. 2, no. 1, pp. 1–2, 2014.
- [36] I. Abayev, A. Zaban, V. G. Kytin, A. a. Danilin, G. Garcia-Belmonte, and J. Bisquert, "Properties of the electronic density of states in TiO₂ nanoparticles surrounded with aqueous electrolyte," *J. Solid State Electrochem.*, vol. 11, no. 5, pp. 647–653, 2007.
- [37] K. Park, Q. Zhang, D. Myers, and G. Cao, "Charge transport properties in TiO₂ network with different particle sizes for dye sensitized solar cells.," *ACS Appl. Mater. Interfaces*, vol. 5, no. 3, pp. 1044–52, 2013.
- [38] F. Fabregat-Santiago *et al.*, "Correlation between Photovoltaic Performance and Impedance Spectroscopy of Dye-Sensitized Solar Cells Based on Ionic Liquids," *J. Phys.*

- Chem. C*, vol. 111, no. 17, pp. 6550–6560, 2007.
- [39] Z. Yang, E. Halvorsen, and T. Dong, “Electrostatic energy harvester employing conductive droplet and thin-film electret,” *J. Microelectromechanical Syst.*, vol. 23, no. 2, pp. 315–323, 2014.
- [40] T. Krupenkin and J. A. Taylor, “Reverse electrowetting as a new approach to high-power energy harvesting,” *Nat. Commun.*, vol. 2, no. May, p. 448, 2011.
- [41] W. Kong *et al.*, “Ionic liquid based vibrational energy harvester by periodically squeezing the liquid bridge,” *RSC Adv.*, vol. 4, no. 37, p. 19356, 2014.
- [42] L. E. Helseth and X. D. Guo, “Contact Electrification and Energy Harvesting Using Periodically Contacted and Squeezed Water Droplets,” *Langmuir*, vol. 31, no. 10, pp. 3269–3276, 2015.
- [43] A. V. Mamishev, K. Sundara-Rajan, F. Yang, Y. Du, and M. Zahn, “Interdigital sensors and transducers,” *Proc. IEEE*, vol. 92, no. 5, pp. 808–844, 2004.
- [44] Z. Yang, E. Halvorsen, and T. Dong, “Power generation from conductive droplet sliding on electret film,” *Appl. Phys. Lett.*, vol. 100, no. 2012, pp. 7–11, 2012.
- [45] N. Miljkovic, D. J. Preston, R. Enright, and E. N. Wang, “Jumping-droplet electrostatic energy harvesting,” *Appl. Phys. Lett.*, vol. 105, no. 1, p. 13111, 2014.
- [46] M. T. Rahman, Z. Barikbin, A. Z. M. Badruddoza, P. S. Doyle, and S. a. Khan, “Monodisperse polymeric ionic liquid microgel beads with multiple chemically switchable functionalities,” *Langmuir*, vol. 29, no. 30, pp. 9535–9543, 2013.
- [47] M. Galiński, A. Lewandowski, and I. Stępniaik, “Ionic liquids as electrolytes,” *Electrochim. Acta*, vol. 51, no. 26, pp. 5567–5580, 2006.
- [48] S. Yamada, H. Mitsuya, and H. Fujita, “Vibrational Energy Harvester based on Electrical

- Double Layer of Ionic Liquid,” *J. Phys. Conf. Ser.*, vol. 557, p. 12013, 2014.
- [49] R. Kumar *et al.*, “Ion transport and softening in a polymerized ionic liquid,” *Nanoscale*, vol. 7, no. 3, pp. 947–55, 2015.
- [50] M. Williams, “Dielectric Constant,” *Universe today*, no. October, p. 2016, 2011.
- [51] B. N. Aleksandrov and N. N. Antonova, “Variation of the electrical resistance of solid mercury at low temperatures,” vol. 26, no. 1, 1967.
- [52] M. K. Nazeeruddin, E. Baranoff, and M. Grätzel, “Dye-sensitized solar cells: A brief overview,” *Sol. Energy*, vol. 85, no. 6, pp. 1172–1178, 2011.
- [53] J. Tiihonen, I. Markkanen, M. Laatikainen, and E. Paatero, “Elasticity of ion-exchange resin beads in solvent mixtures,” *J. Appl. Polym. Sci.*, vol. 82, no. 5, pp. 1256–1264, 2001.
- [54] D. Melekaslan, N. Gundogan, and O. Okay, “Elasticity of poly (acrylamide) gel beads,” *Polym. Bull.*, vol. d, pp. 287–294, 2003.
- [55] A. Black, “Fluoropolymer Tubing,” pp. 1–2, 2012.
- [56] J. Tan, J. H. Xu, S. W. Li, and G. S. Luo, “Drop dispenser in a cross-junction microfluidic device: Scaling and mechanism of break-up,” *Chem. Eng. J.*, vol. 136, no. 2–3, pp. 306–311, 2008.
- [57] F. Baumgart, “Stiffness - an unknown world of mechanical science.pdf.” *Injury, Int. J. Care Injured* 31 (2000) S-B 14-S-B23, pp. B14–B23, 2000.
- [58] A. Warshawsky and D. A. Upson, “Zerovalent metal polymer composites. I. Metallized beads,” *J. Polym. Sci. Part A Polym. Chem.*, vol. 27, no. 9, pp. 2963–2994, 1989.
- [59] T. Scientific and C. T. Handbook, “Crosslinking technical handbook,” *Thermo Fish. Sci. Rockford, IL, USA*, 2009.
- [60] I. Miami, “TIBTECH Innovations,” *Development*, no. April, pp. 9–11, 2010.

